

THERMO
SENSITIVE

SENSOR /
ACTUATOR

*Thermo-sensitive actuator capabilities assessment of a composite material
based on a two-way shape memory semicrystalline polymer*

Thesis presented in partial fulfillment of the requirements for the degree of

MASTER'S IN CONSTRUCTION

CCComposites Research Group

Materials Research Group



Construction Master's Degree
Construction school
Architecture Faculty

Universidad Nacional de Colombia

Medellín, Colombia 2018

THERMO-SENSITIVE ACTUATOR
CAPABILITIES ASSESSMENT OF A
COMPOSITE MATERIAL BASED ON A
TWO-WAY SHAPE MEMORY
SEMICRYSTALLINE POLYMER

John Edison Rodríguez Villegas / bachelor's in architecture (Hons.)

Thesis Direction Ph.D. Henry A. Colorado / *Thesis Co-direction* Ph.D. Juan Camilo Restrepo Gutierrez

“

Daniel Libeskind

Architecture should make us feel different, if not, engineering would be enough.

Science is a way of thinking much more than it is a body of knowledge.

Carl Sagan

”

ABSTRACT

Evidence suggests that energy efficiency is one of the most crucial factors to be addressed in XXI century by building industry, and the study of the building envelope, which includes passive systems of dynamic activation that works with intrinsic properties of materials has risen significantly since the early 2000s as alternative. Hence, there is a growing body of literature that recognizes the advantages of polymers among others stimulus sensitive materials to define systems of dynamic activation.

The adaptive building envelopes state of the art, as well as, semicrystalline shape memory polymers, is assessed in this work. In this way, the thermosensitive potential of a composite material based on a bidirectional shape memory polymer that could be used in responsive building skins was studied. Crosslinked ethylene-vinyl acetate copolymer prestressed, and functionalized sheets were encapsulated into a polyurethane rubber matrix to obtain a thermosensitive functional composite.

The programming process which enhance the shape memory effect and the stability of the phenomenon through thermal cycling were studied, as well as, actuator capacity.

keywords

CRYSTALLIZATION-INDUCED ELONGATION
SHAPE MEMORY ACTUATOR
ADAPTIVE BUILDING SKINS

*EVALUACIÓN DEL POTENCIAL DE ACTUACIÓN
TERMOSENSIBLE DE UN MATERIAL COMPUESTO A
BASE DE UN POLÍMERO SEMICRITALINO CON MEMORIA
DE FORMA BIDIRECCIONAL*

RESUMEN

La evidencia sugiere que la eficiencia energética es uno de los factores más importantes a abordar en el siglo XXI por la industria de la construcción. Es así como el estudio de la envolvente del edificio que incluye sistemas pasivos de activación dinámica con propiedades intrínsecas de los materiales ha aumentado desde el 2000 como alternativa. Por lo tanto, existe un cuerpo creciente de literatura que reconoce las ventajas de los polímeros sobre otros materiales sensibles a estímulos para definir sistemas de activación dinámica.

En este trabajo se evalúa el estado del arte de las envolventes de construcción adaptables, así como los polímeros semi cristalinos con memoria de forma. De esta forma, se estudió el potencial termosensible de un material compuesto basado en un polímero de memoria de forma bidireccional que podría usarse en pieles arquitectónicas adaptativas. Copolímero reticulado de etileno-acetato de vinilo pretensado, y láminas funcionalizadas se encapsularon en una matriz de caucho de poliuretano para obtener un compuesto funcional termosensible.

Se estudió el proceso de programación que mejora el efecto de memoria de forma y la estabilidad del fenómeno a través del ciclo térmico, así como la capacidad del actuador.

*ELONGACIÓN INDUCIDA POR
CRISTALIZACIÓN
ACTUADOR CON MEMORIA DE FORMA
PIELES ARQUITECTÓNICAS ADAPTATIVAS*

*Palabras
clave*

AKNOWLEDGMENTS

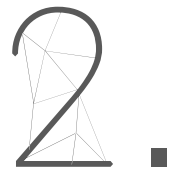
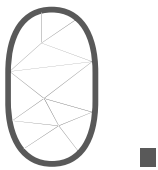
To *my family*, for always supporting me in achieving my goals I want to say thank you, for helping me, even when I am far from home in all the ways that you could. Especially for my mother and brothers for pushing me when I need to be pushed.

To *my directors*, Henry and Juan Camilo, for believing in my research purpose, helping me to find the ways to achieve all the proposed goals and encourage me as a researcher.

To *the research groups and the staff*, for the permanent feedback, for helping me to make this research real, and to be a crucial part of this educational experience; my viewpoint about the construction and building was enhanced because all of you. Especial thanks to professor Diego H. Giraldo, Universidad de Antioquia polymers processing lab staff, and materials research group members under the leadership of professors Juan C. Ochoa and Yhan P. Arias.

To *my friends and fellows*, for sharing ideas, viewpoints, meals... and supporting each other in this process. Especial thanks to Carolina Chalarca, José R. Zelaya and Ricardo A. Rave

CONTENT



1
Preliminary

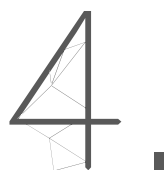
1
Preface
2
Tables List
2
Figures List
5
Symbols List

6
Introduction and overview

7
What is happening
7
What is being done
8
How can be seen
8
What is proposed
9
How is presented
10
References

11
Adaptive Building Envelopes

14
Introduction
16
Active adaptive envelopes
22
Passive adaptive skins
43
Conclusions and further works
44
References



51
Semicrystalline Shape
Memory Polymers

54
Introduction

56
One-Way shape memory effect

58
Thermally induced shape
memory effect

60
Two-Way shape memory effect

67
Conclusions and further works

68
References

71
Thermosensitive functional
composite

73
Introduction

Experimental Objectives

77
Materials and methods

86
Results and discussion

Shape memory lamina synthesis

Shape memory study

Functional composite synthesis

Thermocycling and stability study

108
Conclusions and further works

111
Supplementary information

113
References

115
Overall Conclusions and
recommendations for
future works

117
Overall Conclusions

118
Recommendations for
future works

119
Architecture skin application
Proposal

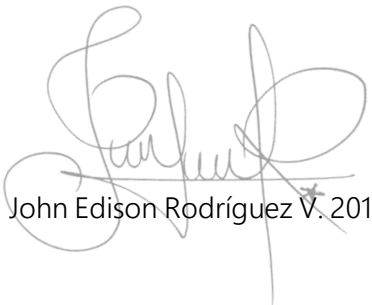
127
References

Figures references

PREFACE

At this moment I declare to the best of my knowledge, that the content of the thesis is original in its entirety and contains no material which has been previously published by another person, except where due reference is stated. Besides, no part of this work has been submitted for the award of any other degree or diploma in any university.

I guarantee that the work has been undertaken solely by the candidate, except where the due acknowledgment is given. The text of the thesis, exclusive of bibliography does not exceed 30,000 words.



John Edison Rodríguez V. 2018

Funding | This Thesis was partially funding by:
Universidad Nacional de Colombia, Support for postgraduate thesis, 2017-2018 national call
Project 40812
Fundación para la promoción de la Investigación y la tecnología, affiliated to *Banco de la Republica de Colombia* cultural network
Project 4198

TABLES LIST

Table 1. Active Control Systems.....	16
Table 2. Passive control systems reported.....	24
Table 3. SMA and SMP Comparative primary features	53
Table 4. Polymeric systems and reversible switch transitions in OW-SME reported.....	55
Table 5. Thermally induced shape memory polymers reported	57
Table 6. Reversible switch transitions in 2W-SME reported in polymer systems.....	59
Table 7. Semicrystalline networks with evidence of 2W-SME reported.....	61
Table 8. Shape Memory Effect key parameters, shape fixity ratio, and shape recovery ratio	65
Table 9. Methodological activities and phases summary	78
Table 10. Used materials.....	78
Table 11. Synthesis and curing summary	79
Table 12. Programming summary.....	81
Table 13. Shape memory study summary	81
Table 14. Surface treatment summary.....	83
Table 15. Composite matrix summary	84
Table 16. Thermomechanical properties of the samples.....	90
Table 17. Mechanical properties of the samples.....	101

FIGURES LIST

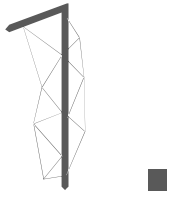
Fig. 1 The Curia. The meeting house of the Senate of Rome,	13
Fig. 2 North rose window, inside view, Notre Dame Cathedral,.....	13
Fig. 3 Seagram Building, Ludwig Mies Van der Rohe, Main entrance view,.....	13
Fig. 4 Data Acquisition protocol of close loop.....	15
Fig. 5 multi-layer Skins.	15
Fig. 6. Arab world institute (Paris) envelope panel.	17
Fig. 7 Arab world institute (Paris) Diaphragms.....	17
Fig. 8. Kiefer technic Showroom (Bad Gleichenberg).....	17
Fig. 9. Al Bahar Towers (Abu Dhabi)	17
Fig. 10. RMIT Design Hub (Melbourne)	17
Fig. 11. Q1 ThyssenKrupp Quarter (Essen)	17
Fig. 12. One Ocean Theme Pavilion (Jeollanam-do).....	19
Fig. 13. Lamella One Ocean Theme Pavilion (Jeollanam-do).....	19
Fig. 14. Arab World Institute (Paris) actuator	19
Fig. 15. Hierarchical location of stimuli-responsive materials on the materials world.....	21
Fig. 16. pinecone scales. Axial cut view,	27
Fig. 17. 3D printed programmable hygroscopic material,	27

Fig. 18. Motion with Moisture.....	27
Fig. 19. Sodium Polyacrylate Swollen process.....	27
Fig. 20. Hydroceramic. Scheme of the components of the cooling systems module,	29
Fig. 21. Bimetal Strip.	29
Fig. 22. Bloom Research Installation (Los Angeles), Panel behavior Position	29
Fig. 23. non-diffusional phase change Austenite – deformed martensite.	31
Fig. 24. Adaptive [Skins]. The dynamic control unit. operated by NiTi springs,	31
Fig. 25. kinetic façade actuated by NiTi wires.....	31
Fig. 26. Vanadium dioxide temperature transition.....	33
Fig. 27. Thermochromic glass coating.....	33
Fig. 28. Temperature against time PCM behavior.....	35
Fig. 29. Schematic dielectric electroactive mechanism of actuation.	37
Fig. 30. Homeostatic Façade Prototype (New York) basic skin unit.	37
Fig. 31. Homeostatic Façade Prototype (New York). System operation, inside view.	37
Fig. 32. Electrochromic multilayer system.	39
Fig. 33. Tungsten Oxide Electrochromic coated window.....	39
Fig. 34. Polymer Thermal-switching transitions.	41
Fig. 35. Translated geometries. Standing structure actuated by SMP.....	41
Fig. 36. <i>Stable molecular structures, bases of the SME in polymers</i>	53
Fig. 37. Stimulus sensitive domains transitions	55
Fig. 38. Thermally induced SME, programming process.....	57
Fig. 39. Lamellae TEM Image.....	59
Fig. 40. Schematic Stretch Induced Crystallization SIC process of a network chain during two-way SME	62
Fig. 41. Plot of storage modulus versus temperature.....	63
Fig. 42. Ethylene Vinyl Acetate Copolymer.....	74
Fig. 43 <i>Customize forced convection thermal chamber with temperature controller</i>	80
Fig. 44. Contact angle θ and surface energies γ for a liquid drop on a solid surface	83
Fig. 45. Interfacial bonds formed in a composite	83
Fig. 46. <i>Machined stainless-steel mold with slots view</i>	84
Fig. 47 thermocycling experiments assembly recording.....	85
Fig. 48. <i>Chemical structure of cEVA (pre-polymer) Left, and dicumyl peroxide (cross-linker agent) Right, Sigma Aldrich</i> ®	87
Fig. 49. <i>ATR-IR spectra of cEVA with 18%Wt vinyl groups</i>	87
Fig. 50 <i>Torque against blending time and temperature plot</i>	88
Fig. 51. Basic principle of the main curing reaction of cEVA during radical crosslinking.....	88
Fig. 52. <i>Raw material/processed material appearance</i>	89
Fig. 53. <i>Annealing process pictures</i>	89
Fig. 54. <i>Non-isothermal DSC curves of cEVA cured and pristine samples</i>	90
Fig. 55. <i>DMTA Test for cured and pristine EVA samples</i>	91
Fig. 56. Stress-Strain curves, pristine and crosslinked EVA.....	91
Fig. 57. <i>Second heating DSC run T_{low} and T_{high} Temperatures</i>	92
Fig. 58. Two-Way shape memory test under several stress programming levels	93
Fig. 59 Second heating DSC run Skeleton and actuator domains transitions for 2W-SME experiments	94
Fig. 60. DSC first heating ramp. Various programming stress level	95
Fig. 61 Contact angle water/cEVA-DCP pictures.....	96
Fig. 62. <i>Contact angle as-received and after low plasma exposure</i>	97

Fig. 63. Surface energy as-received and after low plasma exposure	97
Fig. 64 Low plasma discharge reactor appearance	98
Fig. 65 ATR-IR Spectra as-received and treated surfaces.....	98
Fig. 66 Roughness profiles. As-received and treated samples.....	99
Fig. 67. ATR-AR spectra PU matrixes	100
Fig. 68. Non-isothermal DSC curves of PU matrixes	101
Fig. 69. Stress strain curves PU matrixes.....	101
Fig. 70. Obtained actuator configuration views.....	102
Fig. 71. T-peel strength values as-received and treated encapsulated composite	102
Fig. 72. T-peel strength curves SMC treated and as-received samples	103
Fig. 73 T-peel after test samples. Left as-received, right treated	104
Fig. 74 Expected composite actuator response under thermal cycling	105
Fig. 75 Actuator response for the first thermal cycle SMC1 sample	105
Fig. 76 Transverse displacement recorded during thermal cycling	106
Fig. 77 second thermal cycle SMC2 samples.....	107
Fig. 78 Mimosa pudica pulvinus left. relexed righth. bended.....	120
Fig. 79 Morphing structures of a pulvinus and a petiole movement of Mimosa pudica after thermal stimulation of pinnules and the top of a rachis by a flame, adapted from [281]	120
Fig. 80 Fundamental unit of actuation DaCM.....	121
Fig. 81 DaCM 3D views	121
Fig. 82 Skin module open and close positions.....	122

SYMBOLS LIST

2W-SME	Two-way shape memory effect	<i>SMP</i>	Shape-memory polymer
2W-SSMP	Two-way Semicrystalline shape memory polymer	<i>OW-SME</i>	One-way shape memory effect
		<i>tanδ</i>	Loss factor
β_c	Cooling rate	T_{prog}	Deformation temperature
β_h	Heating rate	T_g	Glass transition temperature
ϵ	Nominal strain	T_{high}	Temperature at which recovery is performed
ϵ_b	Strain at break	T_{low}	Temperature at which temporary shape is fixed
ϵ_m	Default strain in a cyclic, thermomechanical experiment	T_m	Melting temperature
ϵ_p	Recovered strain in a cyclic, thermomechanical experiment	$T_{m,onset}$	Start Melting temperature (AD)
ϵ_u	Fixed strain after unloading in a cyclic, thermomechanical experiment	$T_{m,offset}$	Finish Melting temperature (AD)
σ	Stress	T_c	Crystallization temperature
σ_m	Stress after stretching a sample to ϵ_m in a cyclic, thermomechanical experiment	$T_{sw,act}$	Switching temperature, fixation temporary shape in SME
<i>DMTA</i>	Dynamic mechanical thermal analysis	$T_{sw,rec}$	Switching temperature, recovery permanent shape in SME
<i>DSC</i>	Differential scanning calorimetry	T_{trans}	Thermal transition temperature (T_m or T_g)
<i>E</i>	Young's modulus	$T_{trans,A}$	Thermal transition temperature of shape A for materials with two shapes in memory
<i>E'</i>	Storage modulus	$T_{trans,B}$	Thermal transition temperature of shape B for materials with two shapes in memory
<i>E''</i>	Loss modulus	<i>wG</i>	Gel content
<i>G</i>	Shear modulus	<i>DCP</i>	Dicumyl Peroxide
<i>Xc</i>	Fractional Crystallinity	<i>DHBP</i>	2,5-bis(tert-butylperoxy)-2,5-dimethylhexane
<i>HRMAS</i>	High resolution magic angle spinning in NMR-spectroscopy	<i>TMPMP</i>	trimethylolpropane tris(3-mercaptopropionate)
<i>Hz</i>	Hertz	<i>POM</i>	Polarized Optical Microscopy
<i>N</i>	Interpenetrating polymer network	<i>N</i>	Consecutive number in a cyclic, thermomechanical experiment
<i>AD</i>	Actuation Domain	<i>NMR</i>	Nuclear magnetic resonance
<i>SD</i>	Skeleton Domain	<i>Q</i>	Degree of swelling
<i>MA</i>	Methacrylate	R_f	Shape fixity ratio
m_d	Mass of the extracted and dried network	R_r	Shape recovery ratio
m_{iso}	Mass of the unextracted polymer network	<i>SME</i>	Shape-memory effect
M_n	Number average molecular weight	<i>SEM</i>	Scanning Electron Microscopy
m_s	Mass of the swollen polymer network	<i>M</i>	Transmission Electron Microscopy



INTRODUCTION AND OVERVIEW

What is happening

Buildings have been rated as the responsible for about one-third of the total anthropogenic CO₂ emissions to the atmosphere [1], and at least 40% of the energy produced is consumed by buildings [2]. This consumption is presented from the moment when the building is constructed, as capital energy (CE), and during its life cycle as operating energy (OE), measured in an estimated period of 50 years. In the case of housing, the OE constitutes approximately 65% [3] of the total energy required by the building, a remarkable percentage not only for housing but any kind of building. The OE is mainly used as HVAC because of their direct influence on the comfort perception. Thus, the OE represent more than a half of the energy consumed by the building activity.

Several strategies have been formulated by government organizations on the field of the energy consumption, for instance, the net-zero energy buildings (NZEB) [4], [5]. Strategy focused on achieving a balance close to zero, between the consumed and the produced energy by buildings, with the aim to reach self-sufficient buildings unplugged from the network. Some countries have been implemented the NZEB as the strategy to diminish the energy consumption and the environmental impact of buildings to the short and medium term [6]–[8].

In the case of Colombia, the *Ministerio de Vivienda, Ciudad y Territorio* issued the 0549 resolution from July 10 of 2015, where the water and energy mandatory reduction percentages by new buildings were established; This resolution is nowadays an applicable law in the whole nation. The resolution considers the use of active strategies (systems which energy is required for the operation) and passive strategies (systems which energy is not required for the operation) as well.

What is being done

Architecture has had evolved and developed to satisfy human and city necessities since its origin. Every day, new essentials in addition to severe weather changes need to be solved by buildings. This process, in the last years, has been accelerated because of the complexity of the "modern life" and their impact on the environment [9]. For those reasons, in response to these fluctuating variables, the architecture needs to adapt permanently to remain current.

The bioclimatic strategy, as an approximation for the energy consumption issue, in one of his areas has been focused on the façade or building envelope. The strategy looks for the compatibilization between buildings and the local weather of their surrounding area to reduce the additional energy consumption. Nevertheless, the strategy is focused on the air conditioning of large areas and not in the individual space's needs; it means that the efficiency of the strategy could be improved.

In accordance with Kolaveric and Parlac [10] "passive systems of dynamic activation that works with intrinsic properties of materials are perhaps the most promising direction for development adaptive building envelopes". For those reasons, the development of systems with *reduced in size elements* and independent controls is introduced as the stake to improve building energy performance, in front of the general weather and micro-climate variations.

The buildings adaptation has two dimensions, the first one, as the relationship between architecture and the users, and the second one, as the relationship between architecture and the environment. The last one, through the envelope, as the element, which limits the inside and the outside [11], has been focused on affording comfort and security inside buildings. It makes the envelope a crucial component of the building aesthetics and its internal environment.

How can be seen

As the *skin* in the human body, envelope in buildings has the responsibility to regulate internal physical conditions[12]. The envelope has become since the last century a lightweight and flexible component, instead to be robust and heavy, improving its performance [13]. These buildings and systems, are being developed following *the state of the art technology* and together with disciplines as materials science and engineering, achieving every time a more interactive and efficient interface [14], [15].

As was addressed, the improvement of the building as humanmade shelter managed by the architecture, cannot be done without the support of other disciplines. XXI century buildings, as I think, cannot be static anymore; they must be developed reactively or responsively with the user necessities and the microclimate variations, because they change continuously, the building interfaces need to be flexible and do the same. Therefore, architects as the responsible of the non-structural elements of the building play an essential role in the definition of those interfaces.

The objective of this study is to determine, at laboratory scale, the thermomechanical potential of a composite material based on a low-cost commodity shape memory semicrystalline polymer under thermal cycling, as a thermo-sensitive actuator with the potential to be used in passive adaptive building skins.

What is proposed

This work has three different scopes to reach the proposed objective as follow.

Theoretical. To define the state of the art of the building façade development as adaptation to the environment, from dynamic envelopes to responsive architectural skins. As well as, the study of shape memory polymers as stimulus-responsive materials focused on the state of the art of semicrystalline networks.

Experimental. Thermosensitive laminate functional composite synthesis based on shape memory semicrystalline polymer as reinforcement.

Study. Thermosensitive potential, programming processing parameters, actuation response

In this way, the path to define the scope was the following: an exploration of the adaptive building envelopes and the definition of state of the art focused on the materiality was done to define a work line with the potential to be broader. Once the line was recognized, a state of the art of the shape memory semicrystalline polymers, as stimulus-responsive material, was done and a work line to improve the application of the system as an actuator was identified as well as the work scope.

How is presented

This study is organized into five sections. Section one provides the panorama and the motivation for developing, as an architect, the evaluation of the thermomechanical potential of a composite material based on a stimulus-responsive material capable of being used in a building.

Section two addresses the systems and materials used in the building's envelope adaptation to the environment in concordance to the state of art technology of every decade. A brief overview of façade development in the last century is presented, and then the active, adaptive envelopes are introduced with a focus on their protocol and actuator classes. Finally, passive adaptive skin systems as the most promising research direction, are classified described and analyzed by every variable of control and the physical or chemical protocol followed to obtain a dynamic response.

Section three reviews the shape memory polymers SMP as stimulus-responsive material and compare them with shape memory alloys SMA as the most used shape memory material SMM. Then the one-way shape memory effect OW-SME and the thermally induced shape memory effect is assessed, to finally describe the 2W-SME focused on the semicrystalline polymers. This last apart is divided into the parameters which affect the phenomenon and the polymer networks which evidence this effect reported was presented.

Section four addresses the functional composite experimental study. The research problem is defined, the guiding question is presented, as well as, the objectives and the scope of the experimental study. Moreover, the materials and methods are presented focuses on the shape memory properties study, the surface properties study, and the laminate actuator composites.

Moreover, experimental studies of the thermomechanical behavior are presented, the results and discussion are focused on the synthesis of both reinforcement lamina and laminate composite, as well as, the two-way shape memory behavior of the lamina and the composite thermocycling evaluation.

Finally, section five provides overall conclusions applicable to both theoretical and experimental developed studies, as well as, recommendations for future works and an approximation proposal for an architectural application of the composite material evaluated.

REFERENCES

- [1] Levermore GJ., "A review of the IPCC assessment report four, part 1: the IPCC process and greenhouse gas emission trends from buildings worldwide. *Build Serv Eng Res Technol* 2008;29:349e61.v."
- [2] International Energy Agency (IEA), "Energy Technologies Perspectives: Scenarios and Strategies to 2050, OECD/IEA," Paris, 2008.
- [3] C. Muñoz, C. Zaror, G. Saelzer, and A. Cuchí, "Estudio del flujo energético en el ciclo de vida de una vivienda y su implicancia en las emisiones de gases de efecto invernadero, durante la fase de construcción Caso Estudio: Vivienda Tipología Social. Región del Biobío, Chile," *Rev. Constr.*, vol. 11, no. 3, pp. 125–145, Dec. 2012.
- [4] Y. Song, J. Sun, J. Li, and D. Xie, "Towards Net Zero Energy Building: Collaboration-based Sustainable Design and Practice of the Beijing Waterfowl Pavilion," *Energy Procedia*, vol. 57, pp. 1773–1782, 2014.
- [5] I. Sartori, A. Napolitano, and K. Voss, "Net zero energy buildings: A consistent definition framework," *Energy Build.*, vol. 48, pp. 220–232, May 2012.
- [6] European Parliament, "Directive 2010/31/EU Energy performance of buildings. Off J Eur Union 2010. L 153/13-L 153-35.," 19-May-2010AD.
- [7] European Parliament, "Concerted action (CA) Energy performance of buildings directive (EPBD). www.epbd-ca.eu."
- [8] European Parliament, "Directive 2012/27/EU."
- [9] G. S. Brager and R. J. de Dear, "Thermal adaptation in the built environment: a literature review," *Energy Build.*, vol. 27, no. 1, pp. 83–96, Feb. 1998.
- [10] B. Kolarevic and V. Parlac, Eds., *Building dynamics: exploring architecture of change*. London; New York: Routledge, 2015.
- [11] J. Douglas, *Building adaptation*, 2nd ed. Amsterdam: Butterworth-Heinemann, Elsevier, 2006.
- [12] G. Koçlar, A. K. Yener, and N. T. Bayazit, "Building envelope design with the objective to ensure thermal, visual and acoustic comfort conditions," *Build. Environ.*, vol. 39, no. 3, pp. 281–287, Mar. 2004.
- [13] S. B. Sadineni, S. Madala, and R. F. Boehm, "Passive building energy savings: A review of building envelope components," *Renew. Sustain. Energy Rev.*, vol. 15, no. 8, pp. 3617–3631, Oct. 2011.
- [14] S. di Salvo, "Smart Materials in Architecture," *Int. J. Eng. Res. Afr.*, vol. 23, pp. 72–79, Apr. 2016.
- [15] R. M. Fortmeyer and C. D. Linn, *Kinetic architecture: designs for active envelopes*. Mulgrave, Victoria: Images Publishing Group, 2014.

2.

A D A P T I V E

B U I L D I N G

E N V E L O P E S

2.1 INTRODUCTION

2.2 ACTIVE ADAPTIVE ENVELOPES

2.3 PASSIVE ADAPTIVE SKINS

2.4 CONCLUSIONS AND FURTHER WORKS

2.5 REFERENCES



Fig. 1 The Curia. The meeting house of the Senate of Rome,

©Bertholf (2007)

Fig. 2 North rose window, inside view, Notre Dame Cathedral,

©Nyetta, Ken (2013)

Fig. 3 Seagram Building, Ludwig Mies Van der Rohe, Main entrance view,

©Fernandez, Gabriel (2015)

2.1 INTRODUCTION

Building envelope as the limit between inside and outside, defined by horizontal (roof) and vertical (façade) elements has been developed by the architecture taking concepts, features, and systems from other disciplines, following *the state of the art technology* of each decade. The relationship between buildings and environment has transcended, from a hole in a wall as can be seen in a structure built around 238 CE in Rome Fig. 1, to a one based on complex systems as can be seen in Fig. 6, these developments have been allowed structures to better adjusted to the necessities of each interior space and the fluctuating conditions of their surrounding environment.

The most remarkable changes on the architectural envelope are directed related to the materials and the structural system of the building. As we can see in Fig. 2 Notre Dame Cathedral (Paris 1345), the incorporation of flying buttress as exoskeleton structure [16] enabled the redistribution of the envelope mass and new large aperture sizes to the outside can be achieved.

Another significant change comes with the modern architecture movement [17], [18], established after the World War I with the incorporation of new materials as, steel, concrete, and glass together with the mass fabrication technologies added into the building industry. These new features allowed the façade for releasing from their structural function, since this moment, it stopped being heavy and solid to being lightweight and translucent [19][20]. For the first time, the limits between inside and outside were blurred, as can be seen in Fig. 3, Seagram Building [21] (New York, 1954). Since this moment the façade can be referred as an envelope, and their development can focus on their primary function, ensure internal building comfort conditions.

After the moment when architectural envelope released from their structural function and start to be translucent, the changes in their development are focused on kinetic systems with a dynamic response [22] with the aim to have real-time control over outdoor variables. These systems can be divided into two main categories, on the one hand active, responsive systems which need the electric current to keep their components running, and on the other hand passive, responsive systems which do not require electrical current because they can move or react in response to a specific stimuli[23].

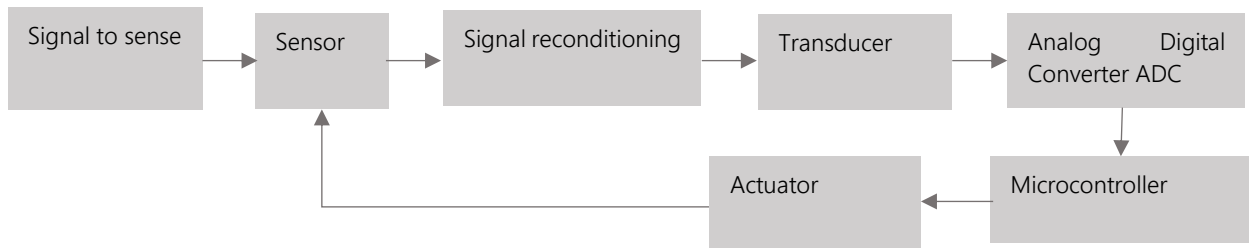
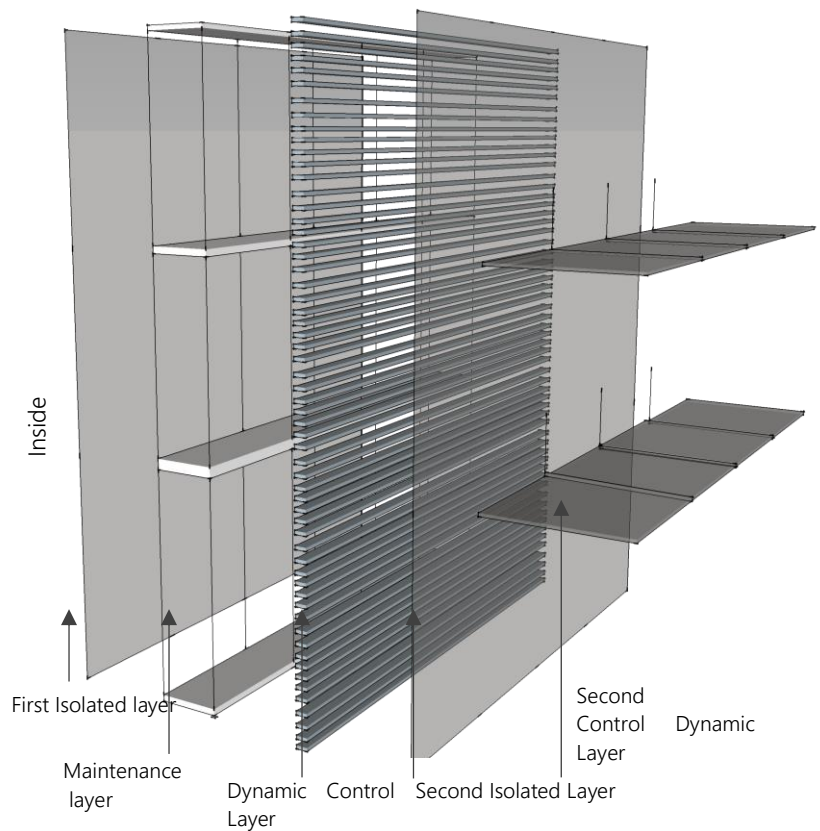


Fig. 4 Data Acquisition protocol of close loop.

Signal: Physic stimulus to being measure such as temperature, light, humidity, pressure, as well as presence. Sensor: a component in direct contact with the environment and the variable to be measured. Signal reconditioning: a process where the signal transmitted by the sensor is adjusted, amplified and filtered on demand. Transducer: a process where the magnitude measured by the sensor is taken and traduced to an operative magnitude for the system. ADC: a process where an analog signal was converted to a binary set. Microcontroller: a process wherein by a logic control the work method is sequenced and controlled. Actuator: control component, which makes a specific motion function, such as electric, mechanic, hydraulic and others.

Fig. 5 multi-layer Skins.

New dynamic envelope interfaces are developed as multilayer systems, according to the stimuli of control, the active layer can be located on the outside (direct contact with the environment), between the layers of the system (in the middle), or in the inside (direct contact with the interior). Most of them are made of matrixes of repetitive elements with independent control that make up a continuum surface, due to the similitude with the organ that covers the living beings, these systems are called as architectural skins.



2.2 ACTIVE ADAPTIVE ENVELOPES

Until recent times, the attention to improving building envelope was focused on increasing thermal insulation. Nevertheless, those systems are not enough to solve the efficiency challenges in the nowadays buildings [24], because of the remarkable use of glass and the increasing of additional energetic reliance on HVAC systems before the modern architecture movement.

A noticeable change about architectural skins appeared in the second half XX century by some postmodern architecture movements [18], they incorporate into the envelope, electromechanical systems equipped with sensors, processing units, and actuators that can be program and answer in real time to weather changes. Obtaining In this way, a dynamic interface [25], These active systems are based on Data Acquisition Systems (DAS) of a closed loop protocol [26], operation diagram can be seen in Fig. 4 there, the stimuli are sensed, and their processing is used as a control device.

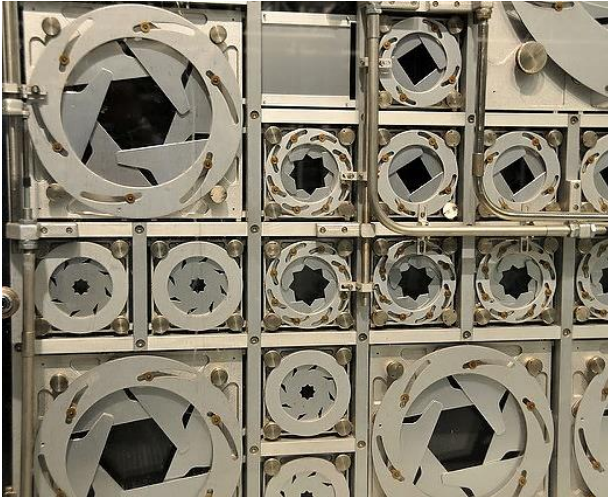
In the DAS protocol, the components that are in contact with the environment are sensors and actuators. The system sensing the stimuli from the environment and generate an electric pulse that can be processed [27]. Any physical variable can be measured, such as temperature, light, pressure, force, moisture, among others, even two or more variables can be controlled as can be seen in Fig. 5, by the same system through a multi-layer skin. Although until now, the systems incorporated on buildings have focused on controlling light and temperature. As can be seen in Table 1, different actuators and mechanisms are reported on the control of these variables as follow.

Table 1. Active Control Systems

Response	Physical Variable	Protocol	Actuator	Author
Reactive	Light / Heat-gain control	Data Acquisition Systems of closed loop	Pneumatic	[28]
			Electric	[29]–[32]
	Temperature / Air-flow control		Hydraulic	[33]

Protocol and actuators reported by active dynamic systems, all of them are base their operation under the Data Acquisition System of close loop.

6.



7.

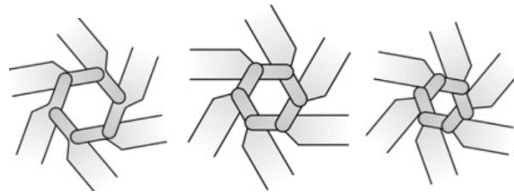


Fig. 6. Arab world institute (Paris) envelope panel.

The South elevation skin are one of the first with a dynamic layer, it is made up 30.000 stainless steel light-sensitive diaphragms, like mechanical irises, ©Melki, Serge (2009).

Fig. 7 Arab world institute (Paris) Diaphragms

Every panel has modules with different sizes and orientations that work with a parametric discretized aperture.

8



Fig. 8. Kiefer technic Showroom (Bad Gleichenberg)

the exterior finishing made of individual metal layer panels is moved by a mechanical actuator in a vertical path succession. The system can be actuated autonomously by weather changes as well as user's preferences, Giselbrecht, ©Ernst (2007)

9



Fig. 9. Al Bahar Towers (Abu Dhabi)

system controlled by a central processing unit linked in to climatological stations in the surrounding area. The active layer was located on the outside after a first glass skin, every unit made of ETFE fiber is actuated by a pneumatic system, AHR (2012)

10

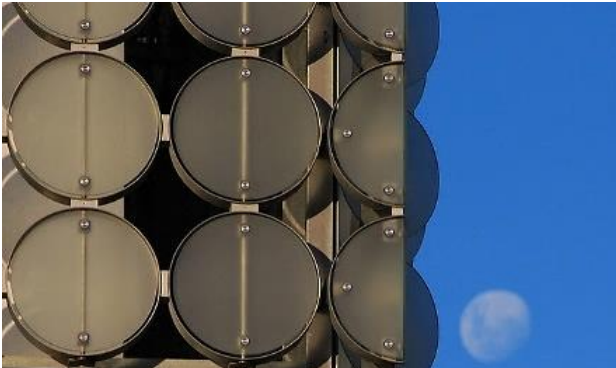


Fig. 10. RMIT Design Hub (Melbourne)

skin made of reflecting and photovoltaic coated glass modules, every unit is in a stainless-steel frame which allows movement to reflect sun-rays and catch them to generate electric current all day long, ©Deutscher, Rob (2013)

11



Fig. 11. Q1 ThyssenKrupp Quarter (Essen)

outside layer made of thin stainless-steel lamella as brise-soleil arranged in a vertical actuator as movement axis in discretized angles, ©Arnoldious (2011).

Light active control systems

The light is the most controlled variable in dynamic systems in buildings skins. Nouvel & Partners (1987), were pioneers with the development of an envelope with automatic control of the light indoors in the 90's decade. As can be seen in Fig. 6, the south elevation of the Arab World Institute is formed by a matrix of mechanical diaphragms between two glass sheets, which permits entry of 10 to 30% of daylight controlled by individual light sensors [34]; every Diaphragm has a discretized aperture shown in Fig. 7.

Different systems were focused on the control of light and sun heat-gain through a layer located outside of the building. Giselbrecht and AEDAS [30],[35] , developed systems where a mechanical actuator turns bi-dimensional sheets one by one into three-dimensional elements Shown in Fig. 8. These systems after a signal by the sensor, allow the light indoors, the visual connection with the exterior, the heat-gain control by shadowing, and in the case of AEDAS, sand storms protection as can be seen in Fig. 9, and improve the HVAC reducing heat gain in 50%. Otherwise *Architekten + Chaix & Morel et Associés* and Godsell [32] developed systems where a matrix of elements moves to reflect the sun-rays shown in Fig. 10, Fig 11, those system allows the heat-gain control and visual contact. Thanks to their location, in direct contact with the environment, these systems enable the control of more than one feature.

Fig. 12. One Ocean Theme Pavilion (Jeollanam-do) skin made of glass fiber reinforced polymer triggered by pneumatic actuators SOMA 2012



Fig. 13. Lamella One Ocean Theme Pavilion (Jeollanam-do) every lamella is compressed/stressed changing their shape to allow natural air circulation

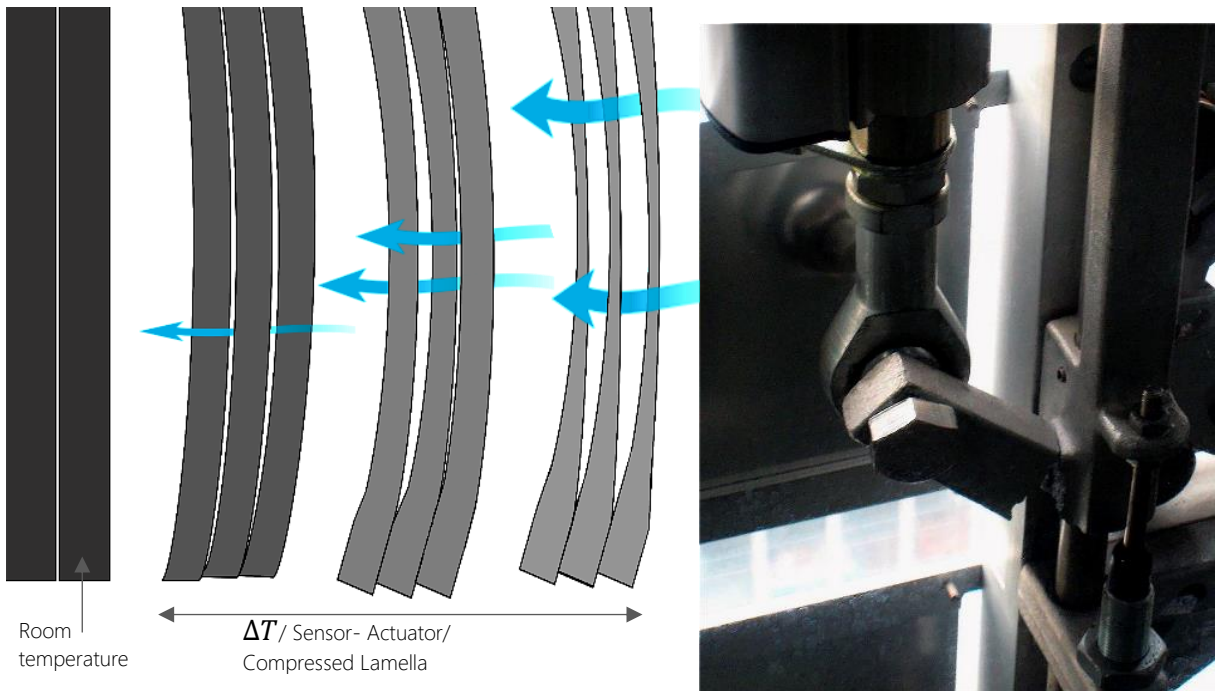


Fig. 14. Arab World Institute (Paris) actuator
An actuator of diaphragms broken. The elements of the envelope have high, costly and burdensome maintenance rate; for those reasons, this skin entered disuse of their dynamic components at an early stage[36].

Temperature active control systems

Temperature as a variable of control on buildings must be developed as a single-layer system because its performance is based on the exchange of losses and gains with the environment. On those systems, the direct contact between inside and outside is need it. As the case of SOMA [33], to enable the contact with the outside in the *Ocean Thematic Pavilion*, a succession of vertical strips was arranged to obtain a deformation and a change of lamella orientation. This movement was achieved by a pneumatic actuator compression shown in Fig. 12, allowing thermal losses from the inside as can be seen in Fig. 13.

The versatility of the DAS protocol of closed loop was highlighted, as it was seen, it enables the development of systems with different kind of actuators (mechanical, pneumatic, hydraulic). A broad-spectrum envelope materials and sizes from *brise soleil* unto laminar structures of some floors have been used. Moreover, Multi-layer systems has been used to achieve a real time response to solar radiation and outdoor temperature firstly [37], because of their influence on thermal and visual comfort.

Nevertheless, all of them requires, firstly an external electric current source to operate [38], and secondly, they are made of mechanical systems with multiple components with high maintenance rate. Both conditions take these active systems to a rapid state of obsolescence [36], for instance, in the Novel's building (1987) the active elements on the envelope were abandoned few years after the project opened, because of the costly maintenance. Moreover, some actuator components are broken as can be seen in Fig. 14. For those reasons, current research developments of building envelopes are improving their performance to be more efficient exploring flexible and jointless solutions with other disciplines, as follow.

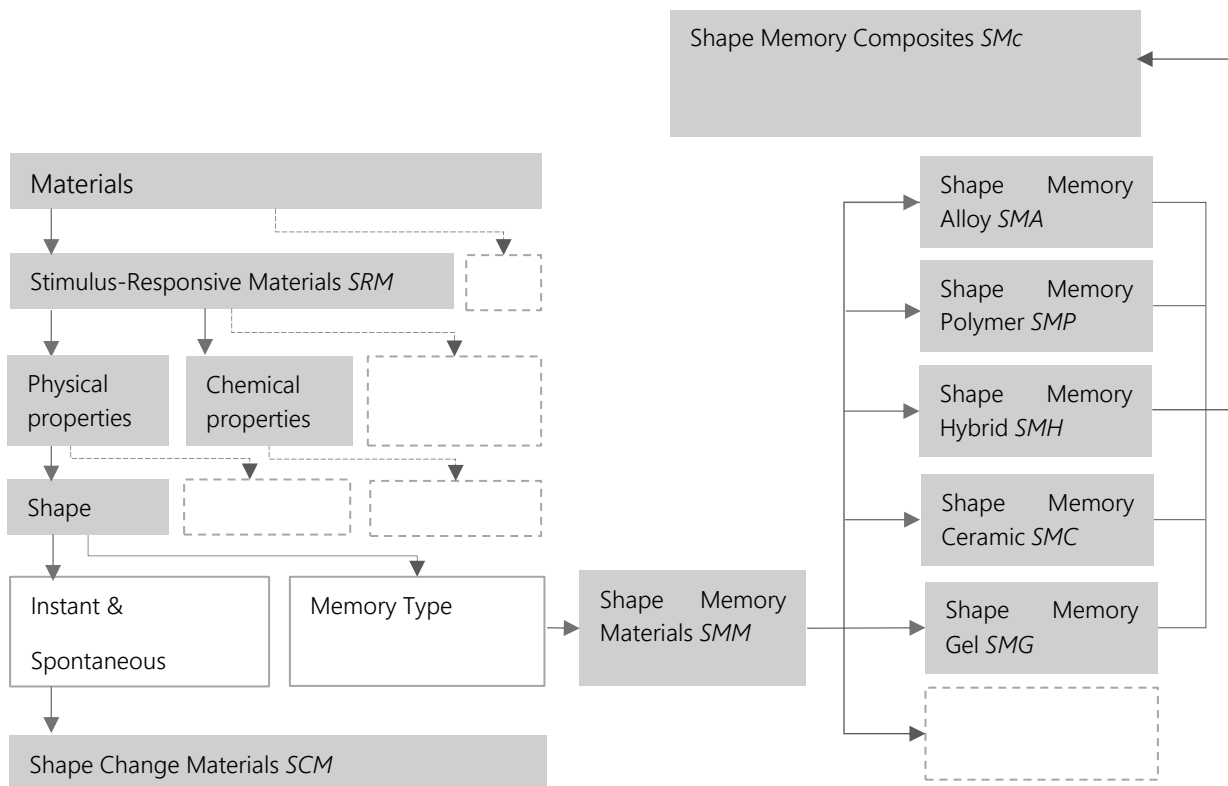


Fig. 15. Hierarchical location of stimuli-responsive materials on the materials world. Adapted from [39].

2.3 PASSIVE ADAPTIVE SKINS

Even when active systems changed the conceptualization of architectural envelopes in the second half XX century and continues being produced nowadays, their energy supply dependence and obsolescence triggered a new change on the perspective of the building skins development [40]. So that, now to translate properties from nano- to macro-scale, is the challenge to the architecture as a discipline to adapted in a passive way [41]. Therefore, by the hand of material science and engineering as an active member in this multidiscipline development [42]. This work has been focused on the research and application of smart materials, with a reversible change of shape capabilities by external activation in response to the increase in HAVC energy demand in buildings.

A hierarchical classification of this materials can be seen in Fig. 15, Other authors as Ritter [43] proposed a classification of smart materials by their use in architecture and a brief overview was done, but it was not focused on shape memory properties, and a review of the new reports must be done. These systems through the study and application of materials from microscopic to the macroscopic scales show kinetic properties and can move without motors, electricity or mechanical parts improving buildings performance[44].

In this way, in accordance with Kolaveric and Parlac [10] passive systems of dynamic activation that works with intrinsic properties of materials are perhaps the most promising direction for development adaptive building envelopes. Hence, from this moment, building envelope can be a skin like the organ in human beings, this kind of systems can take buildings to an autonomous homeostatic state without additional energetic sources and contribute to adapt it to their environment.

PASSIVE ADAPTIVE ACTIVATION PROTOCOLS

Building performance can be improved with passive systems in their energy consumption levels and greenhouse gas emissions as well [45], and new dynamic building interfaces to control outdoor conditions can be done [46]. In this way, prior the application in buildings, performance prediction must be done [47], nevertheless this field is in an early stage and new developments must be focused on the integration between design, material and operational features [48] because of the substantial differences between active and passive kinetic systems, as follow.

In active systems, sensors and actuators are part of an integrative system, but in the case of passive ones, they are the system by itself. From microscopic to macroscopic scale passive systems merge sensing and actuating functions [49], for this reason, they do not follow a general activation protocol; the protocol is relative to each material properties.

Nano- and smart-materials application into architecture and building as a new field have been classified by Daveiga [50] Loonen [51] Basarir [52] Fiorito[53]; In spite of those classifications, in architecture skins these systems are being used mainly to control physical variables, for this reason, the classification of the newest reports will be done by the outdoor weather variables to control, the chemical or physical protocol followed, and the materials proposed to achieve it. As can be seen in table 2, the passive systems reported are listed and then break down by each protocol of activation.

Table 2. Passive control systems reported

Response	Physical Variable	Protocol	Class / effect	Material	Author
Passive	Humidity/Rain water Control/ Air flow Control	Hygroscopy	Shape memory Hybrid	co-polyester composite with high cellulose content	[54]
				<i>Fagus sylvatica</i> veneer - Polyethylene Terephthalate	[55]
				<i>Lime</i> veneer - nylon - plastic	[56]
				<i>Birch</i> veneer - Epoxy resin- Fiberglass textile	[57]
				<i>Fagus sylvatica, Acer pseudoplatanus, Picea abies venner</i> - polyurethane HBS309 / HB-S709 Henkel®	[58]
				<i>Picea abies, Fagus sylvatica</i> venner - polyurethane HB-S709, Henkel	[59]
		Hydrophilicity	Shape memory Gel	Sodium Polyacrylate	[60]
				Sodium Polyacrylate 1mm powder, 7mm Crystals, 20 mm Spheres - Clay - Rubber	[61]
			Shape memory Hybrid	Sodium Polyacrylate - Gelatin - Glycerin - Elastic hydrophobic fabric	[62]
				Silicon - Latex - Expanding Hydromorph composite	[63]
	Temperature / Air flow control / Heat-gain control	Differential Thermal Expansion	Shape memory Hybrid	Thermobimetal	[45], [64]
		Reversible non-diffusional phase-change	Shape memory Alloy	NiTi	[65]–[76]
	Thermo-chromic effect				Al-doped VO ₂
			VO ₂ -ZnO	[78]	
			VO ₂ Single Crystals	[79]	
			W- and F-doped VO ₂	[80]	
			VO ₂ /SiO ₂ composite	[81]	
			VO ₂	[82]–[86]	
			W- VO ₂	[87]	
			Zr-doped VO ₂	[88]	
Eu/Tb/W- codoped VO ₂			[89]		
Hydroxypropyl cellulose			[90]		
Crosslinked polymer	[90]				
WO ₃ - O ₂ /Ar - H ₂ /Ar	[91]				
Thermochromic pigments	[92]				
Sunrays / Heat-gain control					

Response	Physical Variable	Protocol	Class / effect	Material	Author
Passive	Sunrays / Heat-gain control	Phase-Change	Latent heat thermal energy storage	Waxes, Paraffin, Salt hydrates	[93], [94]
				Shape-stabilized PCM	[95]
				Paraffin wax/expanded graphite	[95]
				Paraffin wax/polyurethane	[95]
				Tetradecanol	[95]
				Hexadecanol	[95]
				Caprylic acid	[95]
				Capric acid	[95]
				Butyl Stearate	[95]
				Capric-stearic acid/White Carbon Black	[96]
				Paraffin	[97], [98]
				Paraffin / polymeric matrix	[99]
				MgCl ₂ -6H ₂ O / CaCl ₂ -2H ₂ O	[100]
				1-Tetradecanol / bisphenol A /Wood	[86]
				Paraffin-wax capsule / Concrete matrix	[101]–[103]
	Organic paraffin	[104]			
	Paraffin MG29	[105]			
	Azobenzene dopant - Paraffin /Wax	[106]			
	Light / heat-gain control	Attraction-repulsion electrostatic forces	Shape memory Hybrid	Elastomer- Corrugated Silver Electrodes	[107]
				VHB Elastomer / Carbon Black / Silicone - Cooper electrodes	[108]–[112]
				EAP/PET/ETFE	[113]
		Ion Extraction /insertion	Electrochromic	Alumina	[73]
				W oxide /Ni oxide	[114]
				Sage® Glass	[115]
				WO ₃	[116]
		Elongation Induced by thermal transition	Shape memory polymer	Polyurethane	[117]
				Veritex® SMP	[118], [119]
Polyolefin shrink tape	[120]				

Physic Variables, protocol and materials used by passive responsive systems. Current uses and experimental proposals in architecture. It does not mean that other variables which affect building comfort cannot be controlled with this kind of passive responsive systems.

HUMIDITY PASSIVE CONTROL SYSTEMS

Hygroscopic-based protocol

Hygroscopy is a property of physical systems of absorbed or give humidity to the environment. In this way, systems that attract water as steam or liquid from their medium are hygroscopic. Wood as a material with that feature, through the cellulose as their constituent, attract water molecules from the environment when it is dry, and give water to the environment when it is wet, to be in the balance [121], hygroscopic properties of different classes of wood was evaluated by Glass [122].

This property is usually seen as a disadvantage as a building material, so that thermal treatment effect on the hygroscopic properties of some wood species was studied to inhibit it to react with moisture [123]. Nevertheless by This phenomenon, cellular structure and wood fiber orientation allow a dimensional change up to 10% in the grain perpendicular orientation [124]. Expansion and contraction in a specific direction can be obtained by anisotropic deformation controlled by cell wall architecture through cellulose swelling and shrinkage [125]. In this way, changes in the cellulose volume by humidity exchange, allows movement Fig. 16, for instance, the pine cone scales hydrated/dried behavior [126].

Recently by this protocol, different authors have reported the application of hygroscopic properties on buildings passive control [127]–[129] as remarkable examples, three types of individual laminate pieces systems with a specific fibers direction were reported, as a principal component to obtain a moisture responsive with autonomous movement. An architectural skin with close modules under low humidity conditions and open modules under high humidity conditions as can be seen in Fig 17 was reported by Correa [54], this system was applied on an experimental hydro-sensitive pavilion (*Orléans-la-Source*). Otherwise, with the same protocol, Chen [56] achieved the same goal with a performative architectural surface and a sensor of wet made of a matrix of tiles made of lime veneer, nylon and plastic with hydro-sensitive capabilities because of different porous densities.

Different class of veneer wood: *Prunus serotinal*, *Acer saccharum*, *Juglans nigra* and *Fagus sylvatica* was evaluated and analyzed to shaped up a bilayer dynamic system which finally was compose by Polyethylene Terephthalate and *Fagus sylvatica* veneer with a specific fiber orientation joined by an epoxy resin [55].

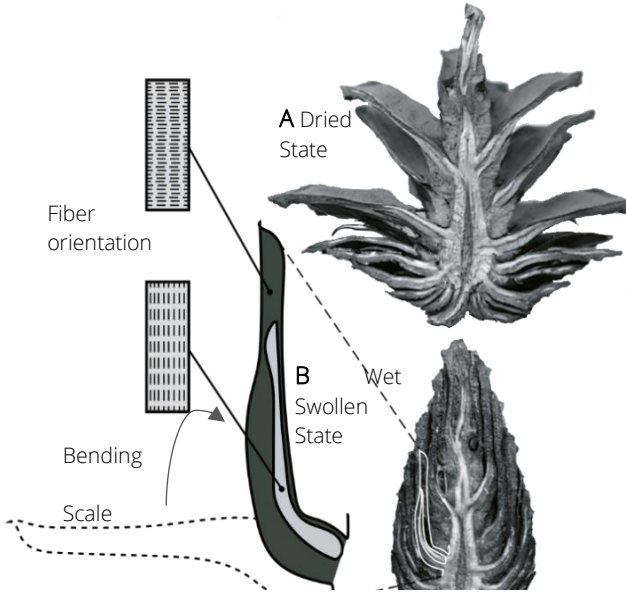


Fig. 16. pinecone scales. Axial cut view, Dried and swelled state, upper and lower tissue cellulose orientation can be seen on one scale. The first one is located parallel to scale axis, and the second one found perpendicular. Because both tissues are linked, the system shrink in the axial direction of each tissue allowing bending when are wet.

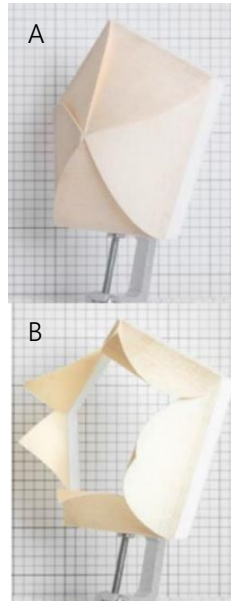


Fig. 17. 3D printed programmable hygroscopic material, through additive manufacturing of a co-polyester composite thermoplastic with high cellulose content from wood fibers, layers with different orientation and thickness was obtained as well as a multidirectional movement [54]

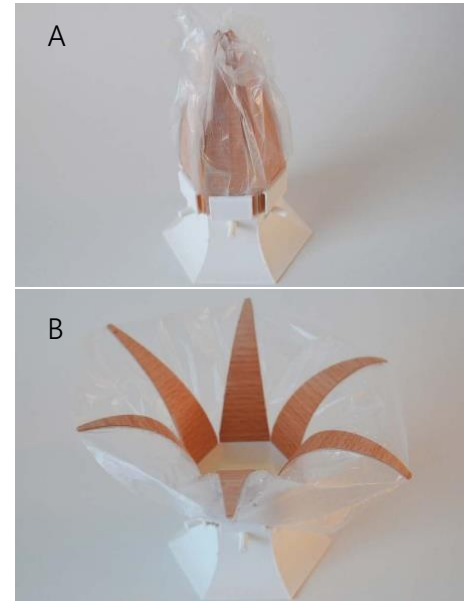
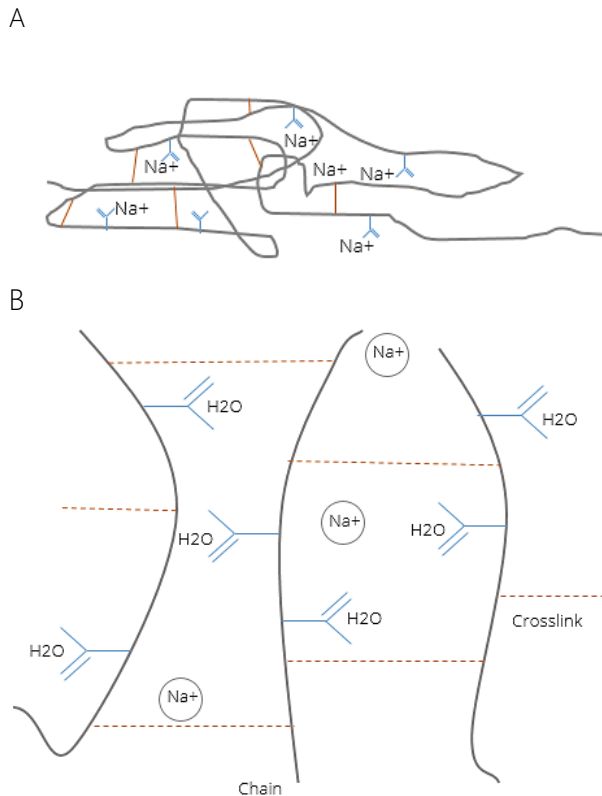


Fig. 18. Motion with Moisture. Responsive biomimetic bilayer module view with two positions A low humidity, B high humidity, A close final module, B completed open final module [55]

Fig. 19. Sodium Polyacrylate Swollen process. A. Polymer in coiled chains state (dry). B. Swollen polymer ionized with water molecules caught by carboxylic groups by hydrogen bonding into their crosslinked network (wet)



This bilayer composite allows the development of a biomimetic module that can be seen in Fig. 18 in a closed and open position, this system can be applied in an envelope system sensible to humidity in the meso- environment and the macro environment as well. Other studies focused on different bilayer veneer made of *Picea abies* Karst, *Fagus sylvatica*, and *Birch* veneer was reported by Vailati [59] Torres [57], and hygroscopic actuated wood elements with simple upscaling and shape complex were proposed by Wood [58].

Hydrophilic Swelling/shrinkage-based protocol

Synthetic Superabsorbent polymers as hydrogels were introduced in early 70's in replace of cellulosic fibers, which based their absorption properties in their hygroscopic behavior without significant swelling of their fibers [130]. They are a hydrophilic polymers that can swell in water , for instance, crosslinked sodium polyacrylate gel is the most used hydrogel in pharmaceutical and cosmetic industries because of their absorption properties, 10 -1000 % above their original weight [131], and their facile synthesis with sodium to obtain a neutral pH product.

The polyacrylic hydrogels are commonly obtained by aqueous polymerization of acrylic acid and crosslinked with vinyl groups; the result is an anionic polyelectrolyte with negative charged carboxylic groups in the main chain [131]. This group ionizes in water, and the negative charge make they repel each other compelling the polymer net to expand, then polar water molecules were attracted to the negative charged carboxylic groups, and they stay caught into the chains between crosslinks. Without those crosslinks, the polymer would collapse [130], and dissolution with the solvent, in this case, water will be obtained. So that, more crosslinks conduce a less water absorption.

This class of environmentally sensitive polymers [132], was incorporated in dynamic envelope systems with two different approaches based on their properties. The first one, is focused on the capacity of the material to retain large amounts of water, and the second one, is focused on in the change of volume by swollen. As the first approach, a multi-cavity system that catch rainwater, made of clay and filled with hydrogel spheres was proposed by Mitrofanova [61]. The system is focused on the passive cooling of an envelope module looking for the store of water for long-term and their slowly release through the day to improve thermal exchanges from the building to the outdoors.

Fig. 20. Hydroceramic. Scheme of the components of the cooling systems module, Sodium polyacrylate spheres held into clay layers for the slowly water/moisture releasing.

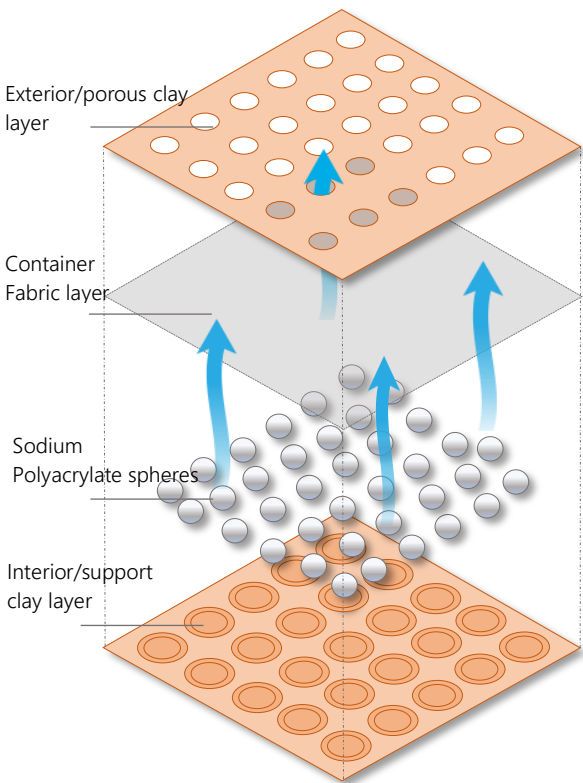


Fig. 21. Bimetal Strip. Two metals bonded together with different expansion coefficients.

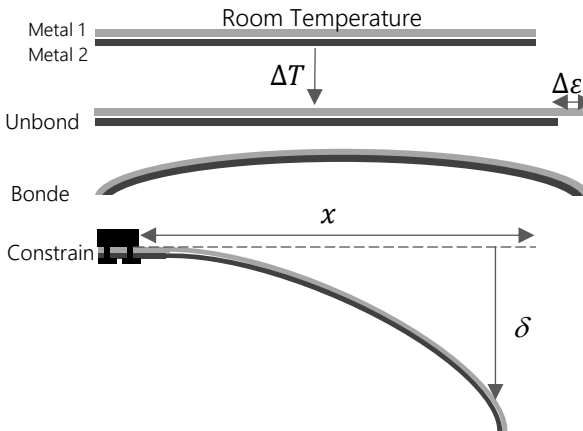
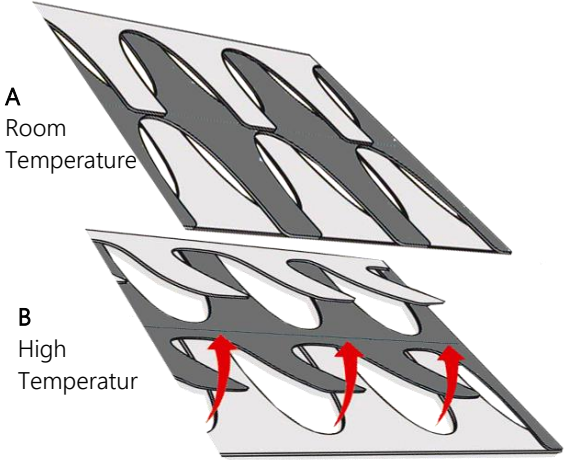


Fig. 22. Bloom Research Installation (Los Angeles), Panel behavior Position A. Room temperature, closed module, Position B. High temperature, opened module.



As the second approach, a force generating systems to be used in an envelope was developed by Kyriakou [60] and Ayala [62]; the devices are based on an acrylic piece attached to hydrophobic fabric pockets filled with sodium polyacrylate spheres with a mesh in contact with it. When the humidity goes through, the change of volume of the pockets is triggered and the systems can allow movement from one side to other or can open to allows air-flow.

A different system which uses the generating force of hydrogels was reported by Roth [63], a surface made of a matrix of silicone scales fixed by a composite based on polyacrylates was proposed. When the surface is in contact with water or moisture the composite net points swells, and the scales can open and close when it shrinks.

TEMPERATURE PASSIVE CONTROL SYSTEMS

Thermal expansion protocol

Hybrid shape memory materials are a class of stimulus-responsive material made of two different materials, which do not have shape memory independent capabilities [39]. Bi-metallic shape memory strips are made from two metallic pieces with different thermal expansion coefficient bonded by an elastic adhesive. The system operation is based on the asymmetric stress distribution between both surfaces, because of the expansion/contraction of each strip independently by thermal gradient differences. This phenomenon allows shape changes as bending, shown in Fig. 21, by direct or indirect heating.

This principle has been applied with the scope of obtaining architectural surfaces with active thermal features triggered by sun rays as well as weather thermal changes. An early report focused on the behavior of thermo-bimetals in architecture was done by Sung [45] , after that, a matrix made of crossing panel pieces of bimetallic strips were applied in a physical real scale pavilion [133].

The proposed pavilion has a surface were closed modules were achieved when the temperature goes down and porous ones when it rises, shown in Fig. 22. The proposed system enables sun-protect by shading and natural air circulation. Another bimetal application was reported by Garcia [64], with the same scope, commercial bimetal flat springs were incorporated into a matrix of intertwined bar shape elements, the system was developed to be deployed on windows and enable sun rays protection.

Fig. 23. *non-diffusional phase change Austenite – deformed martensite.*
 The system changes shape macroscopically, as the martensite grows or decreases, with a mechanical strain. The evolution of form can be created in a specific direction obtaining deformed martensite; for this reason, the material needs to be deformed previously as training.

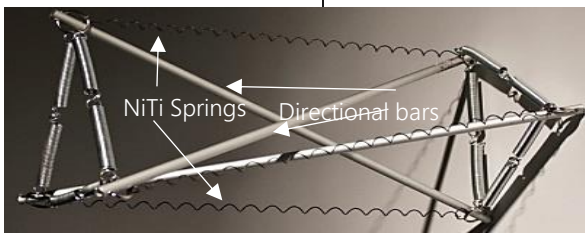
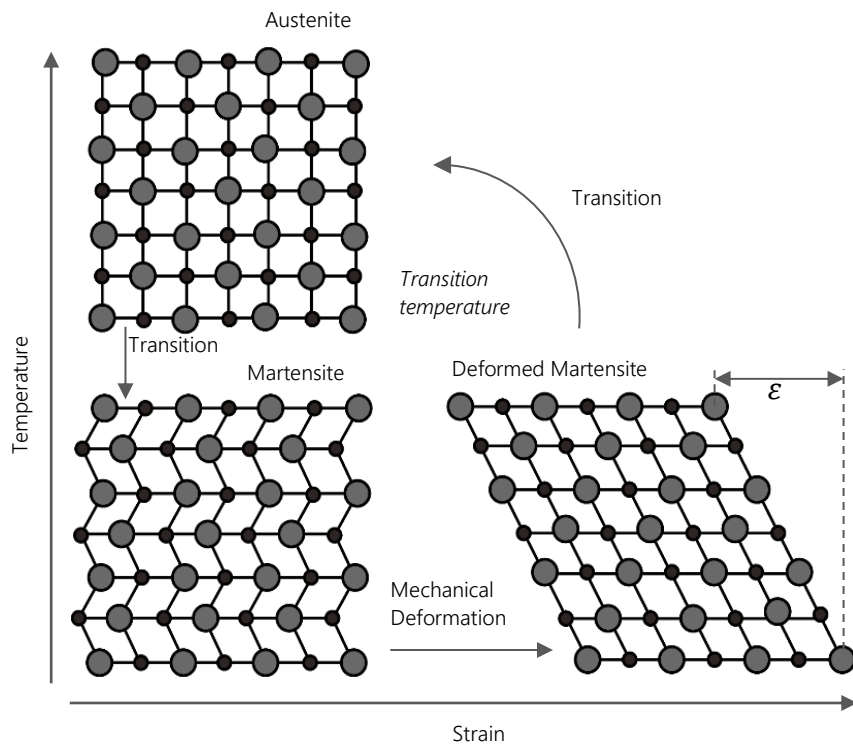


Fig. 24. *Adaptive [Skins]. The dynamic control unit.* operated by NiTi springs,
 ©Cohan, Joe (2013)

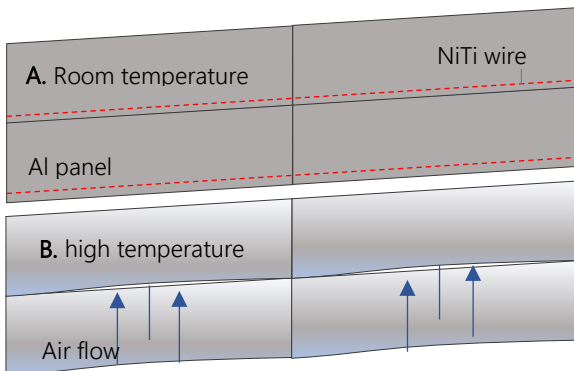


Fig. 25. *kinetic façade actuated by NiTi wires*
 A. close module wire stressed. B. Open module wire contraction.

Reversible phase transition protocol

SMA stress-induced martensite

This protocol bases their operation on the use of Shape Memory Alloys SMA, a class of SRM [39], as their active component, SMA has several features as shape memory effect (SME), super elasticity, and high damping capacity [134]. The first one SME has been used to achieve a bi-directional movement by a martensitic reversible transformation because of warming or cooling. This phenomenon is responsible for the SME. The second one, super elasticity has been applied in civil buildings as bridges, and robust behavior was demonstrated under dynamic loads [135]

The martensitic transformation takes place in a face-centered cubic unit cell structure, solid state austenite, by a cooperative atoms movement without any compositional change. A uniform distorted crystalline network is achieved because of atoms are moved under the inter-atomic distances, producing a new martensite phase as can be seen in Fig. 23. It does not mean that the movement occurs at the same time, but, the transformation spreads through the network [136].

The uses of SMA in architecture either as a dynamic system by itself or as a part of a bigger one, has shown important improvement in performance and energy consumption [137]. NiTi is the most reported SMA in responsive envelope systems developed following the non-diffusional phase transition protocol as an actuator because it is an SMA with one of the most reliable mechanic performance [39]. Focused on the control of heat and light on buildings, several dynamic surfaces were reported using NiTi matrix as an actuator. These systems base the operation in prestressed springs or wires which try to recover their original shape because of thermal fluctuations generating mechanical force in the process.

Prestressed springs as a bracket of a flexible laminate fabric as dynamic surfaces were reported by Verma [65], Sushant [66], Abdelmohsen [69], and Jun [74], [75]. In this system, when the temperature increases up 45°C, the austenite phase for this composition starts, the springs return to their original shape allowing changes in the orientation of the laminate of every module, shown in Fig. 24. With the same protocol but with the use of wires [68] and springs [70]–[73], [76] applied in more stiff and robust panels skins shown in Fig. 25, dynamic indirect illumination and heat-gain control by shadowing was obtained because of the mechanical force obtained by NiTi phase transformation. Finally, the relation between building and users were explored as well by using SMA actuators into integrative systems [67].

Fig. 26. Vanadium dioxide temperature transition. Low-temperature, monoclinic phase (M) zig-zag V-V chains, with two different interatomic distances Insulator/Semiconduct or to high-temperature Rutile (R) phase, linear V-V atom chains Metallic

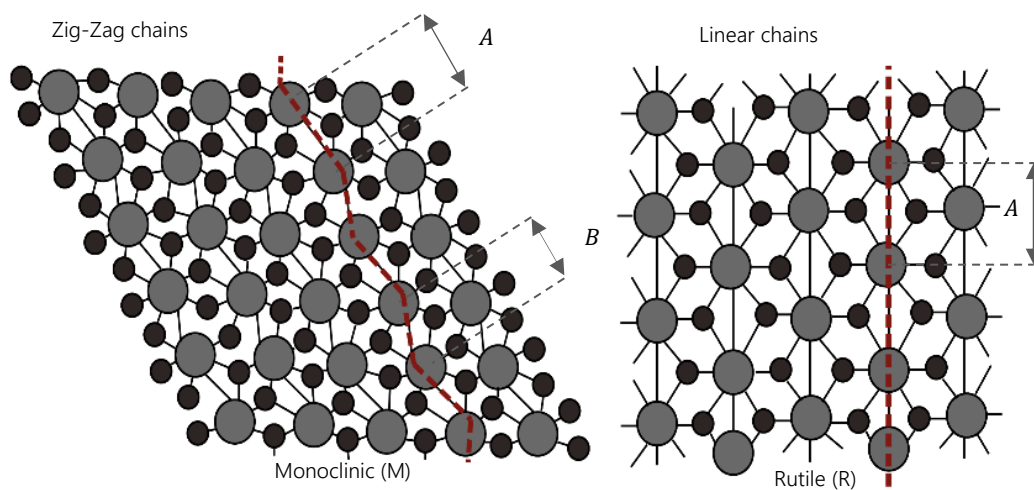
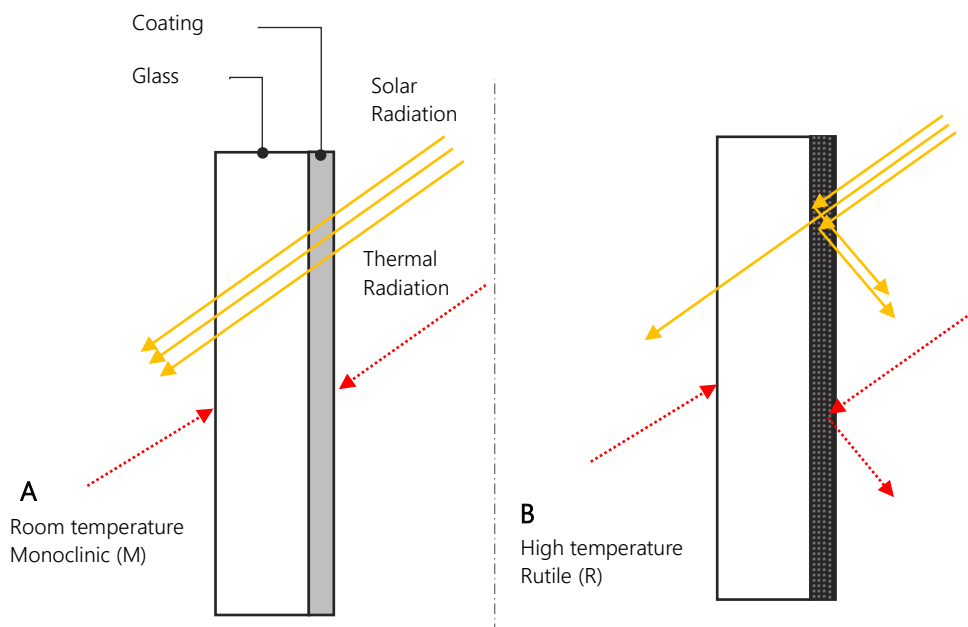


Fig. 27. Thermochromic glass coating. A transmittance mode, B reflectance mode.



Thermochromic effect, monoclinic to rutile phase

Inorganic materials have a change of color by temperature. Electronic properties of these materials at different temperatures cause the thermochromic effect [138]; some of them exhibit a more drastic change of color and variations on their optical properties as transmittance and reflectance. Vanadium dioxide VO_2 and trioxide VO_3 as part of this group, are the most used and study inorganic material with optical temperature-dependent properties [91], [139], [140] .

Vanadium dioxide has a start critical temperature at 68°C for the phase change from semiconductor low-temperature monoclinic phase to metallic high-temperature rutile phase shown in Fig 26. Differences in optical properties are achieved because of changes in V-V bonds angles and interatomic distances [141]. In applications where a thermochromic effect is needed it, as smart windows, this critic temperature is too high in contrast with room temperature, decisive to ensure building thermal comfort. In fact, this is not the only disadvantage of this class of smart coatings, the low transmittance in the semiconducting state and low reflecting rate in the rutile phase as well limits their applications on these areas.

For those reasons to improve this kind of systems to be used on smart windows, several investigations were focused on the most critic features, transition temperature, light transmittance rate, as well as alternative synthesize methods. In general, the VO_2 pure polymorphous coating cannot achieve those goals, for that reason the general performance has been improved by doping or addition as follow.

In the case of the alternative methods and additions, the incorporation of zinc oxide polycrystalline film as a buffer layer between the glass and VO_2 [78], and sol-gel alternative synthesis process with tungsten doping [80], [85], [87], has shown thermal transition reduction, higher transmittance rate and hydrophilicity properties of the coating. Likewise in the line of the synthesis, the introduction of impurities in the VO_2 single crystals growth [79] does not show effects on the energy behavior.

Critical transition-phase temperature has been studied through the doping of VO_2 with: Aluminum where a reduction of temperature and higher transmittance rate were found by Ji at al. [77], Zirconium ions where the temperature is reduced without modifies transmittance [88]. Rare-earth and tungsten (Tb/w, Eu/W) codoping has shown temperature reduction and transmittance enhanced in 60% in the visible range as well as the doping with SiO_2 with a 55.6% of transmittance[89] [81].

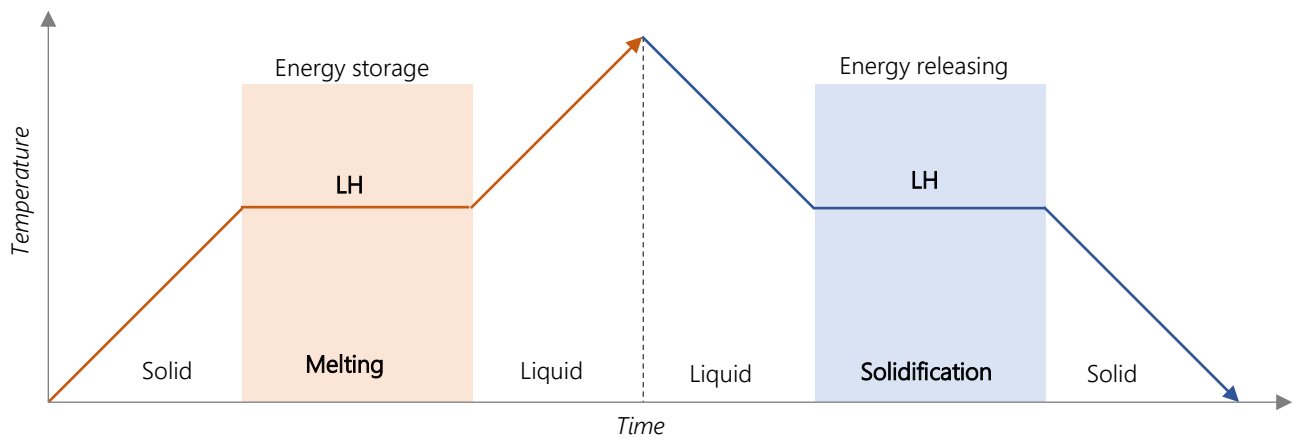


Fig. 28. Temperature against time PCM behavior.

The Latent Heat is stored and released in function of the temperature of the medium, based on © Pazrev, 2014.

Nevertheless, regardless these limitations, the incorporation of thermochromic coatings to building glazing can reduce the energy dependence for HVAC [142], through this systems, reduction on the thermal gain by sunrays can be obtained as shown in Fig. 27. For those reasons, their application in real buildings was studied trough dynamic simulation [82] [83] and full scale application [84], they concluded that near-infrared spectrum thermochromic sensible windows are needed instead visible light thermochromic ones, although 20% energy savings was achieved.

The critic temperature adjustments must look for the temperature of the glass surfaces and not room or outdoor temperature in the development of those devices, as well as, at least 50% transmittance is needed it in the semiconductor state to be energetically efficient were found. Otherwise, different projects not based on vanadium dioxide have been developed. Thermotropic smart windows based on hydroxypropyl cellulose with 22% of energy savings was reported by Allen [90], and Thermochromic pigments incorporated into architectural surfaces was proposed by Bhaktavatsala [92] to display real-time data through the building envelope as a communication way.

Phase change protocol, liquid-solid

Phase change materials (PCM) are substances with the ability to have a phase transition at a specific temperature range [143], During the phase transition a heat absorption, or emission calls latent heat (LH) exist. In the solid-liquid phase transition heat is absorbed and released , the case induced by weather is shown in Fig. 28, this LH can be stored, and this process has been classifying as the most efficient way to store thermal energy with the higher storage density and smaller temperature changes [144]. transition temperature and amount of LH, in this case, used into the fusion are different for each material [95].

Afterward the identification of their efficiency, this protocol has been used in buildings through the inclusion of PCMs in constructive elements with two different scopes. On the one hand, has been used to store the heat gained through the day and liberate it in the night and *vice versa*. On the other hand, has been used in the avoidance of direct thermal transfer from the outdoors to the indoors [145], because with the use of PCMs the heat received is used as LH to change of state, instead to be transmitted as can be seen in Fig. 28. This development is largely focused on the architectural envelope elements [96], [146].

The inclusion of PCMs in elements of construction has been assessed in envelopes as follow: window panels [105], Dynamic shading systems [94], opaque building envelope elements [97], [147], trombe solar walls [103] light weight floors [99] concrete blocks [100] and cellulose insulation [98]. As well as different elements based on: wood composite materials [86] multifunctional concretes [101] doped concretes [102], and mortar based construction materials [104].

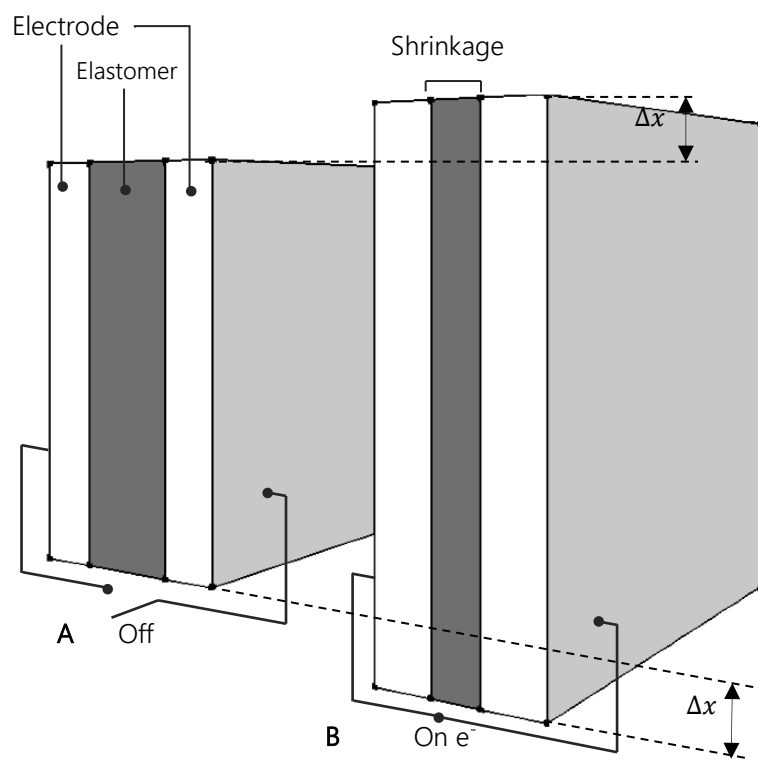


Fig. 29. Schematic dielectric electroactive mechanism of actuation.

A position. The elastomer has a permanent shape. B position. The elastomer is compressed by electrostatic forces, changing their shape in X and Y direction. The performance of this kind of system can be improved by pre-strain training.

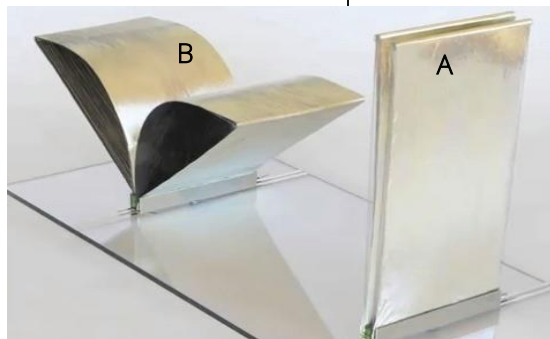


Fig. 30. Homeostatic Façade Prototype (New York) basic skin unit.

Dielectric elastomer coated with silver electrodes. Open and close position view.[107]

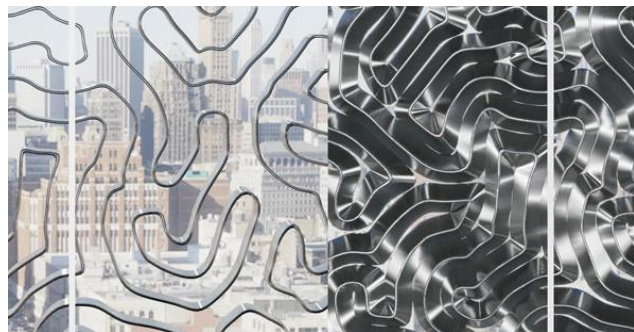


Fig. 31. Homeostatic Façade Prototype (New York). System operation, inside view.

Right. Permanent shape and path (open position); Left, temporal shape after stimuli (closed position) [107].

Likewise, simulation and evaluation methods are proposed to passive cooling envelopes [148], reduced scale evaluation of performance [149] and others focused on general optimization of buildings [150], and more precisely to residential and commercial establishments [151] and local climate case studies performance [93]. Finally, the actual *state of the art* allows the life cycle assessment of PCMs inclusions in buildings [152], and the Improvement in the synthesis, in accordance with the first scope, to obtain long term heat storage systems [106].

LIGHT PASSIVE CONTROL SYSTEMS

Attraction-repulsion electrostatic forces protocol

Following the Coulomb's law, with the use of Electro-Active Polymers (EAP), an elastomer which has electric conduction features [153] [154], a dielectric system has been obtained. The system is a multilayer hybrid defined by a dielectric elastomeric layer restricted both sides by electrodes. The dynamic behavior is triggered when an electric current, as stimulus, goes through the laminate rising the electrostatic forces generating a contraction of the elastomer. As a result, a dimensional change, for instance from a thick plate to a flat and thin, is obtained as shown in Fig. 29, allowing the development of components that can be deformed in a predicted direction [155].

In this way, this protocol is presented as a route to enhanced reactive buildings with the outdoors and users as well [110], [156]. With the aim of control sunlight inside a building, a network made of an elastomer coated with silver electrodes limited by glass layers was developed by Decker [107], as shown in Fig. 30. A bi-directional movement was produced, in the first position, when sunlight is into the building; the elastomers are compressed blocking and reflecting the light, and in the second one, the elastomer recovers their original shape, allowing the direct contact from the inside to the outside as can be seen in Fig. 31.

Different homeostatic skin projects with the use of electro-responsive elements was developed. A lightweight and semi-translucent actuator film defined by a high elastic elastomeric film, coated with a conductive carbon black powder and insulated by a

Fig. 32. *Electrochromic multilayer system.*

The basis is a glass or plastic covered by a transparent conducting film, on multiple cathodic electroactive layers is affixed. A layer of ion conductor follows these, on its turn followed by an ion-storage film or one (or multiple) complimentary anodic electroactive layers and another transparent conducting film.

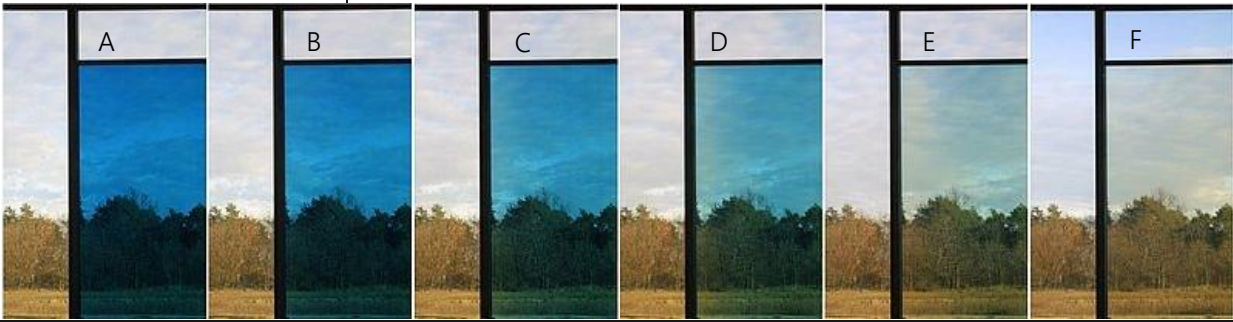
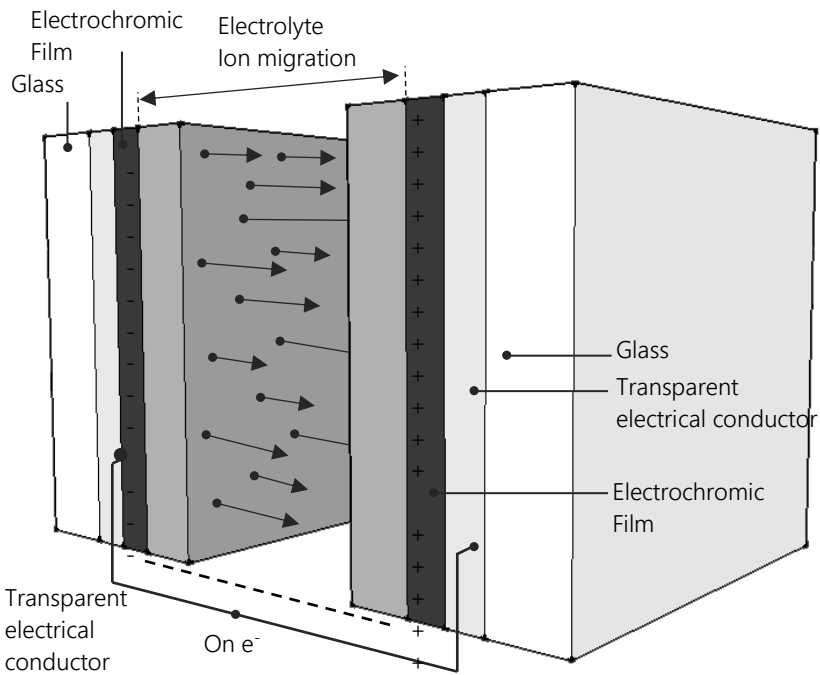


Fig. 33. *Tungsten Oxide Electrochromic coated window.*

the process of change of conductive and reflecting properties From A (blue) to F (transparent) $M_xWO_3 \leftrightarrow WO_3 + xM^+ + xe$ Gesimat (2009).

liquid silicone layer was reported by Joucka [108], and Kretzer [111], [112]. In another approximation, an EAP laminate was joined to water as the second stimulus by Franzke [109] to obtain a hydro-active responsive system.

Finally, as envelope proposals, translucent ETFE cushions actuated by a EAP tape a was reported by Biloría [113], and EAP plates into double glazing façade were simulated by Krietemeyer [157] showing improvement in the energy performance. Nevertheless, in the reviewed proposals, the high voltage needed to actuate the systems, limits the application and detriment the overall efficiency.

Electrochromic protocol

Changes in optical properties is a characteristic of inorganic materials; for instance, the electrochromic effect occurs in partially hydrated transition metal oxides [158]. The effect is a reversible electrochemical reaction where oxides are formed by an ion extraction and insertion. The process triggers changes in physical properties as, conductivity, IR absorption, and color, firstly. The coated systems are made of several thin layers shown in Fig. 32, mainly conform by oxides in an insulator state, and then in a second state as quasi-metallic, through a reversible change if an external potential is applied.

The electroactive layers change their optical properties between their oxidized and reduced form because of electron flow in the system. In the case of tungsten oxide WO_3 , used in the amorphous state in electrochromic coatings, as the most studied [158], the ions exchange used to be H^+ or Li^+ [159], allowing the change in IR absorption as can be seen in Fig 33. The system can be customized to obtain different time response as well as absorbing /reflecting rate.

Although, electrochromic thin layers was developed since 1973 [160], their most promising application, architectural smart windows [161], [162] are designed and commercialized just in the last decade. These systems applied trough flexible layers that can be inserted into a glass or polymer as a substrate with transparent conductors with high electronic conductivity [114], to allow performance of few volts.

The performance of this kind of systems was evaluated in comparison to other glazing technologies as well as by building uses. The evaluation of fritted glass windows and Electrochromic coated windows (EC) reported by Malekafzali [163] shown that EC has significant better performance because it provides a glare control in the areas of the façade which the sun is in contact with, meanwhile, the other zones remain in the visible mode allowing the entry of diffuse light avoiding the use of artificial light sources.

Fig. 34. *Polymer Thermal-switching transitions.*
 A. Crystallization/Melting B. Vitrification/glass. Under appropriate Δt the polymer chains gain mobility allowing a reversible change of shape.

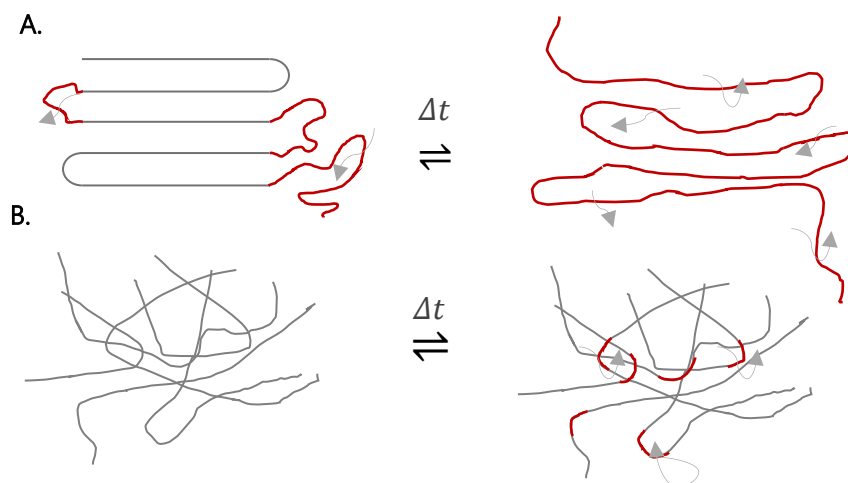


Fig. 35. *Translated geometries.*
 Standing structure actuated by SMP.
 A. open position B. closed position [119].

The use of EC was evaluated in office buildings located in hot and cold zones by Sbar [115], 45% of energy savings and from 35% to 50% of carbon emissions reduction was achieved with EC panels in comparison with no-treated glass windows. Moreover, a long-term performance study of tungsten dioxide coating for 20 months was reported by Lee [164], where a $26 \pm 15\%$ energy savings was obtained. Meanwhile, efficiency simulations conducted shows 16% of energy savings [116], [165], [166].

Despite the use of electric current, this kind of passive system, Attraction-repulsion electrostatic forces and electrochromic protocols, differs from active ones, because the electron flow is used plainly as the stimulus, which triggers the change of shape and properties of the system and has shown important energy savings. In the case of active systems based on DAS protocol, electric current is used as an additional continuous resource to ensure the operation of the electronic components.

Elongation induced by thermal transitions

Shape memory polymers (SMPs) are stable polymer networks with reversible switching transitions triggered by several stimuli as temperature, pH, electricity, magnetic field, light, and ions mainly [154]. There are multiple molecular structures which drive SME in polymers; it is not a property of the material by itself, it is a result of a mix of chemical and processing features, they have been used in several technological areas because of their wide-range stimuli responsiveness.

In the case of thermal-responsive SMPs, they can be based on a polymer with molecule entanglement, chemical crosslinking, crystallization and interpenetrated network. The reversible switching transitions are crystallization/melting and vitrification/glass shown in Fig. 34, in this process can be obtained a change of shape or mechanical force as well.

Based on this protocol, crystallization/melting and Vitrification/glass transitions, commercial temperature SMP have been used to realize self-standing structures actuated by dynamic actuators as flexible hinges [117], [119] as can be seen in Fig. 35, as well as, lightweight 2D structure with no structural elements with prestressed SMP embedded [118]. Likewise, an SMP tape was proposed as an actuator of a flexible metamaterial as indoors light control[120].

2.4 CONCLUSIONS AND FURTHER WORKS

Adaptive building envelopes / skins

As was seen, passive systems of dynamic control in buildings thus far developed has obtained favorable and promising results. However, on the one hand, passive systems which use responsive materials cannot be turned off or work just by one-user preferences, limitation to be recognized, likewise thermal, and comfort indexes must be evaluated on those new experimental projects. On the other hand, they have only been created or applied in buildings in the last decades, for this reason, most of them are found in an experimental phase, where is still necessary continued proving, verifying and optimizing to tuning and spread this kind of envelopes systems massively, because nowadays, among others, the systems high costs limits their applications, as follow.

The systems reviewed be in a different state of the art. On the one hand, PCMs as well as thermochromic and photochromic coated windows, were incorporated in building industry for more than a decade and nowadays are in a stage of evaluation, alternative methods of synthesis, and improving to enhanced building performance. On the other hand, hygroscopic systems, shape memory alloys, bi-metallic strips, and shape memory polymers, all of those are in an experimental stage were measure systems units, legislation or robust commercial solutions cannot be found. All of them presents interesting and different ways to look at the issue of passive response to micro-environmental fluctuations.

The stimulus-responsive materials evaluated are just a part of the categories presented, reversible phase change protocol and elongation induced by crystallization or vitrification the rest are just shape memory hybrids, the more used type of stimulus-responsive systems in architectural envelopes. The use of hybrids is based on several features; to the development of the systems a strong background is not needed it, is based on some basic concepts, and are made of easily accessible materials; for these reasons are the most extensive responsive systems applied. Nevertheless, other categories of this group of materials are still unknown by architecture. Therefore, the possibilities of new developments are broad to improve building efficiency and adaptation from ceramics to polymers.

In this way, Shape Memory/responsive Polymers SMP has been growing research and development because it has some competitive differential features. Wide-spectrum stimuli responsiveness, multiple reaction mechanisms, and programming versatility, among others, this group nowadays is the focus of functional materials in several industries as, medical, pharmaceutical, aerospace, among others. These features establish SMP as a group of materials to focus on near future responsive building skins research because they can shape up active components independently, compound materials or be part of hybrid ones. Studies and possibilities are not just for skins as well self-assembly building components (potential 4D printing), dynamic user interfaces or kinetic to electric building energy production.

2.5 REFERENCES

- [16] M. A. Nikolinakou, A. J. Tallon, and J. A. Ochsendor, "Structure and Form of Early Gothic Flying Buttresses," *Rev. Eur. Génie Civ.*, vol. 9, no. 9–10, pp. 1191–1217, 2005.
- [17] P. Overy, *Light, air & openness: modern architecture between the wars*. London: Thames & Hudson, 2007.
- [18] J. W. Bertens, *The idea of the postmodern: a history*, Reprinted. London: Routledge, 1996.
- [19] D. L. Morse and J. W. Evenson, "Welcome to the Glass Age," *Int. J. Appl. Glass Sci.*, vol. 7, no. 4, pp. 409–412, Dec. 2016.
- [20] M. Wigginton, *Glass in architecture*. London: Phaidon, 2004.
- [21] W. Blaser, *Mies van der Rohe*, 6th, expanded and rev. ed ed. Basel ; Boston: Birkhauser Verlag, 1997.
- [22] H. ACHTEN, "One and Many: An Agent Perspective on Interactive Architecture," presented at the 34th Annual Conference of the Association for Computer Aided Design in Architecture (ACADIA), Los Angeles, California, pp. 479–486.
- [23] M. Barozzi, J. Lienhard, A. Zanelli, and C. Monticelli, "The Sustainability of Adaptive Envelopes: Developments of Kinetic Architecture," *Procedia Eng.*, vol. 155, pp. 275–284, 2016.
- [24] M. Perino and V. Serra, "Switching from static to adaptable and dynamic building envelopes: A paradigm shift for the energy efficiency in buildings," *J. Facade Des. Eng.*, vol. 3, no. 2, pp. 143–163, Oct. 2015.
- [25] G. C. Henriques, "Responsive systems, relevance, state of the art and developments," presented at the 19th Conference of the Iberoamerican Society of Digital Graphics, Florianópolis, Brasil, 2015, vol. 1, pp. 200–206.
- [26] G. Hoover and W. Rempfer, "Closed loop control with data acquisition systems," in *Analog Circuit Design*, Elsevier, 2015, pp. 807–808.
- [27] J. Frazer, "An Evolutionary Architecture." 1995.
- [28] AEDAS, *Al Bahar Towers, The Abu Dhabi Investment Council*. 2012.
- [29] Jean Nouvel, Architecture-Studio, *Arab World Institute*. 1987.
- [30] E. Giselbrecht, *Kiefer Technic Showroom*. 2007.
- [31] JSWD Architekten and Chaix & Morel et Associés, *Q1 ThyssenKrupp Quarter*. 2010.
- [32] S. Godsell and H. Franklin, *RMIT Design Hub*. 2012.
- [33] SOMA, *One Ocean*. 2012.
- [34] Y. Su, "Arab Worl Institute EVDA 621 Formal Strategies in architecture, Case Study Analysis." .
- [35] S. Attia, "Evaluation of adaptive facades: The case study of Al Bahr Towers in the UAE," *QScience Connect*, vol. 2017, no. 2, p. 6, Oct. 2017.
- [36] M. Meagher, "Responsive Architecture and the Problem of Obsolescence," *Int. J. Archit. Res. ArchNet-IJAR*, vol. 8, no. 3, p. 95, Nov. 2014.
- [37] D. Aelenei, L. Aelenei, and C. P. Vieira, "Adaptive Façade: Concept, Applications, Research Questions," *Energy Procedia*, vol. 91, pp. 269–275, Jun. 2016.
- [38] B. L. H. Hasselaar, "Climate Adaptive Skins: towards the new energy-efficient façade," 2006, vol. I, pp. 351–360.
- [39] L. Sun *et al.*, "Stimulus-responsive shape memory materials: A review," *Mater. Des.*, vol. 33, pp. 577–640, Jan. 2012.
- [40] B. Ogwezi, R. Bonser, G. Cook, and J. Sakula, "Multifunctional, Adaptable Facades," presented at the TSBE EngD Conference, University of Reading, 2011.
- [41] R. Ng, *Performative Materials in Architecture and Design*. Bristol: Intellect Ltd, 2013.
- [42] L. A. Momoda, "The future of engineering materials: Multifunction for performance: Tailored structure," presented at the tenth annual symposium on Frontiers of Engineering, Washington D.C, pp. 47–52.
- [43] A. Ritter, *Smart materials in architecture, interior architecture and design*. Basel ; Boston: Birkhäuser, 2007.

- [44] A. Maragkoudaki, "No-Mech Kinetic Responsive Architecture: Kinetic Responsive Architecture with No Mechanical Parts," 2013, pp. 145–150.
- [45] D. Kim Sung, "Skin Deep: Breathing Life into the Layer between Man and Nature." The American Institute of Architects, 2008.
- [46] C. Doumpioti, "Responsive and Autonomous Material Interfaces," in *ACADIA 11: Integration through Computation*, Banff, Alberta, 2011, pp. 318–325.
- [47] R. C. G. M. Loonen, F. Favoino, J. L. M. Hensen, and M. Overend, "Review of current status, requirements and opportunities for building performance simulation of adaptive facades," *J. Build. Perform. Simul.*, vol. 10, no. 2, pp. 205–223, Mar. 2017.
- [48] A. Aksamija, *Integrating innovation in architecture: design, methods and technology for progressive practice and research*. West Sussex, United Kingdom: Wiley, 2016.
- [49] W.-G. Drossel, H. Kunze, A. Bucht, L. Weisheit, and K. Pagel, "Smart3 – Smart Materials for Smart Applications," *Procedia CIRP*, vol. 36, pp. 211–216, 2015.
- [50] J. Daveiga and P. Ferreira, "Smart and Nano Materials in Architecture," presented at the 2005 Annual Conference of the Association for Computer Aided Design In Architecture, Savannah, Georgia, 2005, pp. 58–67.
- [51] R.C.G.M. Loonen *et al.*, "Design for façade adaptability – Towards a unified and systematic character," presented at the 10th Conference on Advanced Building Skins, Bern, Switzerland, 2015, pp. 1284–1294.
- [52] Bahar BASARIR and M. Cem ALTUN, "A Classification Approach for Adaptive Façades," presented at the Interdisciplinary Perspectives for Future Building Envelopes, Istanbul, Turkey, 2017.
- [53] F. Fiorito *et al.*, "Shape morphing solar shadings: A review," *Renew. Sustain. Energy Rev.*, vol. 55, pp. 863–884, Mar. 2016.
- [54] D. Correa Zuluaga and A. Menges, "3D Printed Hygroscopic Programmable Material Systems," *MRS Proc.*, vol. 1800, 2015.
- [55] Nicola Augustin, "Motion with Moisture: Creating Passive Dynamic Envelope Systems Using the Hygroscopic Properties of Wood Veneer," Master Thesis, University of Waterloo, Ontario, Canada, 2018.
- [56] C. Chao, *Reacting architectural surface*. 2015.
- [57] B. Torres, "Programmable Matter Hygroscopic actuation of multidirectional lattice structures," Master Thesis, University of Stuttgart, Stuttgart, Germany, 2014.
- [58] D. Wood, C. Vailati, A. Menges, and M. Rüggeberg, "Hygroscopically actuated wood elements for weather responsive and self-forming building parts – Facilitating upscaling and complex shape changes," *Constr. Build. Mater.*, vol. 165, pp. 782–791, Mar. 2018.
- [59] C. Vailati, E. Bachtiar, P. Hass, I. Burgert, and M. Rüggeberg, "An autonomous shading system based on coupled wood bilayer elements," *Energy Build.*, vol. 158, pp. 1013–1022, Jan. 2018.
- [60] A. Y. Kyriakou, A. Potter, and W. Zhao, "SoftSpaces." Architectural Association AA, London, 2016.
- [61] E. Mitrofanova, A. Rathee, and P. Santayanon, "hydroceramic," Master Thesis, Institute for advanced architecture of Catalonia, Barcelona, 2014.
- [62] I. Ayala Castro, M. Manosong, and Y. C. Chang, "Water-driven Breathing skin," Master Thesis, Institute for advanced architecture of Catalonia, Barcelona, 2017.
- [63] L. Roth, "Hydromembrane," Master Thesis, Institute for advanced architecture of Catalonia, Barcelona, 2015.
- [64] A. Garcia Garcia, M. Srinivas, and M. A. Juarez, "Thermatrix bimetals," Master Thesis, Institute for advanced architecture of Catalonia, Barcelona, 2014.
- [65] S. Verma and P. Devadass, "adaptive[skins]: Responsive building skin systems based on tensegrity principles," in *Future Traditions*, Portugal, 2013, pp. 155–170.
- [66] V. Sushant and D. Pradeep, "Adaptive [skins]: Adaptation through smart systems," presented at the 7th International Conference Proceedings of the Arab Society for Computer Aided Architectural Design, Jeddah, Kingdom of Saudi Arabia, 2014, pp. 275–289.

- [67] N. Diniz, B. Cesar, S. D. Miguel, and T. Alasdair, "Morphosis: A responsive membrane," presented at the 12th International Conference on Computer Aided Architectural Design Futures, Sydney, Australia, 2007, pp. 489–498.
- [68] M. Formentini and S. Lenci, "An innovative building envelope (kinetic façade) with Shape Memory Alloys used as actuators and sensors," *Autom. Constr.*, vol. 85, pp. 220–231, Jan. 2018.
- [69] S. Abdelmohsen, P. Massoud, and A. Elshafei, "Using Tensegrity and Folding to Generate Soft Responsive Architectural Skins," in *Complexity & Simplicity*, Finland, 2016, vol. 01, pp. 529–536.
- [70] C. K. Khoo and F. Salim, "Responsive Materiality for Morphing Architectural Skins," presented at the 33rd Annual Conference of the Association for Computer Aided Design in Architecture (ACADIA), Cambridge, Ontario, 2013, pp. 243–252.
- [71] C. K. Khoo, J. Burry, and M. Burry, "Soft responsive kinetic system: An elastic transformable architectural skin for climatic and visual control," presented at the Annual Conference of the Association for Computer Aided Design in Architecture (ACADIA 11), Bangff, Canada, 2011, pp. 334–341.
- [72] C. K. Khoo and F. Salim, "A responsive morphing media skin," in *Beyond codes and pixels*, Hong Kong, 2012, pp. 517–526.
- [73] C. K. Khoo, F. Salim, and J. Burry, "Designing Architectural Morphing Skins with Elastic Modular Systems," *Int. J. Archit. Comput.*, vol. 9, no. 4, pp. 397–419, Dec. 2011.
- [74] J. W. Jun, M. Silverio, J. A. Llubia, A. Markopoulou, A. Chronis, and A. Dubor, "Remembrance: A Shape Changing Adaptive Structure," presented at the 7th International Conference, CAAD Futures 2017, Proceedings, Istanbul, Turkey, 2017, pp. 180–198.
- [75] J. W. Jun, J. Alcover, and M. Silverio, "Remembrance," Master Thesis, Institute for advanced architecture of Catalonia, Barcelona, 2015.
- [76] N. Gonzales and M. Shreyas, "Self - Adaptive membrane - A passive kinetic system," Master Thesis, Institute for advanced architecture of Catalonia, Barcelona, 2015.
- [77] C. Ji *et al.*, "Al-doped VO₂ films as smart window coatings: Reduced phase transition temperature and improved thermochromic performance," *Sol. Energy Mater. Sol. Cells*, vol. 176, pp. 174–180, Mar. 2018.
- [78] M. Zhu, H. Qi, B. Wang, H. Wang, T. Guan, and D. Zhang, "Thermochromism of vanadium dioxide films controlled by the thickness of ZnO buffer layer under low substrate temperature," *J. Alloys Compd.*, vol. 740, pp. 844–851, Apr. 2018.
- [79] J. B. MacChesney and H. J. Guggenheim, "Growth and electrical properties of vanadium dioxide single crystals containing selected impurity ions," *J. Phys. Chem. Solids*, vol. 30, no. 2, pp. 225–234, Feb. 1969.
- [80] W. Burkhardt, T. Christmann, B. Meyer, W. Niessner, D. Schalch, and A. Scharmann, "W- and F-doped VO₂ films studied by photoelectron spectrometry," *Thin Solid Films*, vol. 345, no. 2, pp. 229–235, May 1999.
- [81] Z. Cao, Y. Lu, X. Xiao, Y. Zhan, H. Cheng, and G. Xu, "Tunable simultaneously visible-light and near-infrared transmittance for VO₂/SiO₂ composite films to enhance thermochromic properties," *Mater. Lett.*, vol. 209, pp. 609–612, Dec. 2017.
- [82] S. Hoffmann, E. S. Lee, and C. Clavero, "Examination of the technical potential of near-infrared switching thermochromic windows for commercial building applications," *Sol. Energy Mater. Sol. Cells*, vol. 123, pp. 65–80, Apr. 2014.
- [83] V. Costanzo, G. Evola, and L. Marletta, "Thermal and visual performance of real and theoretical thermochromic glazing solutions for office buildings," *Sol. Energy Mater. Sol. Cells*, vol. 149, pp. 110–120, May 2016.
- [84] E. S. Lee, X. Pang, S. Hoffmann, H. Goudey, and A. Thanachareonkit, "An empirical study of a full-scale polymer thermochromic window and its implications on material science development objectives," *Sol. Energy Mater. Sol. Cells*, vol. 116, pp. 14–26, Sep. 2013.
- [85] M. M. Seyfour and R. Binions, "Sol-gel approaches to thermochromic vanadium dioxide coating for smart glazing application," *Sol. Energy Mater. Sol. Cells*, vol. 159, pp. 52–65, Jan. 2017.
- [86] H. Yang *et al.*, "Composite phase change materials with good reversible thermochromic ability in delignified wood substrate for thermal energy storage," *Appl. Energy*, vol. 212, pp. 455–464, Feb. 2018.

- [87] Z. Liang *et al.*, "Tungsten-doped vanadium dioxide thin films as smart windows with self-cleaning and energy-saving functions," *J. Alloys Compd.*, vol. 694, pp. 124–131, Feb. 2017.
- [88] W. Lu, G. Zhao, B. Song, J. Li, X. Zhang, and G. Han, "Preparation and thermochromic properties of sol-gel-derived Zr-doped VO₂ films," *Surf. Coat. Technol.*, vol. 320, pp. 311–314, Jun. 2017.
- [89] N. Wang, Q. S. Goh, P. L. Lee, S. Magdassi, and Y. Long, "One-step hydrothermal synthesis of rare earth/W-codoped VO₂ nanoparticles: Reduced phase transition temperature and improved thermochromic properties," *J. Alloys Compd.*, vol. 711, pp. 222–228, Jul. 2017.
- [90] K. Allen, K. Connelly, P. Rutherford, and Y. Wu, "Smart windows—Dynamic control of building energy performance," *Energy Build.*, vol. 139, pp. 535–546, Mar. 2017.
- [91] W. Feng, L. Zou, G. Gao, G. Wu, J. Shen, and W. Li, "Gasochromic smart window: optical and thermal properties, energy simulation and feasibility analysis," *Sol. Energy Mater. Sol. Cells*, vol. 144, pp. 316–323, Jan. 2016.
- [92] N. Bhaktavatsala, "Colourmorph," Master Thesis, Institute for advanced architecture of Catalonia, Barcelona, 2015.
- [93] K. S. Pascha, "The use of Phase-Change-Material as cooling-strategy for buildings in the Chilean climate," *Int. J. Low-Carbon Technol.*, vol. 3, no. 2, pp. 101–109, Apr. 2008.
- [94] L. Bianco *et al.*, "Thermal and optical characterisation of dynamic shading systems with PCMs through laboratory experimental measurements," *Energy Build.*, vol. 163, pp. 92–110, Mar. 2018.
- [95] L. Li, H. Yu, X. Wang, and S. Zheng, "Thermal analysis of melting and freezing processes of phase change materials (PCMs) based on dynamic DSC test," *Energy Build.*, vol. 130, pp. 388–396, Oct. 2016.
- [96] F. Liu, J. Zhu, J. Liu, B. Ma, W. Zhou, and R. Li, "Preparation and properties of capric-stearic acid/White Carbon Black composite for thermal storage in building envelope," *Energy Build.*, vol. 158, pp. 1781–1789, Jan. 2018.
- [97] A. Fateh, D. Borelli, F. Devia, and H. Weinläder, "Summer thermal performances of PCM-integrated insulation layers for light-weight building walls: effect of orientation and melting point temperature," *Therm. Sci. Eng. Prog.*, Jan. 2018.
- [98] K. O. Lee, M. A. Medina, X. Sun, and X. Jin, "Thermal performance of phase change materials (PCM)-enhanced cellulose insulation in passive solar residential building walls," *Sol. Energy*, vol. 163, pp. 113–121, Mar. 2018.
- [99] L. Royon, L. Karim, and A. Bontemps, "Optimization of PCM embedded in a floor panel developed for thermal management of the lightweight envelope of buildings," *Energy Build.*, vol. 82, pp. 385–390, Oct. 2014.
- [100] L. Erlbeck *et al.*, "Adjustment of thermal behavior by changing the shape of PCM inclusions in concrete blocks," *Energy Convers. Manag.*, vol. 158, pp. 256–265, Feb. 2018.
- [101] A. D'Alessandro, A. L. Pisello, C. Fabiani, F. Ubertini, L. F. Cabeza, and F. Cotana, "Multifunctional smart concretes with novel phase change materials: Mechanical and thermo-energy investigation," *Appl. Energy*, vol. 212, pp. 1448–1461, Feb. 2018.
- [102] A. Laura Pisello, C. Fabiani, and F. Cotana, "New experimental technique to investigate the thermal behavior of PCM/doped concrete for enhancing thermal/energy storage capability of building envelope," *Energy Procedia*, vol. 126, pp. 139–146, Sep. 2017.
- [103] E. Leang, P. Tittlein, L. Zalewski, and S. Lassue, "Numerical study of a composite Trombe solar wall integrating microencapsulated PCM," *Energy Procedia*, vol. 122, pp. 1009–1014, Sep. 2017.
- [104] V. V. Rao, R. Parameshwaran, and V. V. Ram, "PCM-mortar based construction materials for energy efficient buildings: A review on research trends," *Energy Build.*, vol. 158, pp. 95–122, Jan. 2018.
- [105] S. Li, G. Sun, K. Zou, and X. Zhang, "Experimental research on the dynamic thermal performance of a novel triple-pane building window filled with PCM," *Sustain. Cities Soc.*, vol. 27, pp. 15–22, Nov. 2016.
- [106] G. G. D. Han, H. Li, and J. C. Grossman, "Optically-controlled long-term storage and release of thermal energy in phase-change materials," *Nat. Commun.*, vol. 8, no. 1, Dec. 2017.
- [107] M. Decker, "Nanotechnology and Emergent Materials in Architecture," presented at the Tectonics of Teaching, Tectonics of Teaching, 2013, vol. 2013, pp. 1–7.

- [108] H. Joucka, "Sound to Polymer 1.0," Master Thesis, Institute for advanced architecture of Catalonia, Barcelona, 2016.
- [109] L. Franzke, D. Rossi, and K. Franinovic, "Fluid Morphologies: Hydroactive Polymers for Responsive Architecture," in *POSTHUMAN FRONTIERS: Data, Designers, and Cognitive Machines*, Ann Arbor, Michigan, 2016, pp. 478–487.
- [110] M. Decker, "Soft Human Computer Interfaces - Towards Soft Robotics in Architecture," presented at the 35th eCAADe Conference, Rome, Italy, 2017, vol. 02, pp. 739–744.
- [111] M. Kretzer, "towards a new softness The aesthetics of soft dielectric electroactive polymers and their application in an architectural context." Morgan Ip, Dino Rossi Chair for Computer Aided Architectural Design, 2010.
- [112] M. Kretzer and D. Rossi, "ShapeShift," *Leonardo*, vol. 45, no. 5, pp. 480–481, Oct. 2012.
- [113] N. Boloria and V. Sumini, "Performative Building Skin Systems: A Morphogenomic Approach towards Developing Real-Time Adaptive Building Skin Systems," *Int. J. Archit. Comput.*, vol. 7, no. 4, pp. 643–675, Dec. 2009.
- [114] A. Azens and C. Granqvist, "Electrochromic smart windows: energy efficiency and device aspects," *J. Solid State Electrochem.*, vol. 7, no. 2, pp. 64–68, Feb. 2003.
- [115] N. L. Sbar, L. Podbelski, H. M. Yang, and B. Pease, "Electrochromic dynamic windows for office buildings," *Int. J. Sustain. Built Environ.*, vol. 1, no. 1, pp. 125–139, Jun. 2012.
- [116] E. S. Lee and A. Tavil, "Energy and visual comfort performance of electrochromic windows with overhangs," *Build. Environ.*, vol. 42, no. 6, pp. 2439–2449, Jun. 2007.
- [117] S. Beites, "Morphological Behavior of Shape Memory Polymers Toward a Deployable, Adaptive Architecture," in *Adaptive Architecture*, Cambridge, Ontario, 2013, pp. 121–128.
- [118] Z. D. Arnellou, E. A. Papakonstantinou, and P. Sarantinoudi, "Fabricflation. Structuring textile techniques," Master Thesis, Institute for advanced architecture of Catalonia, Barcelona, 2015.
- [119] R. shambayati, ece Tankal, and B. Efilena, "Translated Geometries," Master Thesis, Institute for advanced architecture of Catalonia, Barcelona, 2014.
- [120] Y. Tang, G. Lin, S. Yang, Y. K. Yi, R. D. Kamien, and J. Yin, "Programmable Kiri-Kirigami Metamaterials," *Adv. Mater.*, p. 1604262, Dec. 2016.
- [121] C. Skaar, *Wood-water relations*. Place of publication not identified: Springer, 2012.
- [122] Samuel V. Glass and Samuel L. Zelinka, "Moisture Relations and Physical Properties of Wood," in *Wood handbook: wood as an engineering material*, FPL-GTR-190., Madison, WI: U.S. Department of Agriculture, Forest Service, Forest Products Laboratory, 2010.
- [123] V. Kamperidou, I. Barboutis, and V. Vasileiou, "Response of colour and hygroscopic properties of Scots pine wood to thermal treatment," *J. For. Res.*, vol. 24, no. 3, pp. 571–575, Sep. 2013.
- [124] J. M. Dinwoodie, *Timber, its nature and behaviour*, 2nd ed. London ; New York : [England]: E & FN Spon ; BRE, with the support of the Centre for Timber Technology and Construction at BRE, 2000.
- [125] I. Burgert and P. Fratzl, "Actuation systems in plants as prototypes for bioinspired devices," *Philos. Trans. R. Soc. Math. Phys. Eng. Sci.*, vol. 367, no. 1893, pp. 1541–1557, Apr. 2009.
- [126] A. Le Duigou and M. Castro, "Evaluation of force generation mechanisms in natural, passive hydraulic actuators," *Sci. Rep.*, vol. 6, no. 1, May 2016.
- [127] M. T. Marshall, "HYGROSCOPIC CLIMATIC MODULATED BOUNDARIES: A Strategy for Differentiated Performance Using a Natural Circulative and Energy Captive Building Envelope in Hot and Moisture Rich Laden Air Environments," *Perkins & Will research journal*, vol. 02.01, no. 03, pp. 41–54, 2010.
- [128] M. T. Marshall, "Bi-directional thermo-hygroscopic facades: Feasibility for liquid desiccant thermal walls to provide cooling in a small-office building," presented at the Architectural Research Centers Consortium FUTURE of Architectural Research, Illinois, Chicago, 2015, pp. 45–56.
- [129] B. Ogwezi, G. Jeronimidis, G. Cook, J. Sakula, and A. Kilaire, "Development of a passive and adaptable façade element for humidity control." Technologies for a Sustainable Built Environment (T SBE) Centre, University of Reading, 2013.

- [130] T. L. Staples and P. K. Chatterjee, "Synthetic Superabsorbents," in *Textile Science and Technology*, vol. 13, Elsevier, 2002, pp. 283–322.
- [131] E. M. Ahmed, "Hydrogel: Preparation, characterization, and applications: A review," *J. Adv. Res.*, vol. 6, no. 2, pp. 105–121, Mar. 2015.
- [132] Y. Qiu and K. Park, "Environment-sensitive hydrogels for drug delivery," *Adv. Drug Deliv. Rev.*, vol. 53, no. 3, pp. 321–339, Dec. 2001.
- [133] S. D. Kim, *Bloom. Materials & Applications Gallery*. 2012.
- [134] Y. Liu, Y. Li, K. . Ramesh, and J. Van Humbeeck, "High strain rate deformation of martensitic NiTi shape memory alloy," *Scr. Mater.*, vol. 41, no. 1, pp. 89–95, Jun. 1999.
- [135] C. Cismaşiu and F. P. Amarante dos Santos, "Numerical simulation of superelastic shape memory alloys subjected to dynamic loads," *Smart Mater. Struct.*, vol. 17, no. 2, p. 025036, Apr. 2008.
- [136] T. Waitz, V. Kazykhanov, and H. P. Karnthaler, "Martensitic phase transformations in nanocrystalline NiTi studied by TEM," *Acta Mater.*, vol. 52, no. 1, pp. 137–147, Jan. 2004.
- [137] M. Decker and Z. Andrzej, "Designing Resilient Buildings with Emergent Materials," presented at the 32nd eCAADe Conference, England, The U.K., 2014, vol. 2, pp. 179–184.
- [138] M. Kamalisarvestani, R. Saidur, S. Mekhilef, and F. S. Javadi, "Performance, materials and coating technologies of thermochromic thin films on smart windows," *Renew. Sustain. Energy Rev.*, vol. 26, pp. 353–364, Oct. 2013.
- [139] I. P. Parkin and T. D. Manning, "Intelligent Thermochromic Windows," *J. Chem. Educ.*, vol. 83, no. 3, p. 393, Mar. 2006.
- [140] S. Wang, M. Liu, L. Kong, Y. Long, X. Jiang, and A. Yu, "Recent progress in VO₂ smart coatings: Strategies to improve the thermochromic properties," *Prog. Mater. Sci.*, vol. 81, pp. 1–54, Aug. 2016.
- [141] R. Zhang *et al.*, "Metal-to-insulator transition and its effective manipulation studied from investigations in V_{1-x}Nb_xO₂ bulks," *Ceram. Int.*, vol. 44, no. 3, pp. 2809–2813, Feb. 2018.
- [142] M. Casini, "Active dynamic windows for buildings: A review," *Renew. Energy*, vol. 119, pp. 923–934, Apr. 2018.
- [143] M. Kuta and T. M. Wójcik, "Phase change materials in energy sector - applications and material requirements," *EPJ Web Conf.*, vol. 92, p. 02043, 2015.
- [144] M. Iten, S. Liu, and A. Shukla, "A review on the air-PCM-TES application for free cooling and heating in the buildings," *Renew. Sustain. Energy Rev.*, vol. 61, pp. 175–186, Aug. 2016.
- [145] A. Kasaeian, L. bahrami, F. Pourfayaz, E. Khodabandeh, and W.-M. Yan, "Experimental studies on the applications of PCMs and nano-PCMs in buildings: A critical review," *Energy Build.*, vol. 154, pp. 96–112, Nov. 2017.
- [146] H. Akeiber *et al.*, "A review on phase change material (PCM) for sustainable passive cooling in building envelopes," *Renew. Sustain. Energy Rev.*, vol. 60, pp. 1470–1497, Jul. 2016.
- [147] Y. Cascone, A. Capozzoli, and M. Perino, "Optimisation analysis of PCM-enhanced opaque building envelope components for the energy retrofitting of office buildings in Mediterranean climates," *Appl. Energy*, vol. 211, pp. 929–953, Feb. 2018.
- [148] A. Castell and M. M. Farid, "Experimental validation of a methodology to assess PCM effectiveness in cooling building envelopes passively," *Energy Build.*, vol. 81, pp. 59–71, Oct. 2014.
- [149] B. A. Young, G. Falzone, Z. Wei, G. Sant, and L. Pilon, "Reduced-scale experiments to evaluate performance of composite building envelopes containing phase change materials," *Constr. Build. Mater.*, vol. 162, pp. 584–595, Feb. 2018.
- [150] M. Saffari, A. de Gracia, C. Fernández, and L. F. Cabeza, "Simulation-based optimization of PCM melting temperature to improve the energy performance in buildings," *Appl. Energy*, vol. 202, pp. 420–434, Sep. 2017.
- [151] A. Pasupathy, R. Velraj, and R. V. Seeniraj, "Phase change material-based building architecture for thermal management in residential and commercial establishments," *Renew. Sustain. Energy Rev.*, vol. 12, no. 1, pp. 39–64, Jan. 2008.
- [152] A. Kylili and P. A. Fokaides, "Life Cycle Assessment (LCA) of Phase Change Materials (PCMs) for building applications: A review," *J. Build. Eng.*, vol. 6, pp. 133–143, Jun. 2016.

- [153] V. Bobnar, A. Levstik, C. Huang, and Q. M. Zhang, "Enhanced dielectric response in all-organic polyaniline–poly(vinylidene fluoride-trifluoroethylene-chlorotrifluoroethylene) composite," *J. Non-Cryst. Solids*, vol. 353, no. 2, pp. 205–209, Feb. 2007.
- [154] H. Meng and G. Li, "Reversible switching transitions of stimuli-responsive shape changing polymers," *J. Mater. Chem. A*, vol. 1, no. 27, p. 7838, 2013.
- [155] P. Kolodziej and R. Josef, "Responsive Building Envelope as a Material System of Autonomous Agents," presented at the 19th Conference on Computer-Aided Architectural Design Research in Asia, Singapore, 2013, pp. 945–954.
- [156] B. Krietemeyer, "An Interactive Simulation Environment for Adaptive Architectural Systems," in *Architecture and Interaction*, N. S. Dalton, H. Schnädelbach, M. Wiberg, and T. Varoudis, Eds. Cham: Springer International Publishing, 2016, pp. 231–252.
- [157] E. A. Krietemeyer and D. Anna H., "Electropolymeric Technology for Dynamic Building Envelopes," presented at the Parametricism (SPC) ACADIA Regional 2011 Conferenc, Lincoln, Nebraska, 2011, pp. 75–83.
- [158] J. S. E. M. Svensson and C. G. Granqvist, "Electrochromic coatings for 'smart windows,'" *Sol. Energy Mater.*, vol. 12, no. 6, pp. 391–402, Dec. 1985.
- [159] A. Azens *et al.*, "Flexible foils with electrochromic coatings: science, technology and applications," *Mater. Sci. Eng. B*, vol. 119, no. 3, pp. 214–223, Jun. 2005.
- [160] S. K. Deb, "Optical and photoelectric properties and colour centres in thin films of tungsten oxide," *Philos. Mag.*, vol. 27, no. 4, pp. 801–822, Apr. 1973.
- [161] C. G. Granqvist, *Handbook of inorganic electrochromic materials*. Amsterdam; New York: Elsevier, 1995.
- [162] M. Pittaluga, "Electrochromic glazing and walls for reducing building cooling needs," in *Eco-Efficient Materials for Mitigating Building Cooling Needs*, Elsevier, 2015, pp. 473–497.
- [163] A. Malekafzali Ardakan, E. Sok, and J. Niemasz, "Electrochromic glass vs. fritted glass: an analysis of glare control performance," *Energy Procedia*, vol. 122, pp. 343–348, Sep. 2017.
- [164] E. S. Lee, D. L. DiBartolomeo, J. Klems, M. Yazdanian, and S. E. Selkowitz, "Monitored Energy Performance of Electrochromic Windows Controlled for Daylight and Visual Comfort," presented at the ASHRAE 2006 Summer Meeting, Quebec, Canada, 2006.
- [165] T. Aslihan and S. L. Eleanor, "The impact of overhang design on the performance of the electrochromic windows," presented at the International Solar Energy Society (ISES) Solar World Congress, Orlando, Florida, 2018, pp. 199–206.
- [166] N. DeForest, A. Shehabi, S. Selkowitz, and D. J. Milliron, "A comparative energy analysis of three electrochromic glazing technologies in commercial and residential buildings," *Appl. Energy*, vol. 192, pp. 95–109, Apr. 2017.

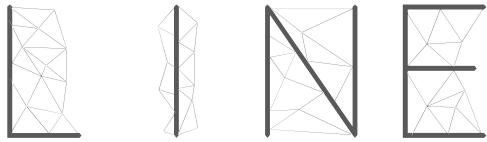
3.

SEMICRYSTAL

SHAPE

MEMORY

POLYMERS



**Shape memory effect [SME]*

3.1 INTRODUCTION

3.2 ONE-WAY *SME

3.3 THERMALLY INDUCED *SME

3.4 TWO-WAY *SME

3.5 CONCLUSIONS AND FURTHER WORKS

3.6 REFERENCES

Table 3. SMA and SMP Comparative primary features

Feature	SMA	SMP
Mechanical strength	High	Low
Shape recovery stress	High	Low
Recoverable strain	Low	High
Stiffness	High	Low
Global cost	High	Low
Density	High	Low
Temperature range	Narrow	Wide
Thermomechanical properties	Fixed	Fitted
Stimuli-responsiveness	Narrow	Wide
Chemical stability	Low	High
SME	Single	Multiple

Comparative features between SMA and SMP in relation with the SME, based on [167]–[171],[172], [173]

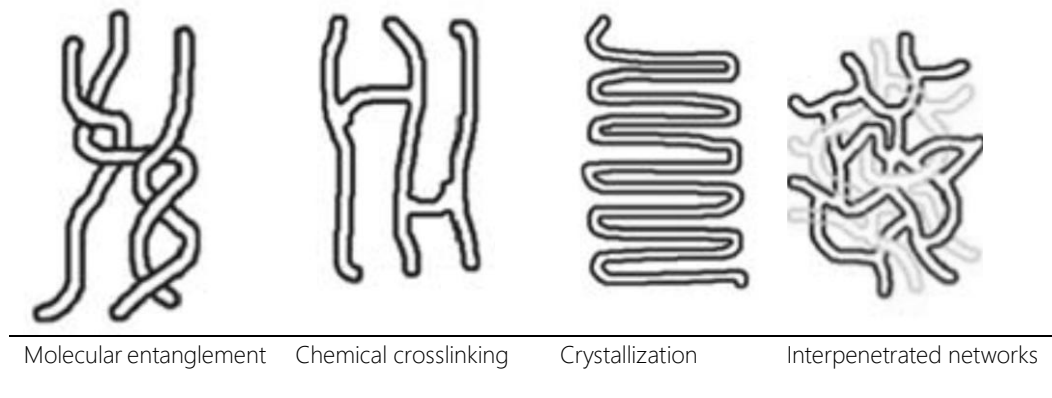


Fig. 36. Stable molecular structures, bases of the SME in polymers

3.1 INTRODUCTION

As was seen in the previous section, SMP's have differential advantages above other stimulus-responsive materials (SRM), because, among others, they are synthetic systems where properties can be tailored by variation of precursors, synthesis, and programming conditions. For those reasons, a review of the shape memory polymeric systems will be addressed, with the aim of identifying a polymeric system which could be assessed in passive dynamic applications with no additional energy supply, focuses on architectural envelopes systems.

SRM are materials able to respond to a specific stimulus by changing particular macroscopic properties, as physical, optical, chemical, among others [167], [174]. Two types of stimulus-responsive materials have a change in their physical properties as a change of shape, as can be seen in Fig. 15. On the one hand, shape change materials (SCM) where the change is instant and spontaneous, on the other hand, shape memory materials (SMM) with a memory type change. Materials with those capabilities can be found in metals, ceramics, polymers and their composites/hybrids [168]. The difference between both are based on the energy barrier from a temporary shape to permanent shape, in the case of SMM this barrier is high enough to need an additional driving force; in the case of SCM, a small energy barrier is found in the viscous-elastic recovery [175].

For a long time, shape memory alloys (SMA) because of properties as superelasticity, shape memory, and high damping capacity was the ideal material for shape memory applications. However, in the case of polymers, the research interest on this group of SRM has been rising in the last decades, because of some comparable properties and features listed in Table 3. The most remarkable characteristic from SMP over SMA is that SMP can reach ϵ_{\max} values up to 800% [176] compared with the 8% of SMA [177]. In industries as engineering [178] [179], and medical [180] [181] [182], several works were carried out.

Reverse elongation during heating and cooling is the same feature studied in SMA and SMP and is in the most cases always entropy-driven. Polymers in contrast to SMA has high versatility [183], but low mechanical strength, to overcoming that inherent deficiency mesoporous nanoparticles, nanotubes, nanocellulose and nanocomposite membranes have been incorporated into SMP matrixes to improve mechanical properties as well as widening stimuli responsiveness [184].

Both shape-changing polymers (SCP) and shape memory polymers (SMP) have as a prerequisite in their composition: functional groups, stimuli-sensitive domains or at least, two segregated domains [185].

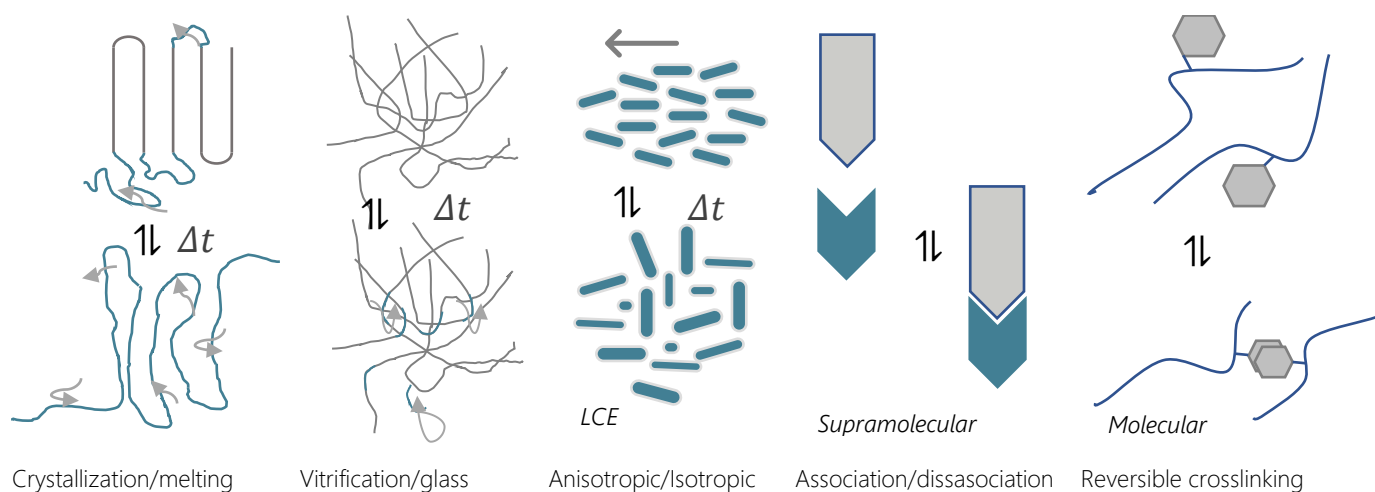


Fig. 37. Stimulus sensitive domains transitions

Table 4. Polymeric systems and reversible switch transitions in OW-SME reported

SME	Reversible Switch	Mechanism	Functional group/Molecule/Matrix	Stimuli
One-Way shape memory effect	Glass/Vitrification Melting/Crystallization	Physically crosslinked	polyurethanes, polynorbornene, 3-caprolactone and L-lactide block copolymers, polyethylene terephthalate-polyethylene oxide block copolymers	Temperature
		Chemically crosslinked	shape memory epoxy, shape memory polystyrene, crosslinking polycyclooctene, crosslinking acrylate, unsaturated polyesters, crosslinking polyurethane, crosslinking poly(3-caprolactone), polyethylene.	
		Hydrogel	poly (propylene oxide) and two hydrophilic blocks of poly (ethylene oxide)	Water, temperature
		Phase transition	Silicon + tin powder nanoparticles	Temperature
	Reversible molecule crosslinking	Photodimerization	cinnamamide, polycaprolactone diol, poly-(L-lactic acid) diol, N,N-bis(2-hydroxyethyl) cinnamamide	Light
		Diels-Alder Reaction	cyclopentadiene-pyridinyldithioformate, furan-maleimide, poly(ε-caprolactones)	Temperature
		Oxidation/Redox	Mercapto group	Chemicals
	Supramolecular association/dissociation	Hydrogen bonding	N,N-bis(2-hydroxyethyl) isonicotinamine. photo-crosslinkable benzophenone	Water Light
		Metal/ligand coordination	Metal salt + low molecular weight poly(butadiene) end-capped with 4-oxy-2,6-bis(N-methylbenzimidazolyl)pyridine	Temperature, light, chemicals

When those domains or functional groups are stimulated with a precise stimulus as light, moisture, electric or magnetic field, pH, and heat among others [168], [174], acts as a switch and the movement is triggered in a macroscopic scale. SCP can change their shape under the exposure of a specific stimulus, but when it is removed, it returns to their original shape [167]. In the case of SMP to achieve this effect, a temporary shape must be fixed, and when it is exposed to the stimulus the original shape can be recovered [169], [174], this work is focused on the second one.

The shape memory effect (SME) in polymers is not an intrinsic property, is the response of a chemical and molecular structure with specific processing parameters. The basis of the effect is focused on a stable molecular structure, as can be seen in Fig. 36. Net points as covalent bonds (crosslinking by polymerization or polyaddition) and physical interaction (hydrogen bonds, crystalline regions, ionic assembly and microdomains, chain entanglements) [176]. Nevertheless, as well as stable structure, elastic capabilities is needed it to allows molecular chain mobility when this is activated by a specific stimulus. As a second requisite, stimulus sensitive domains must be incorporated into the matrix, or a structure with at least two segregated domains must be addressed to reach a stimulus-sensitive polymeric system, as can be seen in Fig. 37.

Once these requirements are met the SME can be addressed, there are two types of SME in a polymer network. On the one hand, one-way shape memory effect (OW-SME) a system where just one cycle of change of shape can be reached. On the other hand, two-way shape memory effect (2W-SME), where the change of shape is reversible and more than one cycle between permanent and temporary shape can be achieved. In both cases, at least two domains are needed it, a hard and a soft domain [175], the first one maintain the original shape of the macrostructure, and the soft domain through a reversible change of shape drive the fixation and recovery [172].

3.2

ONE-WAY SHAPE MEMORY EFFECT

In the case of the OW-SME, The phenomenon takes place when a sample is deformed to "quasi-plastic" levels in a non-equilibrium state, in this state, the molecular chains have held fixing a temporary shape, nevertheless, once the sample is under appropriate stimulus the recovery of the permanent shape is triggered. The amount of energy that the network needs to recover the mobility of their chains is transferred by the stimulus, in this way they return to the original position by an entropic-driven phenomenon.

The phenomenon addressed only occurs once; each new cycle requires the fixation of the temporary shape. This process of fixation describes the principal limitation in applications where more than one cycle is needed it. However, several polymeric systems have been reported with water, temperature, light, and chemical as stimulus, as can be seen in Table 4.

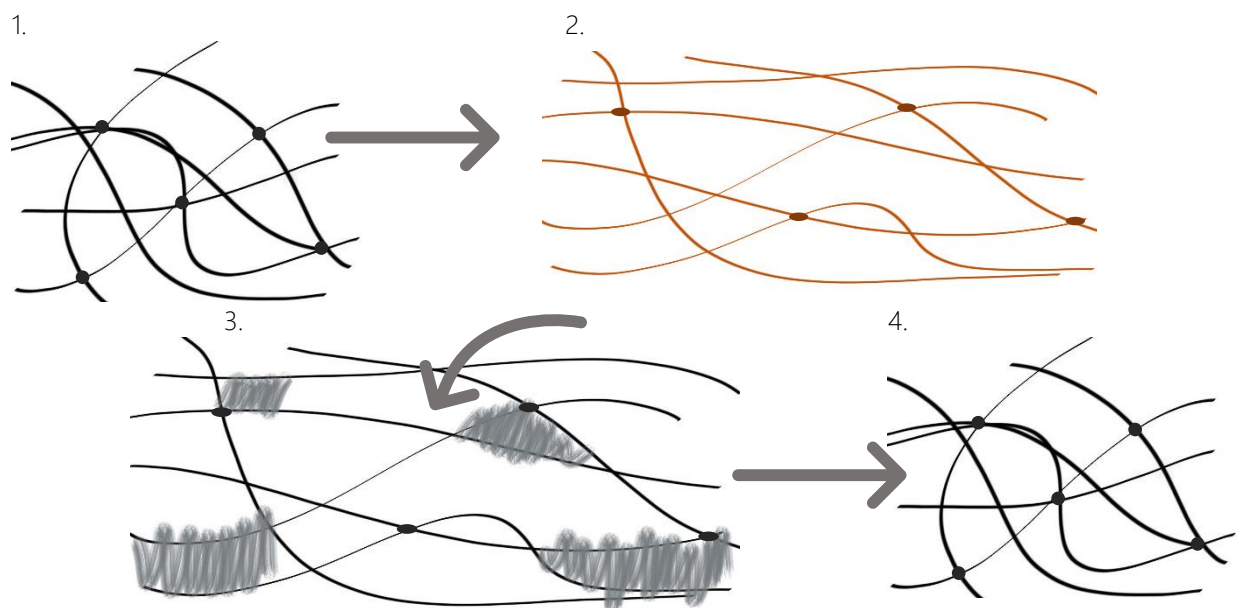


Fig. 38. Thermally induced SME, programming process

1. The permanent shape is obtained after the synthesis, 2. The sample is deformed under high-temperature conditions. 3. The temporary shape is fixed by crystallization or vitrification 4. The recovery of the permanent shape is reached once the sample is heated again.

Table 5. Thermally induced shape memory polymers reported

Physically cross-linked (Thermoplastic)	Block copolymers	Segmented polyurethanes	
		Polyethylene Terephthalate & Polyethylene Oxide copolymers	
		Polystyrene and Poly(1,4-butadiene) copolymers	
		Polybutadiene/PS copolymers	
		Triblock copolymers poly(tetrahydrofuran) and poly(2-methyl-2-oxazoline)	
	High-molecular-weight polymers	Polycaprolactone-polyamide copolymers	
		Polynorborene	
		Branched	Polyethylene-Nylon 6 graft copolymers
		Chemically cross-linked (Thermosetting)	Cross-linked polyethylene
Partly cross-linked/thermosetting SMPU			
cross-linked poly (E-caprolactone)			
Thermosetting epoxy resins			
liquid crystalline elastomers			
Polyolefines			
Thermosetting Polystyrenes			
Polysiloxanes			
Polyethylene- (Vinyl acetate) copolymers			

3.3 THERMALLY INDUCED SME

The case of heat, as stimulus, is the most studied SME in polymers (as temperature variations), because of the sensibility of the polymers network by temperature variations. In that case, the SME phenomenon is driven by a thermal phase-transition, even several activation mechanisms to obtain this kind of transition were developed for conditions where the surrounding temperature cannot be varied. Electrical, magnetic, optical, acoustic and chemical energy can all be converted into thermal energy and cause heating within materials [172].

The thermo-sensitive polymer systems which exhibit SME are based on a reversible glass/vitrification (amorphous) and a melting/crystallization transition (semicrystalline). In these polymer systems, Under Fig. 36, the stable structure is given by a chemically crosslinked glassy polymers, chemically crosslinked semicrystalline polymers, physically crosslinked glassy, and physically crosslinked semicrystalline polymers [186]. In addition to these structures, the two domains could be semicrystalline, and the amorphous segments or the architecture could have domains with different thermal transitions temperatures. The first one, hard domain, must have the highest thermal transition temperature, and the soft domain has the second higher transition. The last one is the responsible for driving the change of shape as switching domain [174].

As the SME is not an intrinsic property of the material, once the matrix was synthesized a processing step as "programming" [187] must be done, as can be seen in Fig. 38 and explained as follow:

<i>Programming</i>	The sample is exposed to temperatures above T_m or T_g , as appropriate, in this state the sample becomes soft and deformation can be quickly done, in this condition a temporary shape is fixed by mechanical deformation.
<i>Fixation</i>	After the deformation under high temperature, the temperature drops to a low one, once the sample is below T_c or T_g , as appropriate, the metastable structure with low entropy energy is formed and the temporary shape is fixed. The work performed on the sample is stored as latent strain energy when the recovery of the sample is forbidden by crystallization or vitrification [176], [184].
<i>Recovery / actuation</i>	Subsequent heating above the critical transition temperature T_g or T_m must be done to trigger the recovery. The stored entropy energy is released, the molecular chains gain high mobility and can come back to their highest entropy state (lowest energy) which corresponds with their permanent shape [176].

Using this kind of change of shape, thermal transitions as a trigger, several physically and chemically crosslinked polymer systems have been reported, as can be seen in Table 5. Nevertheless, the chemically based is more efficient because the change is reached in a shorter time, in the case of physical ones, it is associated to the glass transition which has more extensive temperature range to occur.

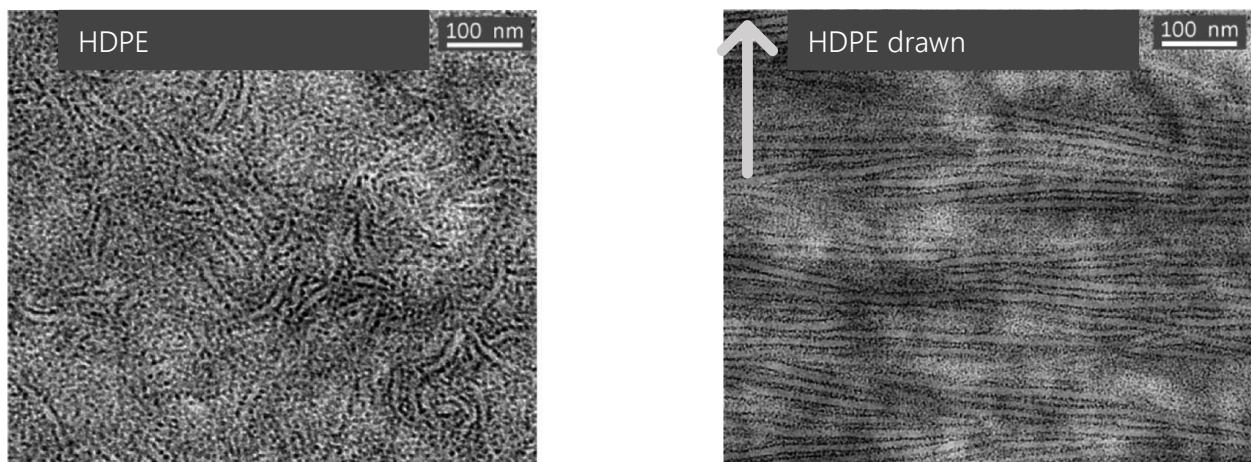


Fig. 39. Lamellae TEM Image.

Left undeformed cross-linked HDPE Right uniaxially stretched during nonisothermal crystallization under load (the arrow shows the load direction), Adapted from [188].

Table 6. Reversible switch transitions in 2W-SME reported in polymer systems.

SME	Reversible Switch	Mechanism	Functional group/Molecule/Matrix	Stimuli
	Nematic-Isotropic transition	Liquid Cristal Polymer	2-tert-Butyl-1,4-bis-4-(4-pentyloxy)benzoylhydroquinone	Temperature
	Stress-induced crystallization	Semicrystalline polymer under constant stress	polyurethane, polyhedra oligomeric silsesquioxane/poly(ϵ -caprolactone) networks, crosslinked poly(ϵ -caprolactone) (PCL)-based polyesterurethane, linear, three- and four-arm star poly(ϵ -caprolactone) functionalized with methacrylate, poly(ethylene-co-vinyl acetate)	Temperature
	Reversible Isomerization	trans-cis	Azobenzene	Light
	Reversible dimerization	4 + 4	9-anthracene carboxylic acid	Light
	Photo-thermal effect		Poly(4-vinyl pyridine) with 7-(carboxymethoxy)-4-methylcoumarin. polydimethylsiloxane, crosslinked polyarylamide contained polyethylene oxide and polyarylamide blocks	Light
	Addition/fragmentation chain transfer reaction	photocleavage	pentaerythritol tetra(3-mercaptopropionate) (PETMP), 2-methylenepropane-1,3-di(thioethyl vinyl ether) (MDTVE) and 25 wt% of 2-methyl-7-methylene-1,5-dithiacyclooctane (MDTO).	
Two-Way shape memory effect	dielectric effect /ions migration	Columb forces	filled copper phthalocyanine into polyaniline/polyurethane, electrostrictive cellulose paper, poly(ethylene oxide)-poly(ethylene glycol), chitosan, poly(vinylidene fluoride-trifluoroethylene) (P(VDF-TrFE)), poly(3,4-ethylenedioxythiophene) doped with poly(4-styrenesulfonate) (PEDOT/PSS),	e-

TWO-WAY SHAPE MEMORY EFFECT

In the 2W-SME, no additional deformation is needed it to achieve the temporary shape[168] , in every new cycle, the phenomenon is driven by each sensitive domain or under the exposure of a suitable stimulus. Each sensitive domain or functional group, shown in Fig. 37, has a different activation protocol and effect on the network which allows the macroscopic change of shape, in Table 6, the polymeric systems reported with evidence of 2W-SME are shown.

For a long, the isotropic-nematic transition in liquid crystal polymers (LCP) were the only systems capable of achieving a 2W-SME because of temperature variations as heat[177]. Nevertheless, the complex process of synthesis reduces the scope of applications of this kind of systems, taking a researchers group to evaluate a polymeric system which has a good OW-SME performance with evidence to obtain a reversible effect. In 2008 a crosslinked semicrystalline network was evaluated by Chung et al. [177], a reversible SME because of heat variations were reached when the sample was under constant stress load. The report of Chung et al. opens a new way to achieved 2W-SME in a cheaper and "Very simple polymer system" as semicrystalline ones.

Because of the report of a reversible change of shape phenomenon induced by temperature, in a "simple" and "facile" polymer system in comparison with the other complex ones, the analysis of the 2W effect was focused on semicrystalline systems, two-way semicrystalline shape memory polymers 2W-SSMP. Moreover, it has potential to be scaled into the architectural building envelope control systems by the low costs of materials and processing, among others.

Until now the process of fixation and recovery of the shape was entirely driven by a flexible-entropy phenomenon, where the sample was deformed, and it could return to their original shape by shrinkage. A complementary phenomenon which also drives the fixity of the shape, measured as Fixity Ratio R_f , and the recovery of the shape, measured as recovery ratio R_r , were found by Chung et al.

As was addressed before, the reported semicrystalline system was under constant stress load; this condition is responsible for the complementary phenomenon which allows the sample to fix the temporary shape between thermal cycles, this is the difference between these and the OW-SME. The fixity of the temporary shape is now partially driven by a phenomenon called *stretch-induced crystallization* (SIC), or *crystallization-induced elongation* (CIE) [189] as follow.

Without stress load conditions, the crystallization pattern of crystalline segments of the network is a lamellae arrangement in a spherulite structure with no preferred direction [190], as can be seen under a transmission electron microscope (TEM) in Fig. 39 *left*.

Table 7. Semicrystalline networks with evidence of 2W-SME reported

Matrix	Crosslinker agent	Author
Poly(cyclooctene) (PCO)	DCP	[191] [192] [193]
Poly(ethylene-co-vinyl acetate) (PEVA)	DCP	[194]
<i>Poly(ethylene-co-vinyl acetate) (PEVA)</i>	<i>DCP</i>	[195]*
<i>Poly(ethylene-co-vinyl acetate) (PEVA) + butylated hydroxytoluene (BHT) as inhibitor</i>	<i>DCP</i>	[196]*
Thermoplastic poly[ethyleneco-(ethyl acylate)-co-(maleic anhydride)](PEEAMA)	DCP	[181]
high-density polyethylene (HDPE) + 1-octene copolymers (EOC)	DHBP	[197]
Highdensity polyethylene (HDPE) + ethylene-1-octene copolymers (EOCs)	DHBP	[198]
Low density polyethylene (type LD100BW) + CB nanoparticles (30e ⁵⁰ nm) + dibutylphthalate number (DBP)	DHBP	[199]
<i>2-Ethyl-2-(hydroxymethyl)propane-1,3-diol 6-hydroxycaproates + ω – pentadecalactone + ε – caprolactone + dibutyl tindilaurate</i>	<i>dibutyl tin oxide</i>	[187]*
<i>Poly(tetramethylene glycol) (PTMG) + polycaprolactone diol (PCL-diol) + 4,4'-methylenebis(phenyl isocyanate) + 1,6-hexamethylene diisocyanate (HMDI) + 1,4-butanediol (BD)</i>	<i>dibutyltin dilaurate (DBTDL)</i>	[200]*
<i>Octylene Adipate (OA) Oligomers + 2-isocyanatoethyl methacrylate</i>	<i>TMPMP</i>	[201]*
<i>Poly(octylene adipate) (POA) + adipic acid + 1,8-octanediol</i>	<i>Scandium triflate</i>	[202]*
Methacrylate terminated PCLs with linear or star-branched (three-arm and four-arm)	DCP	[203]
a,u-hydroxyl-terminated poly(ε-caprolactone)	3-(triethoxysilyl) propyl isocyanate (ICPTS)	[204]
hydroxyl-terminated PCL	2-isocyanatoethyl methacrylate (2-IEM)	[189]
Ionomer poly(ethylene-co-methacrylic acid)	ionic clusters in the ionomer	[205]
Polydopamine-grafted-(poly(E-caprolactone)	4,4'-Methylenediphenyl diisocyanate	[178]
The poly(ester urethane) (PEU) + poly(1,4-butylene adipate) (PBA) + 1,4-butanediol	4,4' methylenediphenyl diisocyanate	[206]
poly(D,L-lactide) (PDLLA) + poly(tetramethylene oxide) glycol (PTMEG)+ 9-hydroxymethylanthracene (AN)	365 nm UV light	[207]
Poly (PEG/PCL/PDMS urethane) copolymer Poly(ethylene glycol) (PEG)+ poly(ε-caprolactone)-diol (PCL-diol)+ Dihydroxylterminated polydimethylsiloxane (PDMS-diol)	dibutyltin dilaurate (DBT)	[208]
oligo(ω-pentadecalactone) (OPDL) + three arm OPDL (AOPDL) + magnetite nanoparticles (MNP) + dibutyltin dilaurate (DBTDL)	1,6-hexane diisocyanate (HDI)	[209]
PPD star-shaped hydroxytelechelic oligomes + ω-pentadecalactone + dibutyl tinoxide (DBTO)	aliphatic diisocyanate	[189]
α, ω-hydroxyl-terminated PCL + 2-isocyanatoethylmethacrylate (2-IEM)	DCP	[210]

In contrast, under stress load the crystallization pattern is changed, distorted crystalline segments are obtained with a preferred lamellae orientation in the perpendicular direction of the load Fig. 39 *Right*; this phenomenon is the responsible for obtaining a macroscopic change of shape in the direction of the load by the crystallization under cooling. The process of the CIE (oriented crystallization) can be graphically viewed in Fig. 40, as the case of shape fixity where the segregated domains amorphous and semicrystalline segments are shown. This process of crystallization was studied in poly(ester-urethane) PEU networks by Bothe and Pretsch [206], and the nanostructural changes of the crystallization in poly(ethylene-(vinyl-acetate) copolymer cPEVA networks by Nöchel et al. [211]

In the case of the shape recovery, the phenomenon is known as *melting induced contraction* (MIC), a complementary effect to the flexible-entropy where the shrinkage of the sample is partially driven by the melting of the oriented crystalline segments. In this way, several works were carried out focused on proofing the evidence of the bidirectional feature on certain semicrystalline polymer networks as can be seen in Table 7.

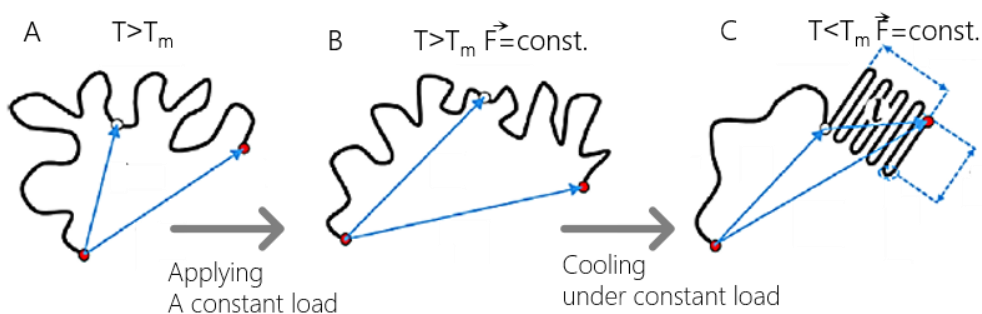


Fig. 40. Schematic Stretch Induced Crystallization SIC process of a network chain during two-way SME Amorphous, undeformed (A) chain; chain deformed by applying a constant load (B); chain crystallized under constant load (C). Red points represent net points; white imagined point divides the chain into amorphous and crystallized sub chains. Adapted from [212]

Once known the phenomenon which drives partially the 2W-SME in the semicrystalline network, the most remarkable parameters in the phenomenon must be addressed. Crystallization, mainly determine the capacity of the covalent networks to evidence 2W-SME [198], their performance as the key parameter is directly related with three variables: The crosslink density, the temperature range, and the stress load, as follow:

Crosslink density

This variable is directly related to the stability of the permanent shape; they act as the links between the chain's network to avoid the slippage of one to another at high temperature under the rubbery state. At the same time, crosslink drives the network to the shape it must reaches when chains recover their mobility at high temperature. A direct relation between the degree of crosslinking and storage modulus when the temperature increases, can be seen in Fig. 41, with low crosslinking levels, the resistance has an asymptotic behavior and drops to 0MPa when the temperature increases; meanwhile higher levels, more than 1%Wt, provides stability and resistance of the sample at high temperatures. Nevertheless, higher levels of crosslink density are not directly related to the high efficiency of the SME, due to their dual effect in the network [201].

When the crosslink density rises, the network gains more strength and stability, crucial to the shape recovery; but at the same time, the polymer chains are higher constrained, and their capacity to crystallize is restricted. For those reasons, the crosslink density must be in a certain level to be high enough to guarantee shape stability, but at the same time, to not constrain the chains allowing them to conform lamellas in any direction; key fact in the fixity of the temporary shape. Several works have been focused on the crosslink density of certain networks as poly(ϵ -caprolactone) PCL/benzoyl peroxide [213], , PCL [210], [214], and (meth)acrylate [215].

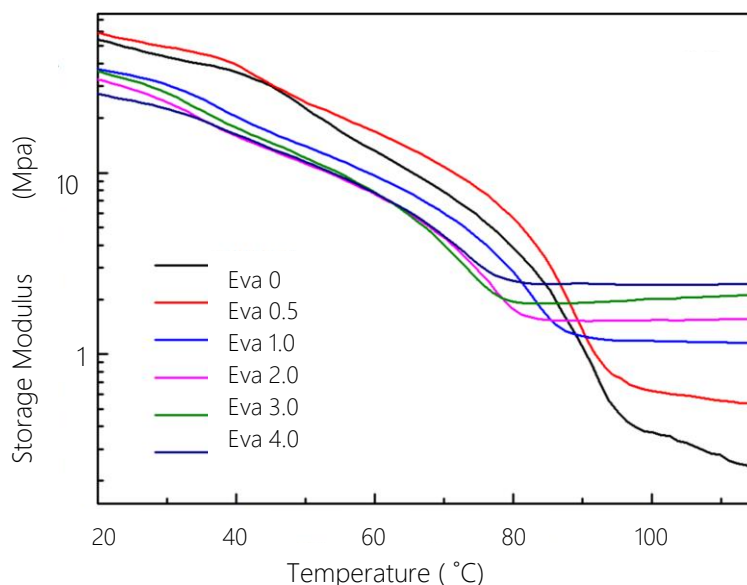


Fig. 41. Plot of storage modulus versus temperature.

Each line represents the %Wt. of the crosslinker agent, Adapted from [195]

This variable as the stimulus which triggers the SME affect the phenomenon in two levels; the first one, the programming process to fix the temporary shape, and the second one, on the thermal cycling to obtain a reversible effect. In the first case, to obtain the temporary shape the crystals of the network must be melted, for this reason, the programming stretch is carried out at a temperature above the T_m , (the T_m of the hard segment), and then the sample is cooled.

Temperature range

In this way, the thermal cycles once the sample was programmed, must be alternated between the T_{high} and T_{low} as follow. The T_{high} must be defined under the higher T_m , to provide the energy that the network requires for the chains recover their mobility; higher temperatures without exceeding the T_m conduces to High R_r values, as can be seen in table 8. The T_{low} must be fixed below the T_c of both segments if the temperature is not low enough the crystallization does not occur, and the CIE is not triggered. Instead, the phenomenon just is driven by elastic-entropy and cannot be reversible.

Stress load

As was recognized the crystallization is directly affected by the constraining effect of crosslinks, but obtaining preferred oriented crystalline segments is crucial to reaching a visible macroscopic effect, this is directly related with the stress induced to the system. For that reason, the effect of the load in the bidirectional result in semicrystalline networks was studied by Chung et al. [191] and Pandani et al. [203] among others. They found that to trigger the phenomenon; each network has a stress point from which the effect is appreciated; this level is called critic stress (σ_{critic}).

If in the programming the σ_{critic} is not exceeded, the stress levels applied are not robust enough to trigger a favored orientation of the lamellae, and the CIE does not occur [205], [216]. Instead, the phenomenon just is driven by elastic-entropy and cannot be reversible. While in contrast, too higher stress levels conduct obtaining unrecoverable oriented chain segments. Because of induced creep into the network [210], avoiding achieving R_r levels close to 100%.

The correlation between the set stress level and the crystallization can be showed in the variation in the T_m of the programmed network. High oriented crystals melt under high temperatures because these crystalline segments need more energy to reach a flexible state.

The effect of those addressed variables has a direct relation to the efficiency of the SME, measured by the R_f and the R_r as crucial parameters. Those parameters and the efficiency of the 2W-SME in the semicrystalline networks reported can be seen in Table 8. Nevertheless, recognizing the parameters highlighted, identified as a critic to the SME, and the basics of a network needs to perform a 2W-SME; different precursors and molecular architectures have been studied with the aim of establishing a relationship between the chemical network and SME phenomenon.

The relation with the precursors as vinyl acetate [194] and ϵ -caprolactone [217] were assessed. Likewise, different works have been carried out looking for the effects of the molecular architecture as follow, different polymer chain length segments of Poly(ω -pentadecalactone) (PPD) [218], chemical changes of ester architecture [200] PEG and PDMS segments [208], crosslinked MACL and CLEG [219], linear and short chain branched polyethylene [188], [198]; PE/PCL, PE/TOR morphology [220], star shaped PCL [221] poly(octylene adipate) networks[201], linear and star branched PCL[203], short aramid/PCL [222], Poly(tetramethylene oxide) glycol PTMEG [207] continuous PE/PP[223] , PPD/PCL [224], [225].

Thus, according to those works, the variation of physical parameters, as the molecular weight of the precursors, different methacrylation, polymerization or polyaddition times, as well as grafted functional groups, among others, can customize the SME performing conditions, and even lead to getting a triple SME.

Table 8. Shape Memory Effect key parameters, shape fixity ratio, and shape recovery ratio

Matrix	Levels %Wt	Stress MPa	ϵ_{prog} %	T_{prog} °C	T_{low} °C	T_{high} °C	Xc(%)	R _F (%)	R _r (%)
PCO	1	0.6	-	-	0	100	28,2	118	95,5
	1,25	0.6	-	-	0	100	27,8	60	97,5
	1,5	0.6	-	-	0	100	26,8	45	98,3
	1,75	0.6	-	-	0	100	26,4	38	98,8
	2	0.6	-	-	0	100	25,7	34	99,3
		0.5	-	-	0	100	-	17,4	99,5
	0.7	-	-	0	100	-	35,5	99,0	
EVA	0,5	0.05	-	-	0	100	-	63,0	-
	1	0.05	-	-	0	100	-	24,5	81,8
	2	0.05	-	-	0	100	-	43,0	98
	3	0.05	-	-	0	100	-	12,0	97
	1	Stress-free	-	-	20	70	17,03	8,41	92,01
			-	-	20	70	16,16	13,41	86,89
	3	Stress-free	-	-	20	70	15,81	16,65	89,82
			-	-	20	50	-	12,0	-
		Stress-free	-	-	20	60	-	22,8	-
		Stress-free	-	-	20	65	-	21,0	-
		Stress-free	-	-	20	70	-	26,0	-
		Stress-free	-	-	20	80	-	30,0	-
	4	Stress-free	-	-	20	80	14,5	12,20	97,91
	PEEAMA	1,0	0.4	400	90	25	70	16	4±1
1,5		0.5	400	90	25	70	15	9±1	70±2
2,0		0.6	400	90	25	70	14	17±2	64±3
Linear HDPE	110*	0.9	-	-	0	165	-	-	-
		1	-	-	0	165	51,8	96	97
		1.1	-	-	0	165	-	219	67
		1.2	-	-	0	165	50,84	311	64
HDPE EOC30	270*	0.45	-	-	0	140	-	95	127
		0.6	-	-	0	140	29,3	97	114
		0.75	-	-	0	140	-	159	81
HDPE EOC60	190*	0.15	-	-	0	120	-	95	123
		0.3	-	-	0	120	12,3	111	103
		0.45	-	-	0	120	-	144	73
LDPE	Fixed	0.855	-	130	45	130	21,3	93.9	99.3

Matrix	Levels %Wt	Stress MPa	ϵ_{prog} %	T_{prog} °C	T_{low} °C	T_{high} °C	Xc(%)	R _f (%)	R _r (%)
LDPE + BC0.5%	Fixed	0.855	-	130	45	130	19,4	92.7	93.5
LDPE + BC1.0%	Fixed	0.855	-	130	45	130	19,1	93.1	94.7
LDPE + BC5.0%	Fixed	0.855	-	130	45	130	17,8	92.2	91.6
LDPE + BC20%	Fixed	0.855	-	130	45	130	15,7	86.6	31.1
PPD-PCL	Fixed	Stress-free	-	90	0	50	-	21	-
MPL	Fixed	Did not show 2W-SME							
HPT	Fixed	Did not show 2W-SME							
HPL	Fixed	Stress-free	100	90	5	50	23±2	75	75
OA	Fixed	Stress-free	20	80	10	47	36	80	85
POA	Fixed	Stress-free	20	70	22	51	44	-	23
PCL-L	2	0.25	0.25	65	-5	65	-	-	-
		0.50	0.50	65	-5	65	-	2.6	82
		0.70	0.70	65	-5	65	-	6.6	98
		1	1	65	-5	65	32	17.7	98
PCL-T	2	0.25	0.25	65	-5	65	-	1.2	68
		0.50	0.50	65	-5	65	-	3.8	72
		0.70	0.70	65	-5	65	-	10.7	93
		1	1	65	-5	65	44	22.8	95
PCL- F	2	0.25	0.25	65	-5	65	-	-	-
		0.50	0.50	65	-5	65	-	4.1	90
		0.70	0.70	65	-5	65	-	7.7	98
		1	1	65	-5	65	34	15.9	99
a,u-hydroxyl-terminated PCL 2200 g/mol ⁻¹	20% stoichiometric excess	0.25	0.25	65	-40	65	-	6	98
		0.50	0.50	65	-40	65	-	16	93
		0.75	0.75	65	-40	65	-	28	97
		1	1	65	-40	65	27	37	96
a,u-hydroxyl-terminated PCL 3400 g/mol ⁻¹	with respect to hydroxyl groups of PCL	0.25	0.25	65	-40	65	-	8	97
		0.50	0.50	65	-40	65	-	19	89
		0.75	0.75	65	-40	65	-	31	96
		1	1	65	-40	65	34	52	96
a,u-hydroxyl-terminated PCL 10000 g/mol ⁻¹	1 groups of PCL	0.25	0.25	65	-40	65	-	9±1	94
		0.50	0.50	65	-40	65	-	26±5	94
		0.75	0.75	65	-40	65	-	54±4	93±6
		1	1	65	-40	65	46	83±9	88±1
lonomer poly(ethylene-co-methacrylic acid)		0.86	79	72	25	65	-	79.1	100
		0.86	79	72	25	80	50.1	100	
Polydopamine-grafted-(poly(E-caprolactone))	0.5 (PDA)		1.7	100	40	150		86-98	69-99
	1 (PDA)		1.7	100	40	150		93-96	82-99
	2 (PDA)		1.7	100	40	150		85-94	75-97

Key parameters which have influence in the 2W-SME and the resulting R_f and R_r on the different semicrystalline networks

3.5 CONCLUSIONS AND FURTHER WORKS

2W-SSMP

As was saw, in the last ten years since the evidence of the 2W-SME in semicrystalline polymers reported by Chung *et al.* the assessment and development of several polymer networks have been carried out with satisfactory and promising results. In this process the phenomenon of the crystallization induced elongation and melting induced contraction were studied deeply, and the key parameters which affects it were identified. Likewise, on the one hand, the advantage of achieving a reversible phenomenon over more complex polymeric systems was highlighted, on the other hand, the restriction in applications where constant stress-load cannot be achieved was highlighted too, in this way different approaches were developed as follow.

The first one is related to the development of elastomer matrix composites where the 2W-SSMP as the reinforcement is encapsulated in a prestressed way to solve the external stress, based on the transference of stress to the matrix. The second, a more complex one, the molecular structure were modified using chemically different domains. The hard domain, with the high thermal transition, acts as a skeleton and has the responsibility of fix the temporary shape; meanwhile, the soft domain with the second highest temperature transition, acts as actuation domain conducting the elongation and shrinkage of the sample [202], [226]. The second approach is based on the building of a molecular scaffold which cannot be broken under the thermal cycling, while the crystallization of the soft segments takes place on the interstices.

In addition to those approaches, increase the responsiveness of the matrixes emerge as research line, where the 2W-SSMP acts as a matrix and have been reinforced by the inclusion of: Carbon Black nanoparticles/PE [173], [199], magnetite nanoparticles/Oligo(ω -pentadecalactone) [209], [227], multiwalled carbon nanotubes/ PCL [228], in these cases with the goal of obtaining electric and magnetically active systems. As well as that research line, other focused on the study of alternative synthesis has emerged, nowadays sol-gel silica domains as crosslinks [204] polymerization-induced phase separation [229], and slide ring movable crosslinks[230] were addressed.

Whereas the medical industry focused on the minimally invasive surgery and self-deployable in-vivo devices have been leading the development of these studies, the potential application in several industries in addition to the aerospace is clear. Nevertheless, the developing spectrum is still broader, for those reasons is essential to continue the exploration of precursors which allow adjusting the thermal transition temperatures or modify properties as strength without thermal transition changes. Likewise, continue with the doping to improve responsiveness, and working on the full fixation and recovery to improve the mechanical performance must be assessed in further studies.

3.6 REFERENCES

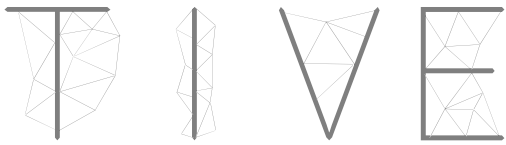
- [167] J. Leng and S. Du, Eds., *Shape-memory polymers and multifunctional composites*. Boca Raton: CRC Press/Taylor & Francis, 2010.
- [168] L. Sun *et al.*, "Stimulus-responsive shape memory materials: A review," *Mater. Des.*, vol. 33, pp. 577–640, Jan. 2012.
- [169] J. Hu, Y. Zhu, H. Huang, and J. Lu, "Recent advances in shape-memory polymers: Structure, mechanism, functionality, modeling and applications," *Prog. Polym. Sci.*, vol. 37, no. 12, pp. 1720–1763, Dec. 2012.
- [170] Q. Meng and J. Hu, "A review of shape memory polymer composites and blends," *Compos. Part Appl. Sci. Manuf.*, vol. 40, no. 11, pp. 1661–1672, Nov. 2009.
- [171] F. Zhang, L. Liu, X. Lv, Y. Liu, and J. Leng, "Properties of smart adaptive composite materials," in *Smart Composite Coatings and Membranes*, Elsevier, 2016, pp. 3–31.
- [172] T. Mu, L. Liu, X. Lan, Y. Liu, and J. Leng, "Shape memory polymers for composites," *Compos. Sci. Technol.*, Mar. 2018.
- [173] X. Wang *et al.*, "Improved Self-Healing of Polyethylene/Carbon Black Nanocomposites by Their Shape Memory Effect," *J. Phys. Chem. B*, vol. 117, no. 5, pp. 1467–1474, Feb. 2013.
- [174] A. Lendlein, Ed., *Shape-Memory Polymers*, vol. 226. Berlin, Heidelberg: Springer Berlin Heidelberg, 2010.
- [175] Y. Zhou and W. M. Huang, "Shape Memory Effect in Polymeric Materials: Mechanisms and Optimization," *Procedia IUTAM*, vol. 12, pp. 83–92, 2015.
- [176] Q. Zhao, H. J. Qi, and T. Xie, "Recent progress in shape memory polymer: New behavior, enabling materials, and mechanistic understanding," *Prog. Polym. Sci.*, vol. 49–50, pp. 79–120, Oct. 2015.
- [177] T. Chung, A. Romo-Uribe, and P. T. Mather, "Two-Way Reversible Shape Memory in a Semicrystalline Network," *Macromolecules*, vol. 41, no. 1, pp. 184–192, Jan. 2008.
- [178] Y. Bai, X. Zhang, Q. Wang, and T. Wang, "A tough shape memory polymer with triple-shape memory and two-way shape memory properties," *J. Mater. Chem. A*, vol. 2, no. 13, p. 4771, 2014.
- [179] J. Hu *et al.*, "Epoxy shape memory polymer (SMP): Material preparation, uniaxial tensile tests and dynamic mechanical analysis," *Polym. Test.*, vol. 62, pp. 335–341, Sep. 2017.
- [180] M. Balk, M. Behl, C. Wischke, J. Zotzmann, and A. Lendlein, "Recent advances in degradable lactide-based shape-memory polymers," *Adv. Drug Deliv. Rev.*, vol. 107, pp. 136–152, Dec. 2016.
- [181] M. Farhan, S. R. Chaganti, U. Nöchel, K. Kratz, and A. Lendlein, "Reversible shape-memory properties of surface functionalizable, crystallizable crosslinked terpolymers: Reversible Actuation of Surface Modified Crosslinked Terpolymers," *Polym. Adv. Technol.*, vol. 26, no. 12, pp. 1421–1427, Dec. 2015.
- [182] B. Yang, W. M. Huang, C. Li, and L. Li, "Effects of moisture on the thermomechanical properties of a polyurethane shape memory polymer," *Polymer*, vol. 47, no. 4, pp. 1348–1356, Feb. 2006.
- [183] E. Hornbogen, "Comparison of Shape Memory Metals and Polymers," *Adv. Eng. Mater.*, vol. 8, no. 1–2, pp. 101–106, Feb. 2006.
- [184] W. Wang, Y. Liu, and J. Leng, "Recent developments in shape memory polymer nanocomposites: Actuation methods and mechanisms," *Coord. Chem. Rev.*, vol. 320–321, pp. 38–52, Aug. 2016.
- [185] M. Behl and A. Lendlein, "Actively moving polymers," *Soft Matter*, vol. 3, no. 1, pp. 58–67, 2007.
- [186] T. Xie, "Recent advances in polymer shape memory," *Polymer*, vol. 52, no. 22, pp. 4985–5000, Oct. 2011.
- [187] M. Behl, K. Kratz, J. Zotzmann, U. Nöchel, and A. Lendlein, "Reversible Bidirectional Shape-Memory Polymers," *Adv. Mater.*, vol. 25, no. 32, pp. 4466–4469, Aug. 2013.
- [188] I. Kolesov, O. Dolynchuk, D. Jehnichen, U. Reuter, M. Stamm, and H.-J. Radusch, "Changes of Crystal Structure and Morphology during Two-Way Shape-Memory Cycles in Cross-Linked Linear and Short-Chain Branched Polyethylenes," *Macromolecules*, vol. 48, no. 13, pp. 4438–4450, Jul. 2015.
- [189] S. Pandini, D. Dioni, K. Paderni, M. Messori, M. Toselli, and T. Riccò, "The network density as tailoring parameter for the two-way shape memory response of crosslinked poly(ϵ -caprolactone)," 2014, pp. 270–273.

- [190] G. Lugito, E. Woo, and W.-T. Chuang, "Interior Lamellar Assembly and Optical Birefringence in Poly(trimethylene terephthalate) Spherulites: Mechanisms from Past to Present," *Crystals*, vol. 7, no. 2, p. 56, Feb. 2017.
- [191] T. Chung, A. Romo-Urbe, and P. T. Mather, "Two-Way Reversible Shape Memory in a Semicrystalline Network," *Macromolecules*, vol. 41, no. 1, pp. 184–192, Jan. 2008.
- [192] K. K. Westbrook *et al.*, "Constitutive Modeling of Shape Memory Effects in Semicrystalline Polymers With Stretch Induced Crystallization," *J. Eng. Mater. Technol.*, vol. 132, no. 4, p. 041010, 2010.
- [193] J. Kunzelman, T. Chung, P. T. Mather, and C. Weder, "Shape memory polymers with built-in threshold temperature sensors," *J. Mater. Chem.*, vol. 18, no. 10, p. 1082, 2008.
- [194] J. Li, W. R. Rodgers, and T. Xie, "Semi-crystalline two-way shape memory elastomer," *Polymer*, vol. 52, no. 23, pp. 5320–5325, Oct. 2011.
- [195] C. Qian, Y. Dong, Y. Zhu, and Y. Fu, "Two-way shape memory behavior of semi-crystalline elastomer under stress-free condition," *Smart Mater. Struct.*, vol. 25, no. 8, p. 085023, Aug. 2016.
- [196] J. Fan and G. Li, "High performance and tunable artificial muscle based on two-way shape memory polymer," *RSC Adv*, vol. 7, no. 2, pp. 1127–1136, 2017.
- [197] I. Kolesov, O. Dolynchuk, and H.-J. Radusch, "Shape-memory behavior of cross-linked semi-crystalline polymers and their blends," *Express Polym. Lett.*, vol. 9, no. 3, pp. 255–276, 2015.
- [198] O. Dolynchuk, I. Kolesov, R. Androsch, and H.-J. Radusch, "Kinetics and dynamics of two-way shape-memory behavior of crosslinked linear high-density and short-chain branched polyethylenes with regard to crystal orientation," *Polymer*, vol. 79, pp. 146–158, Nov. 2015.
- [199] L. Ma *et al.*, "Effects of carbon black nanoparticles on two-way reversible shape memory in crosslinked polyethylene," *Polymer*, vol. 56, pp. 490–497, Jan. 2015.
- [200] A. Biswas, V. K. Aswal, P. U. Sastry, D. Rana, and P. Maiti, "Reversible Bidirectional Shape Memory Effect in Polyurethanes through Molecular Flipping," *Macromolecules*, vol. 49, no. 13, pp. 4889–4897, Jul. 2016.
- [201] Q. Li, J. Zhou, M. Vatankhah-Varnoosfaderani, D. Nykypanchuk, O. Gang, and S. S. Sheiko, "Advancing Reversible Shape Memory by Tuning the Polymer Network Architecture," *Macromolecules*, vol. 49, no. 4, pp. 1383–1391, Feb. 2016.
- [202] J. Zhou *et al.*, "Shapeshifting: Reversible Shape Memory in Semicrystalline Elastomers," *Macromolecules*, vol. 47, no. 5, pp. 1768–1776, Mar. 2014.
- [203] S. Pandini *et al.*, "Two-way reversible shape memory behaviour of crosslinked poly(ϵ -caprolactone)," *Polymer*, vol. 53, no. 9, pp. 1915–1924, Apr. 2012.
- [204] S. Pandini *et al.*, "One-way and two-way shape memory behaviour of semi-crystalline networks based on sol–gel cross-linked poly(ϵ -caprolactone)," *Polymer*, vol. 54, no. 16, pp. 4253–4265, Jul. 2013.
- [205] L. Lu and G. Li, "One-Way Multishape-Memory Effect and Tunable Two-Way Shape Memory Effect of Ionomer Poly(ethylene-co-methacrylic acid)," *ACS Appl. Mater. Interfaces*, vol. 8, no. 23, pp. 14812–14823, Jun. 2016.
- [206] M. Bothe and T. Pretsch, "Bidirectional actuation of a thermoplastic polyurethane elastomer," *J. Mater. Chem. A*, vol. 1, no. 46, p. 14491, 2013.
- [207] H. Xie *et al.*, "Creating Poly(tetramethylene oxide) Glycol-Based Networks with Tunable Two-Way Shape Memory Effects via Temperature-Switched Netpoints," *Macromolecules*, vol. 50, no. 13, pp. 5155–5164, Jul. 2017.
- [208] B. Q. Y. Chan, S. J. W. Heng, S. S. Liow, K. Zhang, and X. J. Loh, "Dual-responsive hybrid thermoplastic shape memory polyurethane," *Mater. Chem. Front.*, vol. 1, no. 4, pp. 767–779, 2017.
- [209] M. Y. Razzaq, M. Behl, U. Nöchel, and A. Lendlein, "Magnetically controlled shape-memory effects of hybrid nanocomposites from oligo(ω -pentadecalactone) and covalently integrated magnetite nanoparticles," *Polymer*, vol. 55, no. 23, pp. 5953–5960, Nov. 2014.
- [210] S. Pandini *et al.*, "The two-way shape memory behaviour of crosslinked poly(ϵ -caprolactone) systems with largely varied network density," *J. Intell. Mater. Syst. Struct.*, vol. 27, no. 10, pp. 1388–1403, Jun. 2016.

- [211] U. Nöchel, K. Kratz, M. Behl, and A. Lendlein, "Relation -between Nanostructural Changes and Macroscopic Effects during Reversible Temperature-Memory Effect under Stress-Free Conditions in Semicrystalline Polymer Networks," *MRS Proc.*, vol. 1718, 2015.
- [212] O. Dolynchuk, I. Kolesov, and H.-J. Radosch, "Theoretical Description of an Anomalous Elongation During Two-Way Shape-Memory Effect in Crosslinked Semicrystalline Polymers," *Macromol. Symp.*, vol. 346, no. 1, pp. 48–58, Dec. 2014.
- [213] M. Huang, X. Dong, L. Wang, J. Zhao, G. Liu, and D. Wang, "Two-way shape memory property and its structural origin of cross-linked poly(ϵ -caprolactone)," *RSC Adv*, vol. 4, no. 98, pp. 55483–55494, Oct. 2014.
- [214] S. Pandini, D. Dioni, K. Paderni, M. Messori, M. Toselli, and T. Riccò, "The network density as tailoring parameter for the two-way shape memory response of crosslinked poly(ϵ -caprolactone)," 2014, pp. 270–273.
- [215] D. L. Safranski and K. Gall, "Effect of chemical structure and crosslinking density on the thermo-mechanical properties and toughness of (meth)acrylate shape memory polymer networks," *Polymer*, vol. 49, no. 20, pp. 4446–4455, Sep. 2008.
- [216] M. Bothe and T. Pretsch, "Two-Way Shape Changes of a Shape-Memory Poly(ester urethane)," *Macromol. Chem. Phys.*, vol. 213, no. 22, pp. 2378–2385, Nov. 2012.
- [217] A. L. Sisson, D. Ekinici, and A. Lendlein, "The contemporary role of ϵ -caprolactone chemistry to create advanced polymer architectures," *Polymer*, vol. 54, no. 17, pp. 4333–4350, Aug. 2013.
- [218] M. Behl, J. Zotzmann, and A. Lendlein, "One-Way and Reversible Dual-Shape Effect of Polymer Networks Based on Polypentadecalactone Segments," *Int. J. Artif. Organs*, vol. 34, no. 2, pp. 231–237, Feb. 2011.
- [219] I. Bellin, S. Kelch, R. Langer, and A. Lendlein, "Polymeric triple-shape materials," *Proc. Natl. Acad. Sci.*, vol. 103, no. 48, pp. 18043–18047, Nov. 2006.
- [220] I. Kolesov, O. Dolynchuk, S. Borreck, and H.-J. Radosch, "Morphology-controlled multiple one- and two-way shape-memory behavior of cross-linked polyethylene/poly(ϵ -caprolactone) blends: SHAPE-MEMORY BEHAVIOR OF POLYETHYLENE/POLY(ϵ -CAPROLACTONE) BLENDS," *Polym. Adv. Technol.*, vol. 25, no. 11, pp. 1315–1322, Nov. 2014.
- [221] K. Y. Mya, H. B. Gose, T. Pretsch, M. Bothe, and C. He, "Star-shaped POSS-polycaprolactone polyurethanes and their shape memory performance," *J. Mater. Chem.*, vol. 21, no. 13, p. 4827, 2011.
- [222] G. Rabani, H. Luftmann, and A. Kraft, "Synthesis and characterization of two shape-memory polymers containing short aramid hard segments and poly(ϵ -caprolactone) soft segments," *Polymer*, vol. 47, no. 12, pp. 4251–4260, May 2006.
- [223] J. Zhao *et al.*, "Triple Shape Memory Effects of Cross-Linked Polyethylene/Polypropylene Blends with Cocontinuous Architecture," *ACS Appl. Mater. Interfaces*, vol. 5, no. 12, pp. 5550–5556, Jun. 2013.
- [224] J. Zotzmann, M. Behl, Y. Feng, and A. Lendlein, "Copolymer Networks Based on Poly(ω -pentadecalactone) and Poly(ϵ -caprolactone) Segments as a Versatile Triple-Shape Polymer System," *Adv. Funct. Mater.*, vol. 20, no. 20, pp. 3583–3594, Oct. 2010.
- [225] J. Zotzmann, M. Behl, D. Hofmann, and A. Lendlein, "Reversible Triple-Shape Effect of Polymer Networks Containing Polypentadecalactone- and Poly(ϵ -caprolactone)-Segments," *Adv. Mater.*, vol. 22, no. 31, pp. 3424–3429, Apr. 2010.
- [226] Y. Meng, J. Jiang, and M. Anthamatten, "Shape Actuation via Internal Stress-Induced Crystallization of Dual-Cure Networks," *ACS Macro Lett.*, vol. 4, no. 1, pp. 115–118, Jan. 2015.
- [227] M. Y. Razzaq, M. Behl, and A. Lendlein, "Thermally Controlled Shape-Memory Investigations of Nanocomposites Based on Oligo(ω -pentadecalactone) and Magnetic Nanoparticles Acting as Crosslinks," *MRS Proc.*, vol. 1718, 2015.
- [228] W. Li, Y. Liu, and J. Leng, "Shape memory polymer nanocomposite with multi-stimuli response and two-way reversible shape memory behavior," *RSC Adv*, vol. 4, no. 106, pp. 61847–61854, Nov. 2014.
- [229] A. H. Torbati, H. B. Nejad, M. Ponce, J. P. Sutton, and P. T. Mather, "Properties of triple shape memory composites prepared via polymerization-induced phase separation," *Soft Matter*, vol. 10, no. 17, pp. 3112–3121, 2014.
- [230] X. Li, Y. Wang, R. Wu, Y. Pan, Z. Zheng, and X. Ding, "Slide-ring shape memory polymers with movable cross-links," *React. Funct. Polym.*, vol. 119, pp. 26–36, Oct. 2017.

4.

THE RMOSENS
FUNCTIONAL
COMPOSITE



4.1 INTRODUCTION

4.2 MATERIALS AND METHODS

4.3 RESULTS AND DISCUSSION

4.4 CONCLUSIONS AND FURTHER WORKS

4.5 SUPPLEMENTARY INFORMATION

4.6 REFERENCES

4.1

INTRODUCTION

Guiding question

Experimental objectives

Work scope

2W-SSMP
Crosslinked
cEVA

Several 2W-SSMP precursors were used in rigid semicrystalline networks as soft domains to drive the SME as was addressed. One of them, the vinyl acetate, for instance as the soft domain in the ethylene-vinyl acetate copolymer cEVA, as can be seen in Table. 8, which is described as follow.

cEVA is an ethylene network with random vinyl groups, shown in Fig. 42 , with different properties because of Wt% of vinyl acetate groups as follow, 4% - 11% (hot melt adhesive), 12% -40% (thermoplastic elastomer), and >40% (rubber) used as an additive in several industries. Chemically crosslinked cEVA is a thermosetting elastomer with toughness features but also flexibility at room temperature, in comparison with linear ethylene; the crosslinked network also present stability at high temperatures above the rubbery state, because of the constraining effect of crosslinks against the chains slippage.

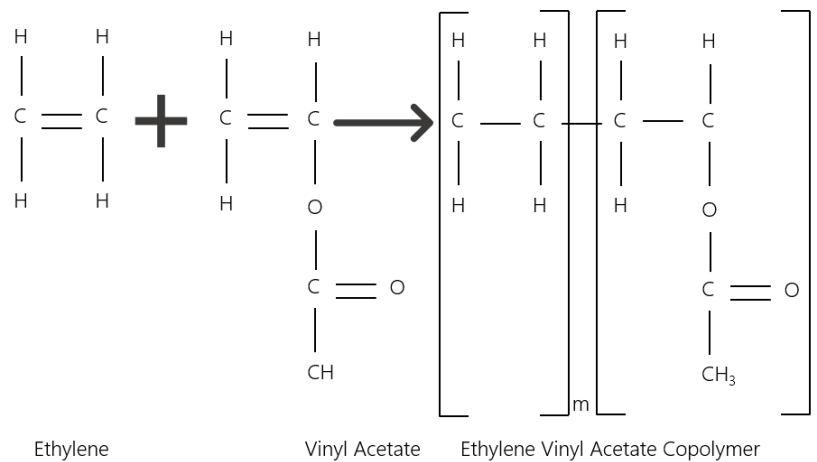


Fig. 42. Ethylene Vinyl Acetate Copolymer. adapted from [231]

In this way, their molecular network has the SME basis, two domains, ethylene as hard, and vinyl acetate as soft, and crosslinks as the guarantee of the stability. Because of the accomplish of those basics, and be a commercial polyolefin elastomer soft and flexible, low-cost commodity polymer; this polymer network has been evaluated with the aim to study their 2W-SME performance.

Li et al. [194], have verified the evidence of the bidirectional SME of crosslinked cEVA in 2011, since that moment, several works have been carried out exploring and improving their performance with certain applications in the scope as follow. Network modifiers as PEVA/poly(L-lactacide)[232] carbon fiber reinforcement [233] electrical active carbon nanofiber inclusions [234], triple SME assessment[235], in this way Behl et al. [236], 2013 have been identified *the potential of cEVA as active building facades temperature-memory actuator*.

The most promising direction in the building adaptation is passive responsive strategies based on material properties. In this way polymers, as was addressed in previous sections, have several advantages above other SRM. Likewise, to building applications, a low-complex polymer system must be selected as the basis for a possible industrial scaling, for those reasons, in accordance with Behl et al. crosslinked cEVA was selected to be assessed. Hence, as was addressed, one of the identified lines to apply the 2W-SME in semicrystalline networks is the encapsulation in a prestressed way to solve the external stress necessity. This line was identified as the work scope.

The potential of polymers to be used as actuators was previously assessed by Ionov [237], and the wide application spectrum was showed, in this way, the soft actuators development is outlined as an important area of development of those matrixes. Other investigations have been reported the conversation of light into mechanical motion trough polymer systems [238], temperature sensors based on poly(cyclooctene) network [193], and active origami by 4D printing by Ge et al. [239]

With those precedents, shape-memory actuators based on binary and ternary polyethylene blends were assessed by Dolynchung [240], cEVA 2W-SME was evaluated under stress free conditions by Qian et al. [195], and High performance artificial muscles based on EVA was reported by Fan and Li in 2017 [196] showing favorable results.

Semicrystalline polymer networks have been encapsulated in a prestressed way by Westbrook et al. [241], The modeling to predict the displacement was carried out, but differences between modeling and experimental data were found, as one of the reasons, the interface between the reinforcement and the matrix could be not entirely coherent because of the polymers low energy surface. Nevertheless, the surface did not be studied; Likewise, were presumed that the effect could be enhanced by the reduction of the transversal area between reinforcement and matrix of the composite.

For those reasons, the study of the 2W-SME behavior of a semicrystalline polymer, with a potential to be used as facade temperature-memory actuator previously identified, is defined. Functionalized crosslinked cEVA strip encapsulated, with variations in the hardness of the matrix is defined as the scope; Looking for the enhancing of the SME phenomenon, their stability in time, and the direction of the movement because of thermo-sensitive actuator applications.

Guiding question

What is the thermosensitive potential of a composite material based on a functionalized crosslinked cEVA and what kind of matrix conditions enhance the 2W-SME phenomenon?

GENERAL OBJECTIVE

Determine the thermomechanical potential of a composite material based on a semicrystalline polymer with bidirectional shape memory effect (2W-SME)

SPECIFIC OBJECTIVES

Complete the synthesis of a semicrystalline polymer matrix with two domains capable of obtaining a 2W-SME

Establish the levels of the processing program parameters to obtain the 2W-SME in a semicrystalline polymer network

Complete the synthesis of a functional composite material which guarantees the permanent stress load of a 2W-SMP encapsulated lamina.

Evaluate the shape memory stability of a functional thermosensitive composite under thermal cycling.

Experimental Work Scope

The thermosensitive potential and programming processing parameters of the reinforcing lamina and the composite material at laboratory scale were studied in this work

4.2

MATERIALS AND METHODS

In this section, the used materials are reported, the followed experimental methodology is described, and the concepts did not previously cover are introduced.

The used methodology is divided into four phases associated with five main activities. Polymer reinforcement lamina synthesis; shape memory effect study; reinforcement lamina preparation and functionalization; experimental matrix design, and thermocycling performance study. Each experimental procedure has been further addressed in the next sections. The experimental development divided into phases is presented in Table 9. From the obtained results of each activity, the next one is carried out; in this way, the procedure allows the improvement of the following actions.

Description | In the first phase, the synthesis of the chemically crosslinked semicrystalline network was carried out, an ethylene-vinyl acetate copolymer and dicumyl peroxide as thermal initiator was selected. In the second phase, the shape memory study was developed according to the literature procedure; and the reported programming parameters were used as the basis to define the range of the study. The third phase was divided into two activities; the first one, the preparation and functionalization of the reinforcement lamina to enhance the surface wettability, the second one, the encapsulation with polyurethane rubber matrix with various hardness as variable.

Finally, in the fourth phase, the thermocycling experiments were carried out to determine the shape memory stability of the composite, focused on the guided obtained displacement.

Table 9. Methodological activities and phases summary

Phase	Activity	Goal
1. Polymer reinforcement lamina	Synthesis of chemically crosslinked cEVA network	Obtain a chemically crosslinked polymer network with two segregated domains
2. Shape memory effect study	Shape memory programming process	Identify the programming parameters to maximize the 2W-SME
3. Polymer Matrix laminate composite	Reinforcement lamina functionalization	Improve the surface wettability
	Matrix experimental study	Identify the hardness relation matrix / reinforcement to enlarge deformation
4. Thermocycling performance study	Thermocycling test	Define the thermocycling behavior and work capacity of the matrix/reinforcement with higher deformation rate

The used materials into the experimental development and their main characteristics are shown in Table 10.

Table 10. Used materials

Material	Supplier	Characteristics
Ethylene-vinyl acetate copolymer	Regional supplier (Asia Polymer Corp.)	18 % vinyl acetate groups
Dicumyl peroxide	Sigma-Aldrich	Scales 98% purity, analytic grade
Polyurethane rubber	Regional supplier (Smooth-on Inc.)	Shore A hardness 30
		Shore A hardness 60
		Shore A hardness 80

REINFORCEMENT LAMINA

The reinforcement as the shape-shifting component was must be reached at first, to obtain a functional composite material with thermosensitive capabilities. CIE and MIS drive the shape memory phenomenon in semicrystalline networks, for that reason, a stable structure with reversible domains must be synthesized as the first step to reach the phenomenon. In this way to obtain a crosslinked semicrystalline network with two domains, the following procedure was carried out.

Shape memory reinforcement sheets cEVA-DCP samples were prepared by mixing 50g (ethylene-co-(vinyl acetate)) copolymer with a vinyl acetate content of 18 wt% (Asia polymers Corp.) and 1,5g (3%Wt.) dicumyl peroxide 99% purity (Sigma-Aldrich) in a torque rheometer (Thermo- Fisher Scientific) at 100°C and 50 rpm. Uncured polymer samples were granulated into 3 mm thickness, then compression molded and cross-linked was performed at 200 °C under 5MPa for 45 min. Finally, an annealing process at 100°C for 10 min was carried out to remove any residual stress because of the molded by compression. Summary can be seen in Table 11.

Synthesis
& curing

Table 11. Synthesis and curing summary

Synthesis	Sample	Blend	Curing	Annealing
cEVA-DCP 3	Ethylene-vinyl acetate copolymer cEVA + Dicumyl peroxide DCP 3Wt%	100°C 50 rpm	200°C 5MPa 45min	100°C 10min

The *crystallization behavior and thermal transitions exploration* of SMS was investigated by TA instruments SDT Q600 differential scanning calorimeter under N₂ atmosphere 50 ml min⁻¹. Thermal transition temperatures were scanned between 40 °C and 150 °C under a cooling and heating rate of 10 °C min⁻¹. The first cooling and the subsequent second heating traces were recorded for analysis. The crystallinity (X_c) of the samples was calculated according to Equation (1):

Characterization

$$X_c = \frac{\Delta H_f}{\Delta H_f^*} \cdot 100\% \quad (1)$$

where ΔH_f^* is the enthalpy of fusion of the perfect polyethylene (PE) crystal and ΔH_f is the enthalpy of fusion of the EVA. The value of ΔH_f^* for PE is 277.1 J/g[242]

The Chemical verification of the obtained polymer network was performed by ATR-IR spectra in the mid-infrared band from 400 to 4000 cm⁻¹ at 4cm⁻¹.

The *Mechanical response*, the *elongation at break* and *toughness* were measured using a Shimazu tensile tester at a strain rate of 10 mm /min-1, at room temperature. Modulus ϵ was measured using an extensometer at a strain rate of 1mm/min-1 at room temperature. The samples evaluated keep a thickness of 2.5mm x 6mm. Several samples were evaluated to obtain a reasonable estimation of error.

The *temperature dependent stiffness properties* were performed by dynamic mechanical analysis E' ; E'' ; loss factor T_g , $\tan\delta$ E''/E' Samples 0.9 mm x 6.0 mm x 50 mm. the sample was fixed in tension mode between clamps. From room temperature to 150 °C.

SHAPE MEMORY *effect* STUDY

As was addressed in section 3 the shape memory effect is not an intrinsic property of a material, is the result of a chemical-specific network with specific processing conditions. In this way, once the network is done, the processing parameters must be addressed as the second step to obtain the SME phenomenon.

Different authors have measured the shape memory effect in semicrystalline polymers in a variety of ways [174]; nevertheless, the deformation to fix a shifting shape and the recoverability of the permanent shape is the most important properties to quantify the SME in the macroscopic level [243]. Cyclic thermomechanical experiments have been performed to define the shape memory properties of a sample.

Those cyclic thermomechanical tests have been focused on determining the percentage of strain produced on the fixing of the shifting shape, *defined as shifting shape fixity ratio* R_f , and the percentage of recovery of the permanent shape, *defined as permanent shape recovery ratio* R_r . The test used to be performed in the tensile mode and the changes in the total length of the sample is recording. In agreement with equations 2 and 3 the main parameters can be defined.

$$R_f = 100\% \times \frac{\varepsilon}{\varepsilon_{load}} \quad (2)$$

$$R_r = 100\% \times \frac{\varepsilon - \varepsilon_{rec}}{\varepsilon} \quad (3)$$

Each full cycle consists of a programming and recovery module, to assess the shape memory stability, and at least five cycles have been performed to describe both, the fixing and recovery ability of the network. The following procedure was followed in the SME assessment, focused on determining the thermomechanical processing conditions which enlarge the SME phenomenon. The *shape memory characterization* was performed using an MTS Universal Materials Testing Frame of 5kN (Digimess) equipped with a customized forced convection thermal chamber to guarantee the heat distribution and a temperature controller as can be seen in Fig. 43.

Fig. 43 Customize forced convection thermal chamber with temperature controller



The dog-bone samples ISO 527–2 were cut from the thermocompression resulting sheets for the thermomechanical programming. Different levels of stress were applied through the fixed temperature reported, as can be seen in Table 12, to explore the induced crystallization enlargement phenomenon.

Programming

The program begins at elevated temperature ($T > T_m$). (1) Deformation: The Sample strip is heated from room temperature to 95 °C during 10 min, then is elongated by increasing the applied load from 0 to the load defined in table 12 at a rate of 0.05 N/min. (2) Fixing: the sample is then cooled to a temperature below T_m under constant load, in this step the shifting shape must quite completely fix (3) Recovery: Finally, heat-induced recovery toward the original length was examined by heating to the temperature range defined in Table 13. Each temperature range addressed was performed during five cooling and heating cycles and the strain was recorded.

Characterization

The *crystallization behavior and thermal transitions exploration* of SMS was investigated by TA instruments SDT Q600 differential scanning calorimeter under N_2 atmosphere 50 ml min^{-1} . Thermal transition temperatures were scanned between 40 °C and 150 °C under a cooling and heating rate of 10 °C min^{-1} . The first cooling and the subsequent second heating traces were recorded for analysis.

Table 12. Programming summary

Programming	Sample	Temperature	Stress Load MPa
			0.55
			0.75
cEVA-DCP	ISO 527–2	95°C 10 min	0.85

Table 13. Shape memory study summary

Programming	Sample	Stress load	Temperature range °C
			40 – 60
			40 – 65
		Sample with the best performance	40 – 70
cEVA-DCP	ISO 527–2	from the programming process	40 – 75

COMPOSITE ACTUATOR

As was concluded in section three, one way to improve shape memory stability in semicrystalline polymers is the encapsulation of the sample into an elastomeric matrix to guarantee the stress level to trigger the CIE which partially drives the SME, defining in this way a functional composite material. Hence, for the synthesis of a polymer matrix composite, different polyurethane networks were selected as a matrix because the material in the rubbery state is needed to allow the deformation of the reinforcement lamina, but also having the toughness, scratch and temperature resistance to perform thermal cycling.

The interface region is set as a critical fact conforming to the composite materials theory:

There is the region where the stress load is transferred from the matrix to the reinforcement and vice versa. It is assumed that the interface region is "perfect" but is not in that way, in fact, many essential phenomena take place in this region, depending on each structure and the stress generated there; these processes tend to promote plastic deformation of the matrix and influence the onset and nature of the failure. [244] pp 133.

Previous works focused on the encapsulation of SSMP [241], does not take into consideration the interface study in functional composites as shape memory, and it has an essential effect because the interface is assumed as perfect into the modeling process to predict the behavior and the data has differed from the experimental results. Hence, the interface study is an important fact in the synthesis of a functional composite material based on crosslinked cEVA lamina in a prestressed way, because of the performances are based in the transference of load between the reinforcement and the matrix.

The bidirectional shape memory capabilities of crosslinked cEVA have been addressed in section four; nevertheless, cEVA use to be used joined to other materials, and it has been reported low adhesion properties because of their low energy surface. Chemical treatments and solvent-based primers have been used to modify the physical and chemical composition of the surface reaching higher polar groups rising the surface energy. Although, the uses of chemical-based treatments must be avoided because of the safety and environmental disposal of the produced toxic waste.

Plasma treatment (or plasma irradiation) is a widely used technique for the effective chemical and physical modification of material surface properties [245]–[247]. Generally, several common effects of plasma treatment can be determined: cleaning, etching, activation, and cross-linking [248]. Plasma is a totally or partially ionized gas which consists of various charge carriers such as electrons, ions and radicals, and is overall electrically neutral. Thus, each component within plasma may interact during plasma irradiation.

Moreover, plasma exposure can activate a polymer surface by creating new polar functional groups including carbonyl, carboxyl, ether, amine and hydroxyl; thus, markedly increasing the free polymer surface energy because of modified chemical composition, the wetting characteristics and surface adhesion of polymeric materials can also be changed [246]. The attractiveness of plasma treatment amongst other conventional surface modification techniques is an ability to alter only surface properties, up to several nanometers thick, without affecting the bulk characteristics of materials [249].

Moreover, short-time plasma irradiation does not overheat materials, so their destruction may be avoided. The critical fact for the treatment of temperature dependent characteristic materials as semicrystalline polymers, because of treatment with overheat can induce the melting of the scaffold crystals and erase the programmed shape avoiding the reach of a reversible effect.

Several investigations were carried out focused on the surface modification of cEVA following alternative treatments as low-plasma exposure [250], and UV exposure [251]. On the one hand, the rising of the energy surface was reported by the etching of the surface and the increase in superficial area from both treatments, on the other hand, chemical functionalization was reported by the UV treatment by the incorporation of carboxyl and hydroxyl groups. Nevertheless, the chemical of the surface on the plasma treatment was not studied.

The surface of two bodies come into contact when are close to each other, In composite materials, one of them use to be in a liquid form, there the "wetting" concept takes place referring to the ability

of a liquid to spread on a solid surface. The wetting is directed related to the surface energy of the constituents, and it is improved if their energy is large and the interfacial surface energy is small.

The wettability of a solid by a liquid can be measured by a drop of liquid on the solid surface on an appropriate atmosphere [252]. The contact angle of a liquid on the solid surface is an essential parameter to characterize wettability. it is measured by the deposition of a drop on the surface, and it is obtained from the tangents along three interfaces: solid/liquid, liquid/vapor, and solid/vapor.

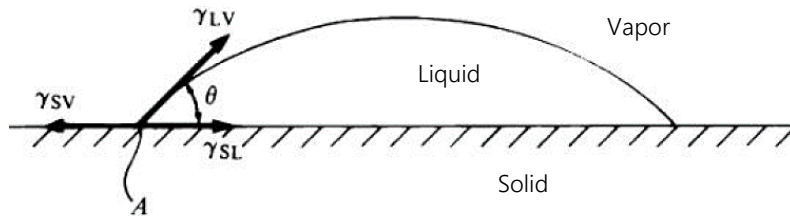


Fig. 44. Contact angle θ and surface energies γ for a liquid drop on a solid surface
Reproduced from [244]

The functionalization of cEVA was proposed with the aim of reach an interfacial bond formed by molecular entanglement (A) and mechanical keying (B) shown in Fig. 45, trough low plasma exposure treatment. The functionalization of the cEVA-DCP surface after the programming process previous the encapsulation was carried out according to the procedure used by Cepeda-Jimenez et al. [250]. The samples were exposure to non-oxidizing Ar and N₂ atmosphere plasma in a reactor (Quorum Q150R ES) under a 35mA current; Voltage 358V; varying the exposure time and the polarity as shown in

Functionalization

Table 14.

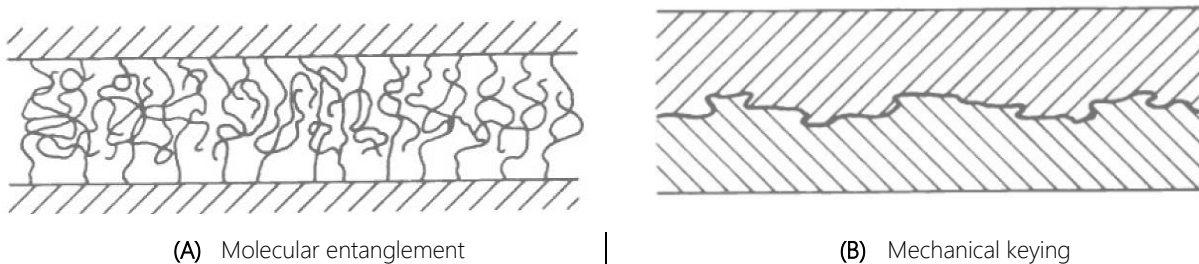


Fig. 45. Interfacial bonds formed in a composite
Reproduced from [244]

Table 14. Surface treatment summary

Sample	Atmosphere	Current	Voltage	Polarity	Exposure Time
					300 s
					600 s
	Ar	35mA	350 V	Positive	900 s
					300 s
					600 s
cEVA-DCP 3	N	35mA	350 V	Positive / Negative	900 s

Contact angle measurements between EVA20 and deionized and bidistilled water were measured in a Rame´ – Hart 100 goniometer at 25 °C, after the chamber was saturated with water. Five different single drops (4 ml) of water were deposited on the surface of the same EVA20 specimen and measurements were obtained 10 min after drop deposition in accordance with equation 4.

Surface
Characterization

$$\gamma_{SV} = \gamma_{SL} + \gamma_{LV} \cos\theta \quad (4)$$

Surface Characterization

The *surface* was studied on the as-received and treated cEVA surfaces by the determination of the peaks and deeps length on the surface by a rugosimeter in the longitudinal and transverse direction of the programmed samples.

The *Chemical characterization* of the as-received and treated samples were performed by ATR-IR spectra in the mid-infrared band from 400 to 4000 cm⁻¹ at 4cm⁻¹.

Composite Fabrication process

1. *Reinforce shape memory strip preparation.* cEVA-DCP3 dog-bone samples ISO 527-2 were cut from the sheets and programmed under XX MPa at 95 °C during 10 min. and then cooled to room temperature, to obtain bars of dimensions of 50 mm x 4 mm x 1 mm the middle section of the programmed bond sample was sectioned.

2. *Reinforcement treatment.* Surface treatment was carried out by 300 seg of low plasma radiation exposure under a non-oxidizing N and Ar atmosphere with positive and negative polarity to improve wettability according to the addressed procedure in the functionalization step.

3. *Reinforcement location.* The programmed and treated cEVA-DCP strip was inserted into the mold machined with slots on each end located off-center in the thickness dimension shown in Fig. 46, the enclosed, interior section of the mold was designed to be more extensive than the required actuator dimensions to allow the different transversal relationships shown in

Table 15 and the removal of any edge defects that may be introduced in the process.

4. *Encapsulation.* The mold was sealed by securing two Teflon coated glass slides on the top and bottom using binder clips, and the polyurethane rubber with different hardness, as shown in table 16, was then injected into the sealed mold using a syringe. The material cure for 12 hours at 40 °C.

5. *Sectioning.* The composite was removed to the mold and cut to obtain the desire dimensions

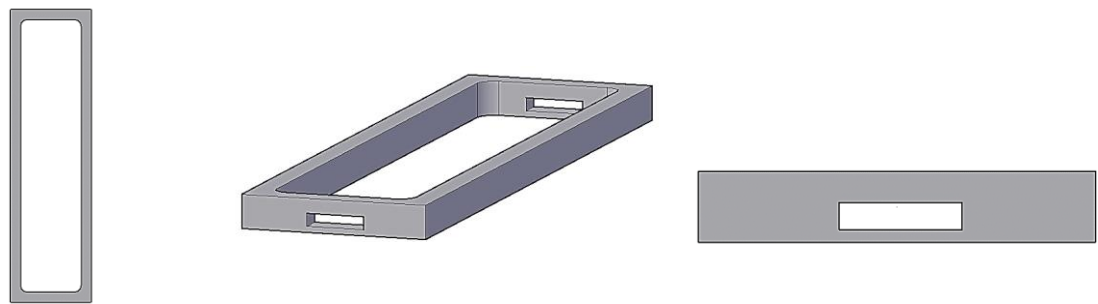


Fig. 46. Machined stainless-steel mold with slots view

Table 15. Composite matrix summary

Sample	Reinforcement	Surface treatment	Matrix	Hardness	Modulus
SMC 1				30 A	65
SMC 2		Low plasma radiation exposure	Poly(Ester-urethane) rubber	60 A	300
SMC 3	cEVA-DCP			80 A	400

The *thermal transitions exploration* of SMS was investigated by TA instruments SDT Q600 differential scanning calorimeter under N_2 atmosphere 50 ml min^{-1} . Thermal transition temperatures were scanned between $40 \text{ }^\circ\text{C}$ and $150 \text{ }^\circ\text{C}$ under a cooling and heating rate of $10 \text{ }^\circ\text{C min}^{-1}$.

The *Chemical verification* of the elastomer matrixes was performed by PerkinElmer ATR-IR spectrometer in the mid-infrared band from 400 to 4000 cm^{-1} at 4 cm^{-1} .

The *Mechanical response*, the *elongation at break* and *toughness* were measured using a Shimazu tensile tester at a strain rate of 10 mm min^{-1} , at room temperature. The samples evaluated keep a thickness of $2.5 \text{ mm} \times 6 \text{ mm}$. Several samples were evaluated to obtain a reasonable estimation of error.

The *adhesion* between reinforced lamina and polyurethane matrixes were performed to as-received and plasma treated samples through T-peel strength test, using a Shimazu universal tester at a strain rate of 10 mm /min-1 , at room temperature. A half the reinforced lamina was encapsulated and the other half was on the outside of the matrix, the matrix end and the reinforced end lamina were mounted between the clamps and stress-strain were recorded.

The *Shape memory stability* was performed by using a forced air convection Binder 9010-0196 oven equipped with a customized glass gate and an independent thermometer. Thermal cycles were performed according to the next procedure. The actuator was mounted inside the oven attached by a grip, a grid was placed behind the sample for tracking the actuator deformation via time-lapse photography as shown in Fig. 47.



Fig. 47
thermocycling
experiments
assembly
recording

Once the actuator was mounted, the glass gate and the thermometer was placed, and a digital video camera was set up outside according to [253]–[256]. The temperature of the cycling was defined according to the range selected in the programming process of the reinforcement lamina, and each of them was performed between the T_{low} and the T_{high} . The displacement distance was measured via time-lapse.

4.3

RESULTS AND DISCUSSION

In this section obtained results from activities set out in the methodology are presented and discussed. Results are arranged following the next order according to the defined experimental objectives:

- Shape memory lamina synthesis*
- Shape memory effect study*
- Functional composite synthesis*
- Thermocycling stability study*

SHAPE MEMORY LAMINA SYNTHESIS

Raw materials & crosslinking process

As defined in the introduction, 4.1 section, the encapsulation of a 2W-SSMP is defined as scope to improve the shape memory stability and define the direction of the movement to be used in actuator applications. In this work, a low-cost commodity polymer, with crystallizable/melting switching domains, ethylene-vinyl acetate copolymer and dicumyl peroxide as the crosslinking agent, were selected as raw materials to obtain a stable network, the chemical structure is shown in Fig. 48, to synthesize the shape memory component, designated as cEVA-DCP reflecting the DCP as thermal initiator used in the crosslinking process. Likewise, an ester-based urethane rubber, PU, is defined as the matrix as exoskeleton to ensure external stress reinforcement, further addressed below, defying in this way a thermally controlled functional composite system.

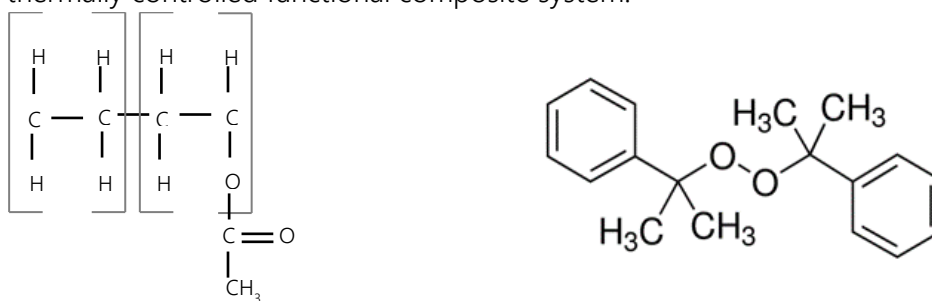


Fig. 48. Chemical structure of cEVA (pre-polymer) Left, and dicumyl peroxide (cross-linker agent) Right, Sigma Aldrich ®

Before reaching a thermally controlled composite, synthesis of 2W-SSMP reinforcement lamina into prestressed functionalized strips must be addressed. The Chemical characterization was carried out to verify the composition of the processed material, ATR-IR displayed in Fig. 49 reveals characteristic peaks of 2918, 2849, 1467, and 1371 cm^{-1} for CH₂. Besides, 1738, 1238, and 1020 cm^{-1} were found by the stretching of the carbonyl group (C=O), and the ester group (C-O). Some insignificant changes (0-4 cm^{-1}) in the peak position were seen, not for the material composition, but for the experimental spectral resolution; the spectra were compared with the *PerkinElmer polymers library*, and a coincidence of 99.56 % was reached. Effectively a crosslinked PE copolymer with 18% of vinyl groups, a thermosetting elastomer was obtained.

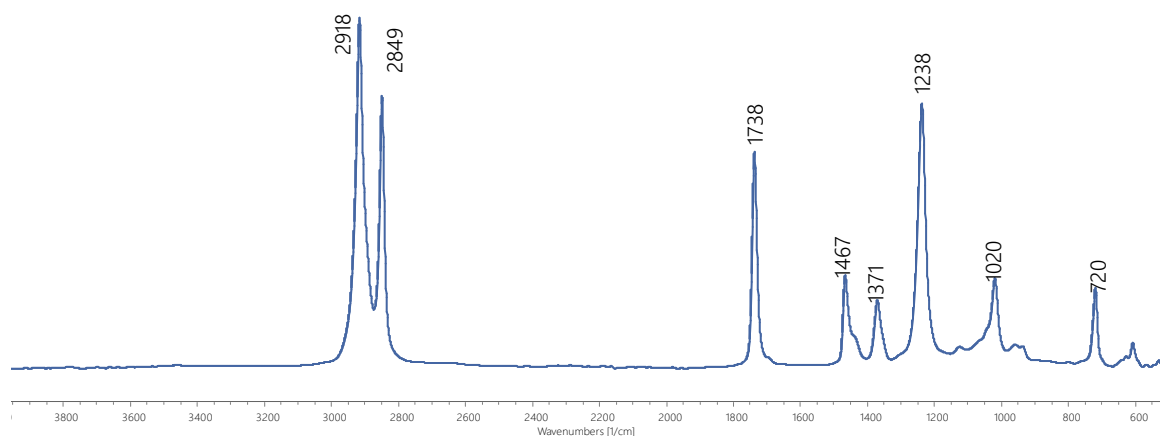


Fig. 49. ATR-IR spectra of cEVA with 18%Wt vinyl groups

Torque against temperature plot presented in Fig. 50 shows the thermally controlled blending process to avoid pre-curing of the batch. When the curve has stabilized, the blending process was finished. The drop in the torque between 1.9 and 2.2 min. Indicates the addition of the DCP 3%Wt. Thermal initiator into the blend once the cEVA pellets were melted and mixed, to guarantee the correct incorporation. According to previous studies [195], DCP 3%Wt addition has shown remarkable cyclability and the highest R_f values in cEVA networks, likewise, previous works were not clear about the step of the addition of the thermal initiator agent in the blend.

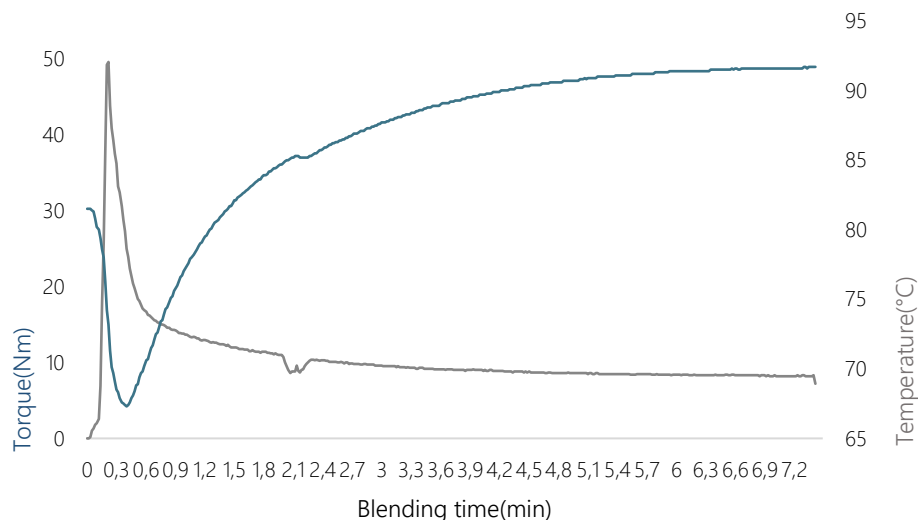


Fig. 50 Torque against blending time and temperature plot.

The reaction displayed in Fig. 51 shows the crosslinking reaction followed by the thermo-compression molding in accordance to Hirschl et al. [257], In the crosslinking process the decomposition of the DCP free radicals takes hydrogen, preferred from the terminal methyl CH_3 of the vinyl group side chain, letting reactive radicals in the cEVA network, the reactive radical bonds each other reaching chemical bonds between chains. The pale white and soft raw material before the curing process turns into a transparent and flexible but stable thermosetting elastomer as can be seen in Fig. 52.

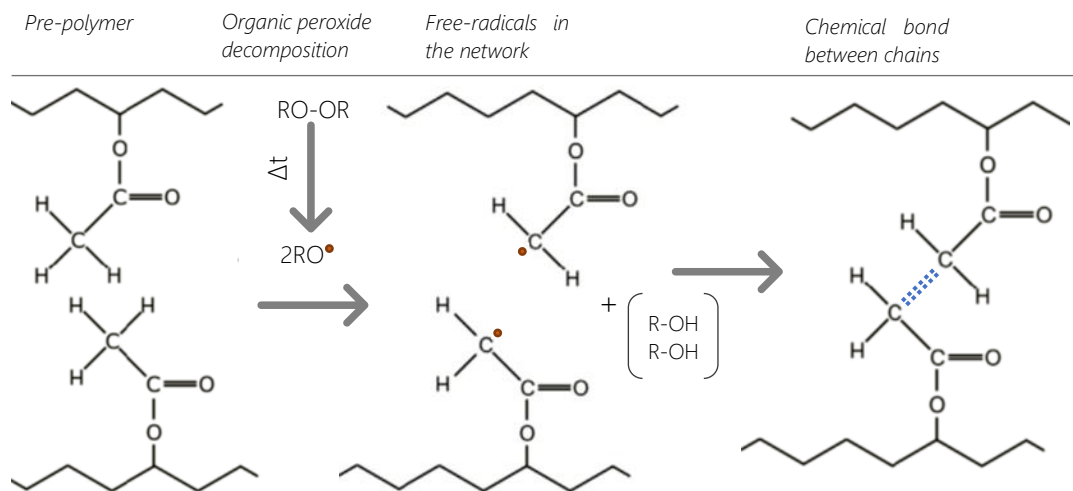


Fig. 51. Basic principle of the main curing reaction of cEVA during radical crosslinking. Adapted from [257]



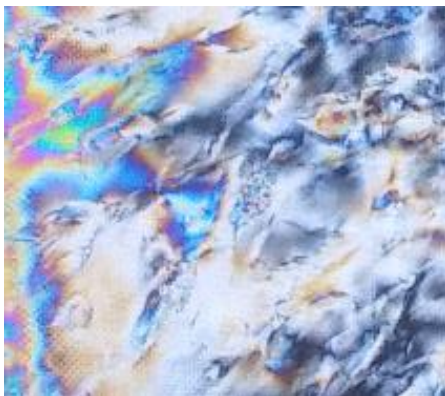
(A) Pristine cEVA



(B) Cured cEVA-DCP

Fig. 52. Raw material/processed material appearance.

Because of the obtain of sheets with a presence of residual stress after the thermo-compression molding, an annealing process was performed as stress releasing with satisfactory results. The optical appearance of the samples was verified before and after the annealing process by a polarizer sheet and a polarized light source as can be seen from Fig. 53. The visualization of different color fringes in the (A) picture is related to the change in the refraction index because of stress concentration; the fringes were not seen after the thermal annealing treatment (B).



(A) As-received



(B) Annealed

Fig. 53. Annealing process pictures

Thermomechanical properties

Thus far, several studies indicated that the crystallization and melting transitions have a straight influence on the shape memory effect in semicrystalline polymers, because of the phenomenon is partially drive by CIE and MIC as was addressed in section 2.3. Thermal properties of crosslinked cEVA were investigated by DSC and are presented in Fig. 54 and Table 16. Nonisothermal crystallization and melting curves of the uncrosslinked and crosslinked cEVA samples were recorded, the melting point at 86°C was identified in the second heating program and the crystallization temperature at 65.8°C in the first cooling as well, corresponding to the PE crystals population in the copolymer[258].

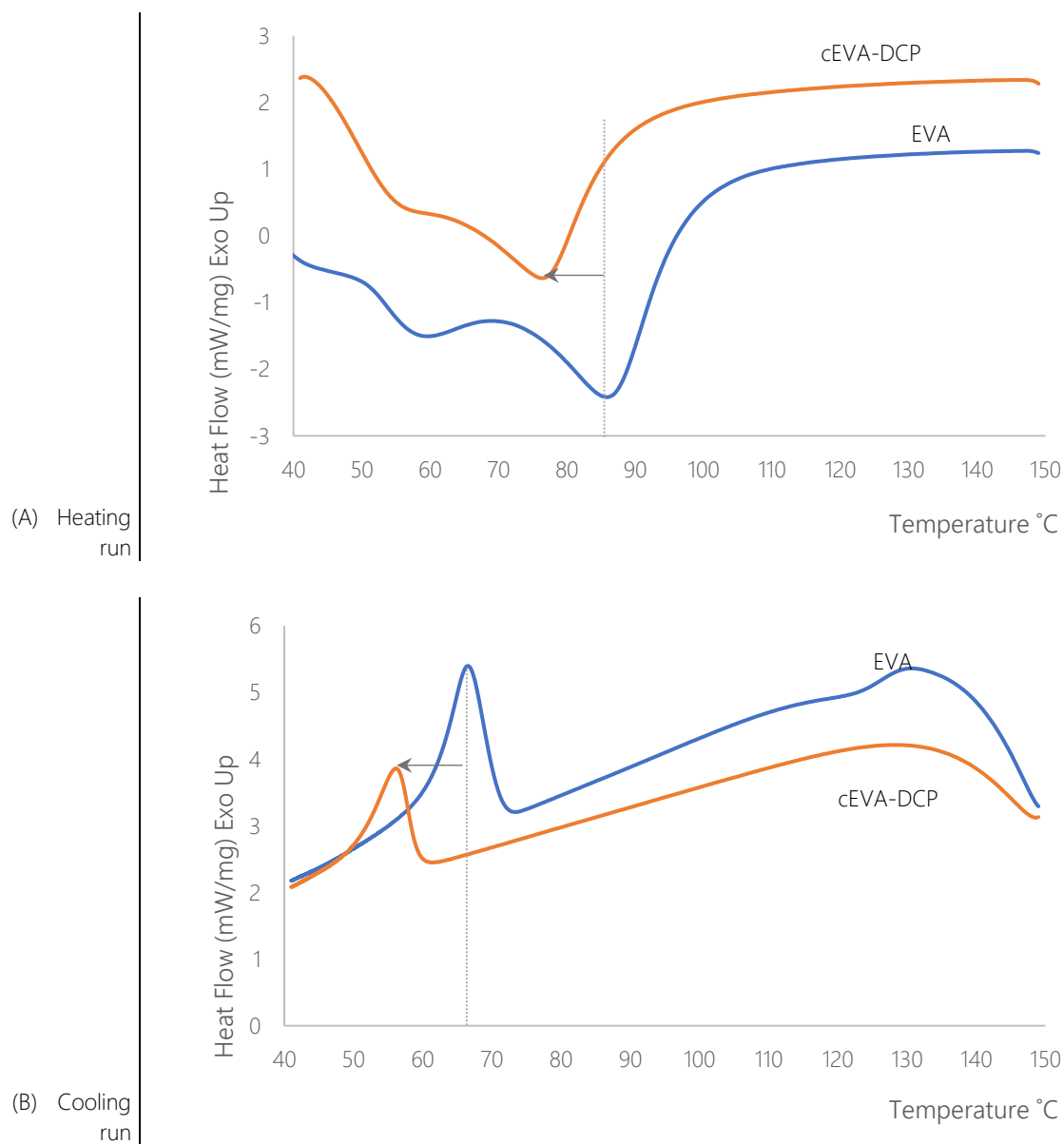


Fig. 54. Non-isothermal DSC curves of cEVA cured and pristine samples

According to DSC analysis, a decrease in the principal thermal transitions in the crosslinked samples can be seen in Fig. 54, T_m after crosslinking shifts to 75°C and T_c to 53,6°C and the intensity of the peaks decreases as well, respect to typical values of a pristine cEVA. This behavior may have been attributed to the dual constraining effect of chemical crosslinks, on the one hand, in the mobility of the polymer chains and on the other hand, on the growth of crystals [259], [260], reason why the overall transition temperature decreases because fewer crystals were formed in the crosslinked network.

Table 16. Thermomechanical properties of the samples

Sample	T_m	T_c	X_c (%)	Young's modulus (MPa)	Tensile strength (MPa)	Elongation at break (%)
cEVA	86	65.8	21.42	10.06	19.46	1622,93
cEVA-DCP3	75	53.6	15.81	8.690	12.25	946.44

Two transition temperatures may exist in the cEVA-DCP which need to be further conformed. So that, dynamic thermomechanical analysis was performed to explore the temperature-dependent properties of the samples directly related with the shape memory behavior.

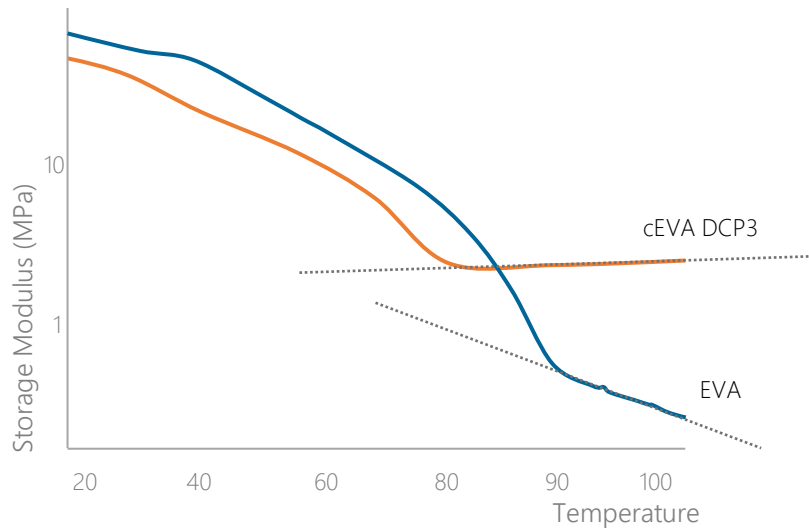


Fig. 55. DMTA Test for cured and pristine EVA samples.

The behavior of the storage modulus at different temperatures is provided in Fig. 55, a noticeable difference in the storage modulus in cured and pristine samples can be seen. In the pristine sample, the modulus above T_m decreases near to 0MPa, and exhibits flow behavior after the melting transition, because of their thermoplastic nature, the molecules slippage each other. In the case of the crosslinked sample, once the temperature is above T_m , a rubbery plateau is reached up to 1 MPa. The crosslinks in the samples define a stable structure of the network, pre-requisite to exhibit the shape memory effect phenomenon, thereby the slippage of molecular chains is restricted maintaining a certain level of strength.

The average value of the elongation at break point, young’s modulus and tensile strength of the samples are presented in Table 16. The effect of the crosslinks into the mechanical properties of the samples was also verified through stress-strain experiments as can be seen in Fig. 56. Crosslink influenced the elongation at break, and tensile strength, both decreases in cured samples, this trend could be attributed to the reduced self-adjustment ability of the chain segments because cured samples have a stable-network structure where crosslinks act as mobility blockage.

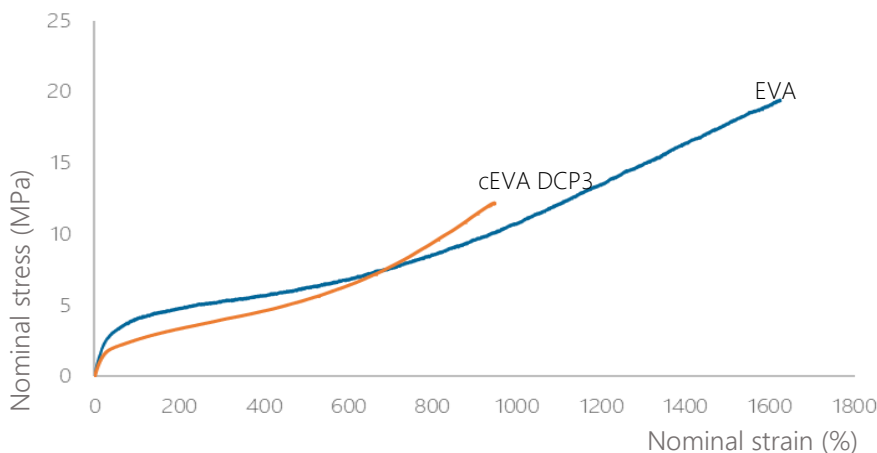


Fig. 56. Stress-Strain curves, pristine and crosslinked EVA

What was obtained

As was verified through the thermomechanical evaluation, a stable polymer network by molecular crosslinking with stimulus-sensitive domains was reached. In the network, the stimulus domains are the crystalline segments sensible to a thermal stimulus, where the response of the system is driven by a crystallization / melting transition, molecular pre-requisites to evidence the shape memory effect phenomenon.

SHAPE MEMORY *effect* STUDY

As was described in section 3, the shape memory effect SME in polymers is not an intrinsic property; the effect is the result of a molecular structure with specific processing conditions. For those reasons, with the aim of identifying the influence of processing parameters: stress load and programming and cycling temperatures in the SME, once a molecular structure capable of exhibiting this effect was reached, shape memory effect experiments were performed.

At first step, Temperature programming conditions were explored by DSC analysis of the cured samples. The melting transitions were explored in the non-isothermal second heating run, and the melting peak of PE crystals was identified between 40°C and 95°C, as shown in Fig. 57.

According to Lendlein et al. [243], external stress must be applied when crystals are entirely melted and must be held cooling down until crystallization temperature was reached, to perform a correct shifting shape fixation. Hence, the shifting shape fixation temperatures for cured cEVA-DCP samples were defined as $T_{prog}=95^{\circ}C$ where crystals are entirely melted to correctly induced a shifting shape, and then cooling down below T_c and $T_{sw} = 40^{\circ}C$, to guarantee the formation of the crystalline scaffold responsible of the shifting shape fixation.

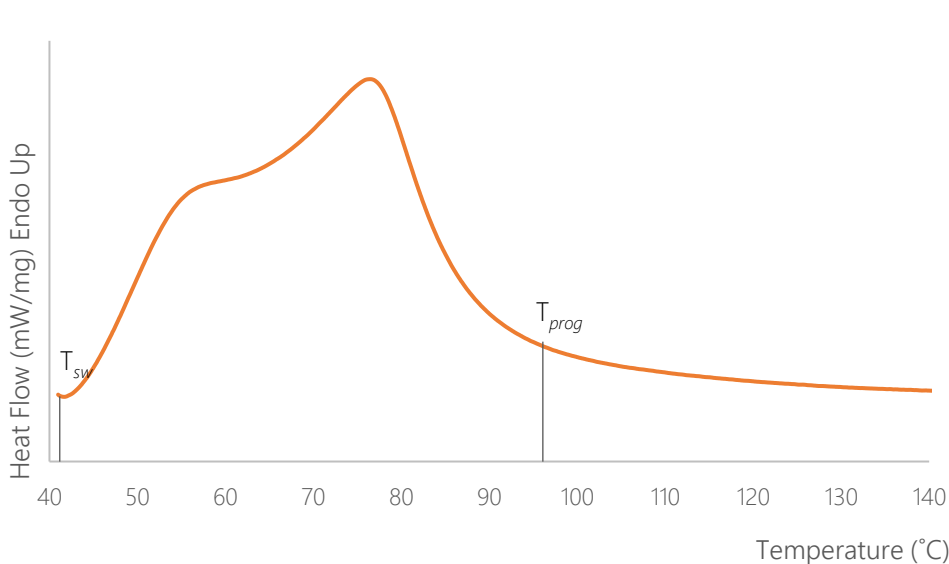


Fig. 57. Second heating DSC run T_{low} and T_{high} Temperatures

Once the programming temperature for the shifting shape fixation was defined, the influence of the stress programming levels and cycling temperatures were simultaneously evaluated through shape memory experiments. At first, various stress programming levels $\sigma= 300,550, 750, 850$ kPa with a small loading rate of $5mm\ min^{-1}$ to minimize creep effect under constant stress conditions, were used to perform the shifting shape fixation prior the experiment; then, samples were cycled between temperatures above T_{sw} and below T_{prog} .

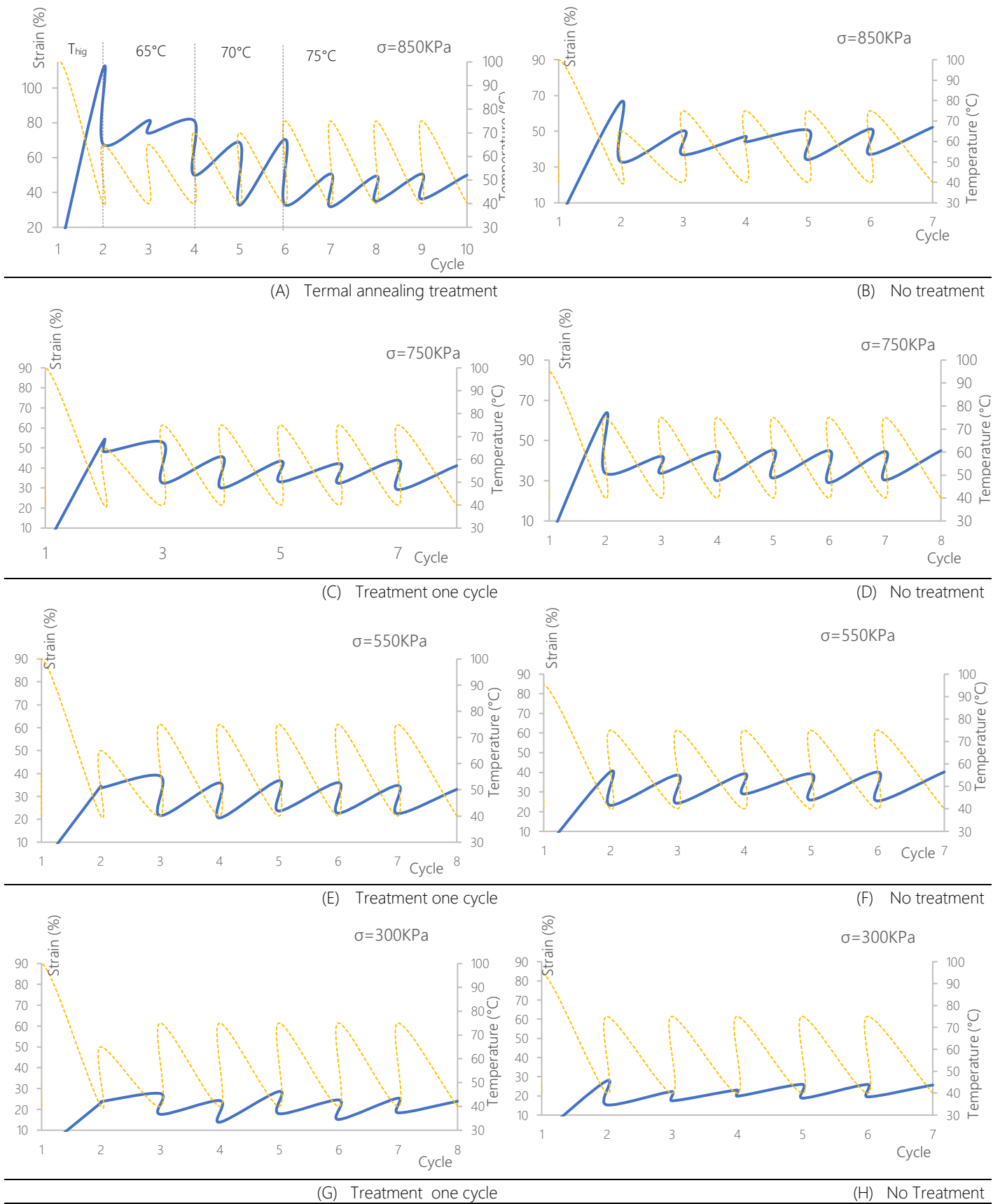


Fig. 58. Two-Way shape memory test under several stress programming levels

Fig. 58 presents the summary results of the evolution of the strain against temperature during each shape memory cycle. From the curves in Fig. 58, a direct relation between programming stress and the generated strain is noticed. The highest reversible strain 31.3% was detected at the highest programming stress 850 kPa as can be seen in Fig. 58 (A), The reversible effect was achieved all over the stress programming levels evaluated, in fact, programmed samples under the lower stress level 300 KPa led to reach strain up to 8%.

Can be observed that the explored tension range was located above the critic stress level needed to trigger the shape memory effect in cEVA-DCP cured samples, nevertheless the effect is displayed more evident at higher load levels, this behavior may due to more align crystalline segments were reached, but it need to be further confirmed. Moreover, the obtained lower strain in shape memory experiments can be compared to the max. strain reported in shape memory alloys, for instance NiTi 6%- 8% [261], [262].

The effect of the cycling temperature is also presented in Fig. 58, the cycles were conducted between 40°C to 75°C in all the samples, pre-heating treatment at lower temperatures of 60°C y 70°C were performed to improve the fixing of the shifting shape and slightly effect was noticed. Pre-heating treatment was previously assessed by Quian et al. [195] , and improvement of the effect, as well as an increase in the upper temperature, were reported.

The high reversible strain was found at 35 °C to 70 °C to 35°C cycling temperatures as can be seen in Fig. 58 (A), in the T_{high} exploration meanwhile, the T_{high} temperature was increased near to T_m , the polymer chains are less restricted. On the one hand, the original shape is more recoverable because the systems have more entropic energy, on the other hand, the shifting shape cannot be fixed because the scaffold as a path is not enough. However, was identified that when the temperature is above 70°C, the remaining crystalline components cannot be able to orient the free chain, thereby inducing the loss of reversible strain capacity, and temperature below 70°C the polymer chains does not have enough energy to trigger the recover.

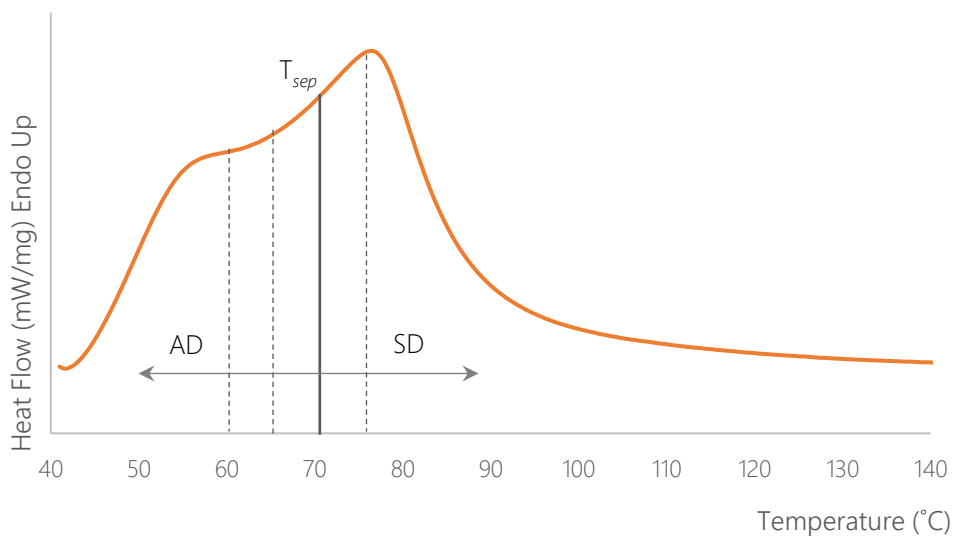


Fig. 59 Second heating DSC run Skeleton and actuator domains transitions for 2W-SME experiments

In this way, as can be seen in Fig. 59, 70°C was identified as the T_{sep} temperature which defines SD and AD range for the cEVA-DCP cured samples, in the case of SD at this temperature, the high strain is generated under cooling because the scaffold can be maintained with the crystals unmelted at this point.

In the case of the AD, on the one hand at 70°C, the crystals are partially melted, and the energy supplied to the network is enough to recover the original shape partially by a flexible entropy process. On the other hand, the melted crystals under cooling have the path to crystallize in a preferred orientation because of the SD. Hence this T_{sep} were selected to perform the temperature cycle for the shape memory stability of the shape memory composite.

As Fig. 60 shows, when DSC traces from samples under various stress programming levels were compared, the process presents, for the primary melting run, a narrower and more pronounced peak as the value of the applied stress increases. The peak corresponding to the secondary melting process becomes less significant and disappears entirely for the highest load.

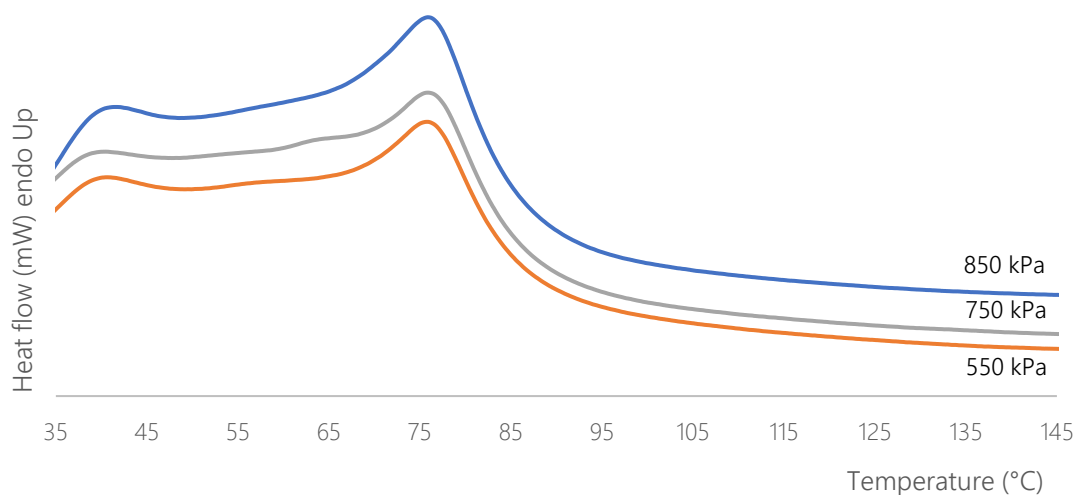


Fig. 60. DSC first heating ramp. Various programming stress level

It is therefore suggested that the application of higher values of load leads to the nucleation of a more ordered crystal structure, but it need to be further confirmed. When the sample is heated again, a second heating trace as the previously reported is found for all cEVA-DCP samples independently from the values of stress applied during cooling. The results suggest nevertheless only slight changes in the heat of fusion, which is higher for the samples subjected to stresses of 750 kPa and 850 kPa than that measured for lower stress levels.

Once various shape memory experiments were performed, the programming conditions which enlarge the phenomenon in cEVA-DCP cured samples were identified. High programming stress values lead to obtaining high reversible strain, and the temperature which defines the correct AD and SD formation were identified to be applied in thermocycling experiments of the samples.

What was obtained

FUNCTIONAL COMPOSITE SYNTHESIS

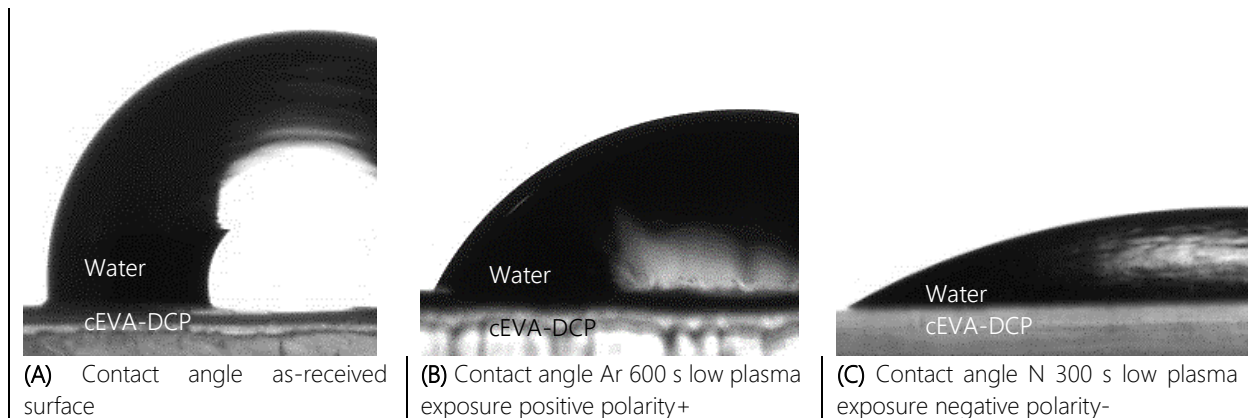
Surface functionalization

According to the identified approach in section 4.1, the improvement of the SME stability and the control of displacement of semicrystalline polymers in actuator applications, a prestressed encapsulation of cEVA-DCP layers into various poly Esther-urethane rubber matrix was proposed. Nevertheless, before the encapsulation process, a surface functionalization must be made due to the low energy surface in Ethylene-vinyl acetate copolymer with the aim to improve their wettability.

Low plasma discharge has shown favorable results into the surface wettability in polymers as an alternative to high-risk chemical treatments for water and soil. In this way, low plasma discharge was performed to cEVA-DCP cured and programmed samples under two inert atmospheres Ar and N₂ with different polarity and exposure time as was defined in the methods section.

Contact angle measurements between water and as-received and treated samples were performed according to Good [263] and Owens & Wendt [264] as shown in Fig. 61. (A) contact angle in the as-received sample and water up to 90° can be seen, the water advancing contact angles decreasing in response of the atmosphere and time exposure (B) y (C) reaching lower levels up to 10° indicating that the treatment has an effect in the surface. Contact angle and surface energy measurements are presented in Fig. 62 and Fig. 63.

Fig. 61 Contact angle water/cEVA-DCP pictures



A linear tendency was identified in the Ar positive polarity plasma, as shown in Fig. 62 when the exposure time increase, a progressive decrease in the contact angle (increase in the surface energy) were found. Nevertheless, on the one hand, the lower contact levels were not found under Ar atmosphere, on the other hand, inhomogeneities were found in the surface may due to the dispersion of the ions in the treatment under the positive polarity of the reactor as shown in Fig. 64. (A).

In the case of N₂ atmosphere under positive polarity, 300 s was found as the critical time of exposure where low contact angle measurements were reached. Higher exposure times increase the contact angle again; this trend could be attributed to a physical smoothing effect of the ions in the surface because of the long-term exposure, where the etchings created in the surface were erased again, but it needs to be further confirmed.

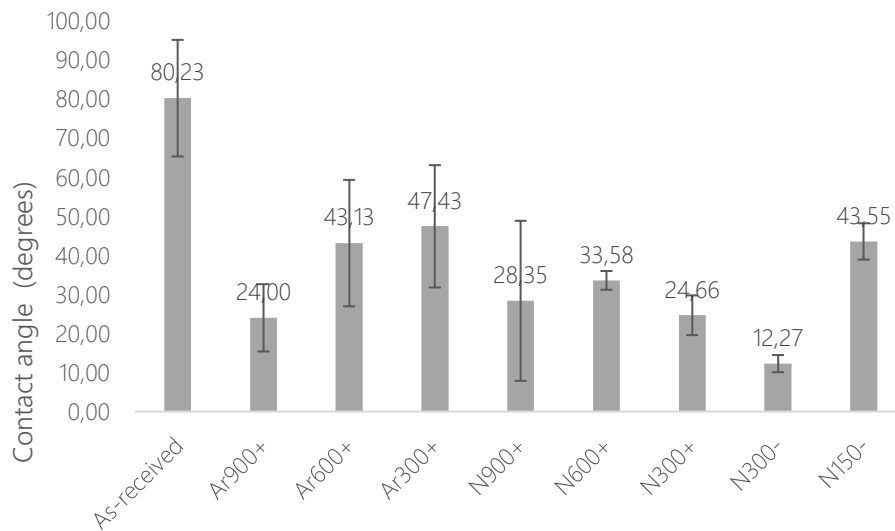


Fig. 62. Contact angle as-received and after low plasma exposure

Fig. 63 compares the surface energy levels reached by the plasma treatment, negative polarity exposure under N₂ atmosphere was shown favorable results, the surface energy increases to 71,16 mJ/m² (the higher value reached), N₂ (-) has shown lower deviation and more uniform treated surfaces under the same exposure times, this effect may due to the concentration of radiation under the negative polarity plasma exposure, as shown in Fig. 64 (B). Lower exposure time under (-) polarity was performed, and the surface energy decreases at 150 s, this time was found not enough to rises the surface energy, yet, the effect was more effective than 600 s of Ar (+) polarity exposure.

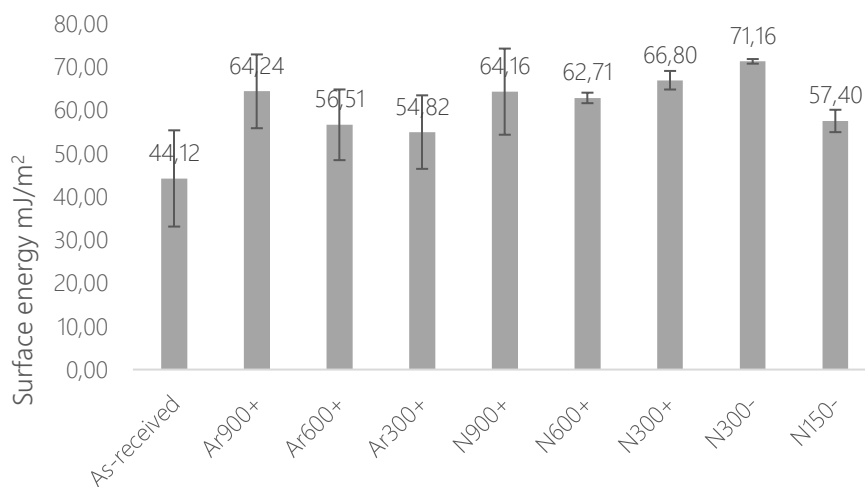
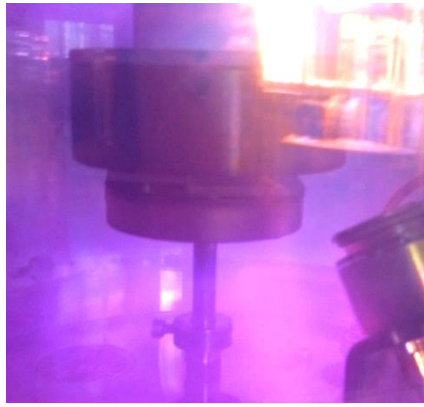


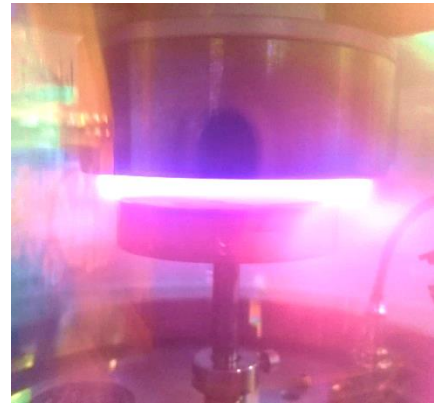
Fig. 63. Surface energy as-received and after low plasma exposure

It is suitable to remember the effect of plasma treatment above polymers surface; the plasma radiation can produce chemical and physical modification of the surface up to several nanometers deep without altering the bulk properties. Effects such as cleaning, etching, crosslinking and activation of the surface can be found because of the mixture of UV radiation, ions, electrons, atoms, and free radicals between electrodes as shown in Fig. 64.

Fig. 64 Low plasma discharge reactor appearance



(A) Positive polarity glow discharge



(B) Negative polarity glow discharge

The chemical effect on the treated surfaces was assessed by ATR-IR spectra taken in a PerkinElmer infrared spectrometer following the methods section, as can be seen in Fig. 65 (C) the overall intensity of the 1738 cm^{-1} decreases but the width of the band increases due to C=O bonds of vinyl acetate groups indicating the formation of new oxygen-containing moieties on the cEVA-DCP surface. A similar effect is noticed at 1020 cm^{-1} , where the overall intensity of the peak and the width of the band increases because of the formation of new C-O bonds, at the surface as shown in Fig. 65 (D), these polar groups have been found in the treatment of Polycarbonate films under low-plasma glow discharge [265]. Some insignificant changes ($0\text{-}4\text{ cm}^{-1}$) in the peak position were seen, not for the material composition, but for the experimental spectral resolution.

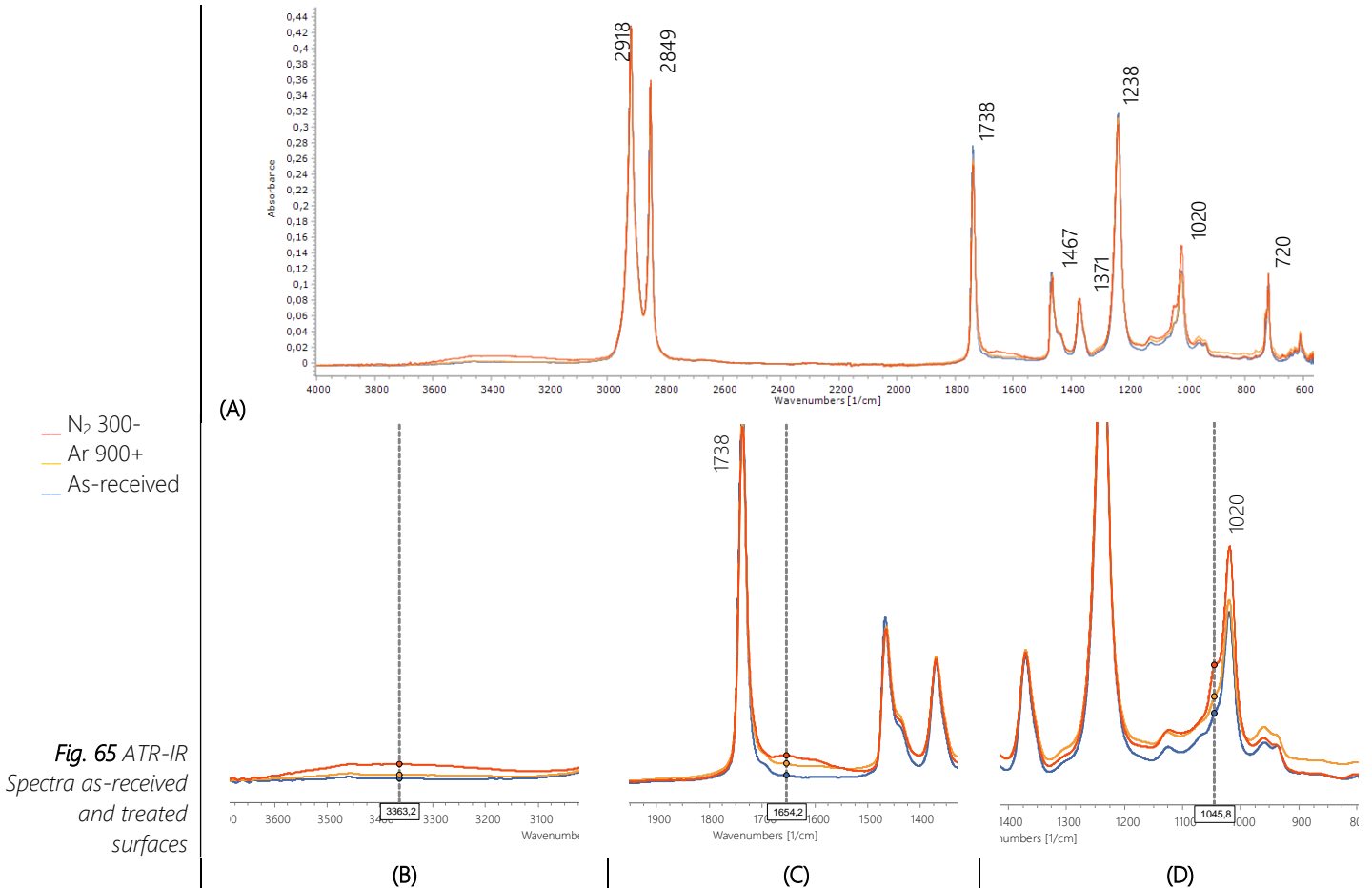


Fig. 65 ATR-IR Spectra as-received and treated surfaces

Fig. 65 (B) displays the creation of a new broader peak of hydroxyl groups O-H [266], on the treated surface under 300 s N₂ and negative polarity. Therefore, these new polar groups are responsible for the surface activation enhancing their wettability by an increase of the surface hydrophilicity of the cEVA-DCP films.

The physical effect on the treated surfaces was assessed by roughness profiles taken in an **XX** rugosimeter following the methods section. Fig. 66 provides the longitudinal and transversal profiles taken from as-received, and treated surfaces, the peak-to-valley that exceed two μm found in all samples can be associated with the thermocompression molding process because of the marks of the coated polytetrafluoroethylene fabric used to avoid the adhesion to the mold. The peak-to-valley roughness below 1 μm found in treated samples shown in Fig. 66 (C) (D) may be due to the etching effect of the plasma exposure in the surface, but it need to be further confirmed.

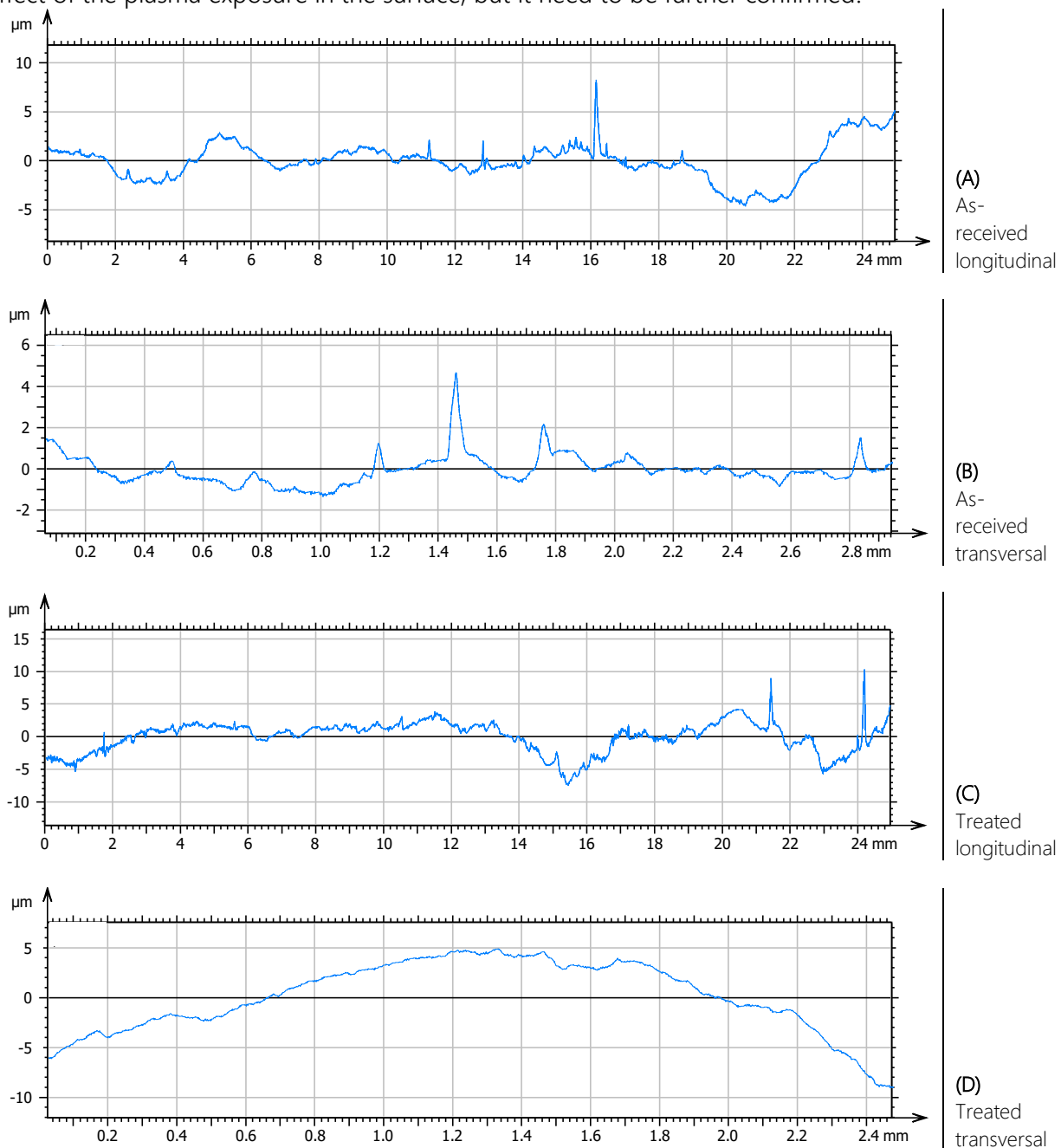


Fig. 66
Roughness profiles. As-received and treated samples

What was obtained

These results suggest that the enhanced on the wettability of the treated surfaces is related to both chemical and physical effect. On the one hand, due to the increase in the hydrophilicity because of the new polar groups generated into the surface, on the other hand, the etching generated on the surface which raises the surface area and promotes the mechanical keying.

Raw materials and synthesis

Focused on the improvement of the shape memory stability to actuator applications, a composite material based on a prestressed crosslinked cEVA lamina, two-way shape memory semicrystalline polymer, encapsulated into polyurethane rubber matrixes with different toughness was reached, with the aim of guarantee the shifting shape obtained by the CIE through thermal cycles.

Various poly Ester-urethane matrixes were selected because of material in the rubbery state flexible enough to comply when the SMP lamina recover their permanent shape upon heating is needed, but also with the toughness to keep the encapsulate lamina straight during cooling. Ester based urethane rubber also has scratch and temperature resistance to perform thermal cycling, better thermo-oxidative stability and property retention at elevated temperatures.

In the first place, ATR-IR spectra were taken following the methods section to verify the chemical composition of the PU matrixes as shown in Fig. 67. Effectively a polyester urethane rubber was obtained after the polymerization by resin and catalyzer based on the taken spectra, characteristic peaks of stretching of 1729 C=O stretching of the ester-carbonyl group [267] were found. Some insignificant changes ($0-4\text{ cm}^{-1}$) in the peak position were seen, not for the material composition, but for the experimental spectral resolution. The slightly differences were found in the matrixes with have long soft segments in their composition which affects their hardness.

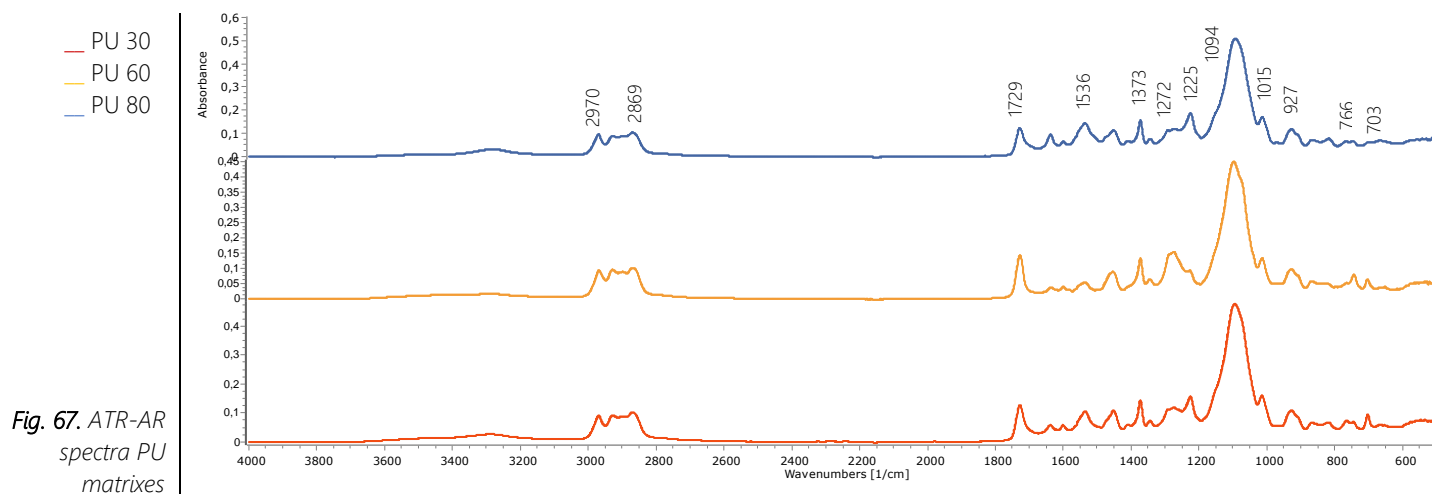


Fig. 67. ATR-AR spectra PU matrixes

Fig. 68 provides the curves obtained from the heating and cooling run analysis taken in an TA instruments differential scanning calorimeter following methods section. There is no evidence of thermal transitions as T_g or T_m in the thermal range explored, so the matrixes are effectively elastomers. At 75°C heat deflection temperature HDT was identified in all the samples, but it is located above the cycling thermal range performed in the shape memory stability experiments.

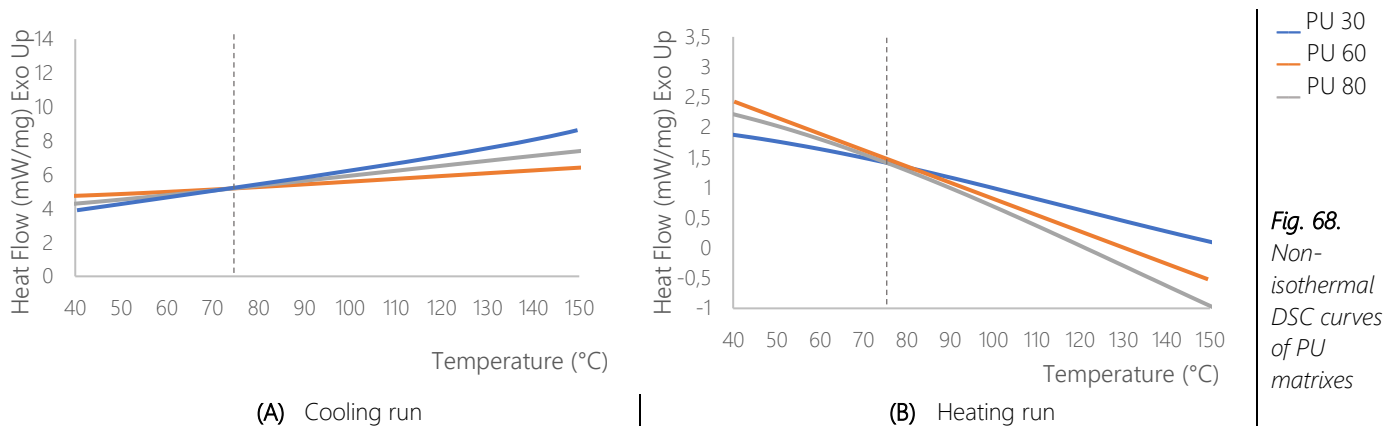


Fig. 68.
Non-isothermal DSC curves of PU matrixes

The mechanical behavior of the matrixes was investigated in a tensile test carried out at room temperature following the methods section. The results obtained are displayed in Fig. 69, the evaluated matrixes PU30, PU60, and PU80 are mechanically different rubbers, a relation between hardness, Young's modulus, and tensile strength was found, the sample with the lower hardness also have lower values of modulus and strength, similar behavior for all the samples can be seen in Fig. 69.

Nevertheless, significant elongation at break differences was not found, all the samples because of their rubbery nature presents elongation values above 1383 %. Therefore, all the samples can comply when the reinforced lamina start the recovery of their permanent shape. The average value of the hardness, elongation at break point, Young's modulus and tensile strength of the samples are presented in Table 17.

Table 17. Mechanical properties of the samples

Sample	Shore A hardness	Young's modulus (MPa)	Tensile strength (MPa)	Elongation at break (%)
PU30	30	0.44	0.66	1460
PU60	60	2.20	4.36	1612
PU80	80	3.00	8.16	1383

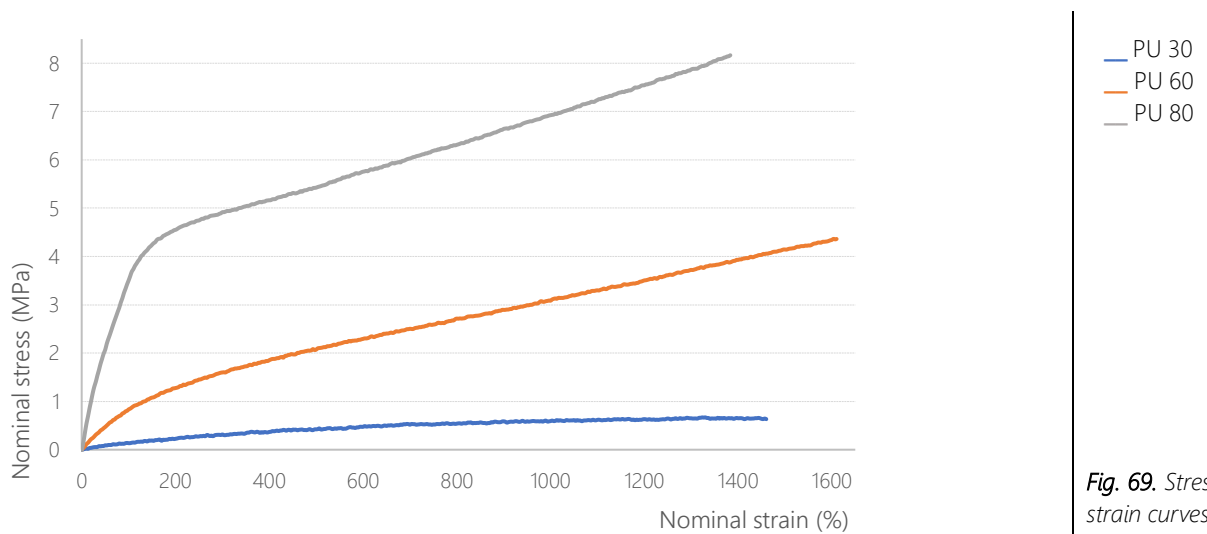


Fig. 69. Stress strain curves PU matrixes

Once the raw matrix materials were characterized, the functional composite material was synthesized following the steps highlighted in the methods section. The resulted geometry from the synthesis can be seen in Fig. 70 (A) multilayered beam actuators with different matrixes were reached Fig. 70 (B), shape memory composites SMC1 (PU30 matrix), SMC2 (PU60 matrix), SMC3 (PU80 matrix).

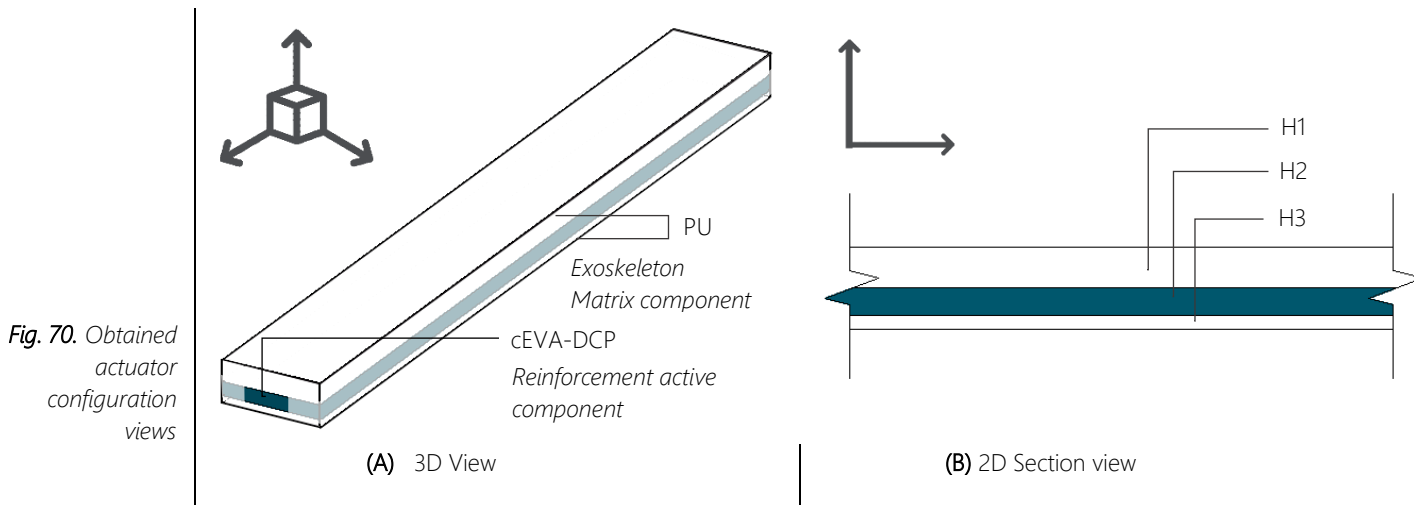


Fig. 70. Obtained actuator configuration views

As previously addressed, the stress load transference is a crucial fact to obtain the expected behavior in composite materials, in this way, the adhesion between the reinforcement lamina and the matrixes was assessed as the first step. T-peel strength test values were taken from functionalized (treated surface), and as-received encapsulated reinforcing lamina in a Shimadzu universal tester frame in accordance to methods section. Looking at Fig. 71, it is apparent that the treated samples group reported high strength values than the as-received group. The behavior of every SMC system was further analyzed as follow.

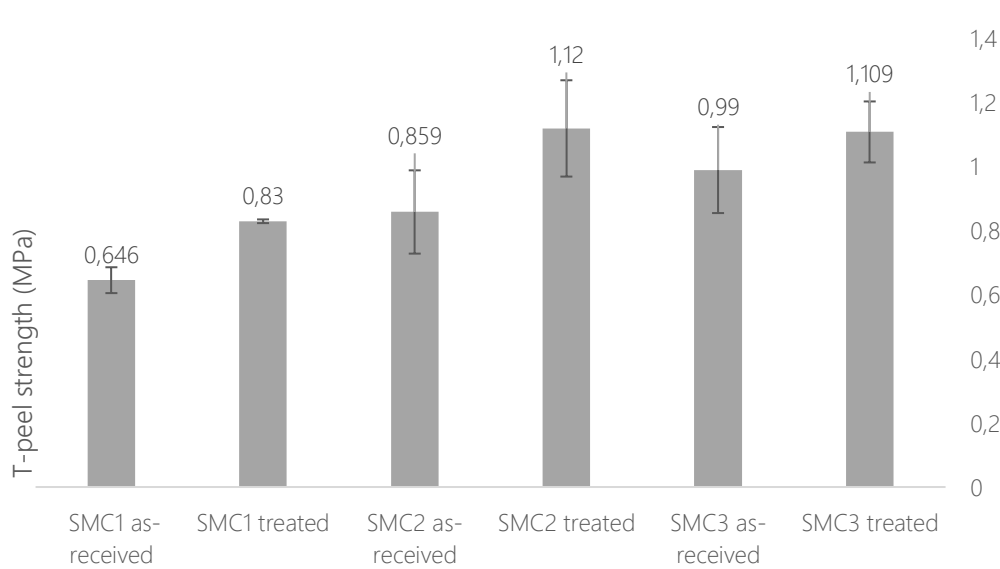
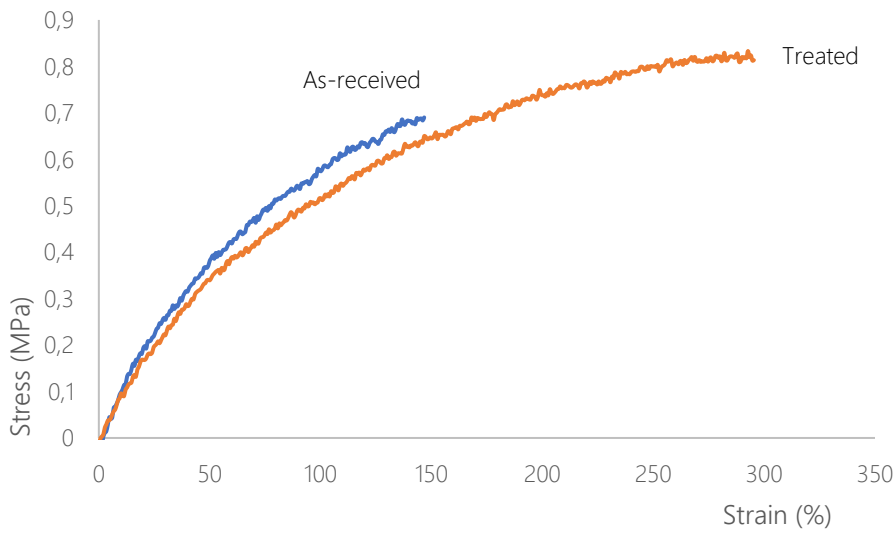
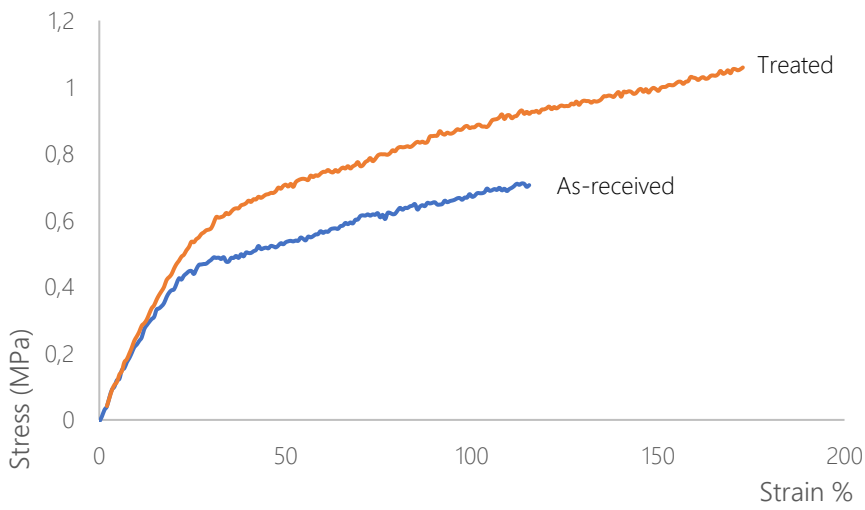


Fig. 71. T-peel strength values as-received and treated encapsulated composite

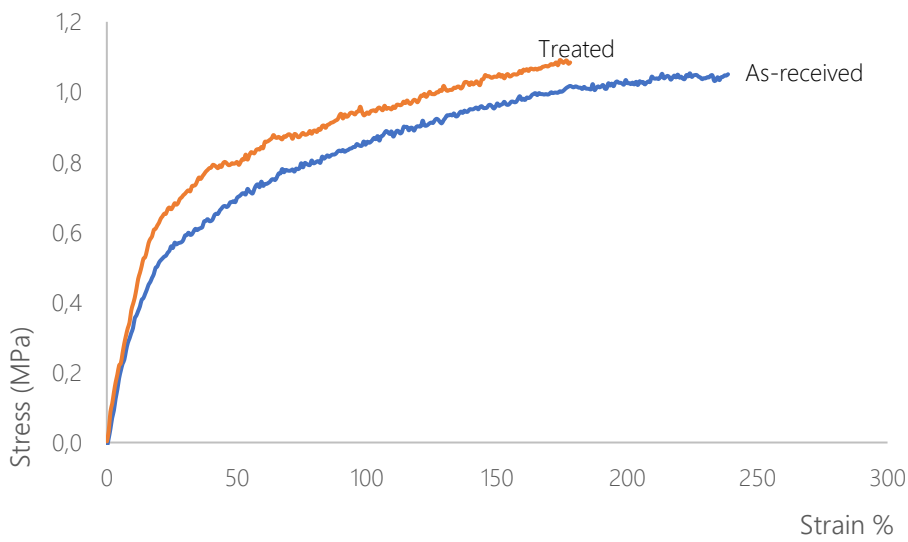
Fig. 72 (A) compares as-receives and treated SMC1 samples. the T-peel strength in the treated samples the lower slope curve is obtained because of a neck was formed in the unreinforced section



(A) SMC1 samples



(B) SMC2 samples



(C) SMC3 samples

Fig. 72. T-peel strength curves SMC treated and as-received samples

then, the neck progresses through the reinforced section and tractioned the interface zone starting the peeling process, the mechanical response is due to the matrix, as can be seen in video S1, *Section 4.5 Supplementary information*. In the as-received SMC1 samples, when the test starts, both matrix and reinforcement materials support the load reaching a higher slope, but the whole system fails sooner because of the interface region presents no opposition to the peel. No inflection point was found in the curves.

In the case of SMC2 and SMC3, matrix samples with a tensile strength above 4MPa a different behavior was observed. Two sections with different slopes and an inflection point were found as shown in Fig. 72 (B) (C). On the first section, a combined mechanical response between matrix and reinforcing was found, leading to getting a higher slope. On the second section the behavior was changed, a lower slope is reached because a neck was formed in the reinforcing lamina, it starts to reduced their transverse section and the interface fails, starting the peeling process as shown in Fig. 73 and S2, S3, S4 videos.



Fig. 73 T-peel after test samples. Left as-received, right treated

In this way, the mechanical behavior of SMC2 and SMC3 shows a combined mechanical response is shown up to 0,6 MPa is found.

THERMAL CYCLING

Once the adhesion of the as-received and treated samples was analyzed, thermocycling experiments were performed with treated samples, those reached higher adhesion values, and were recorded through time-lapse video following the methods section. The transverse displacement was measured tracking the expected actuation as shown in Fig. 74 by scaling the grid placed behind samples using a computer assistant drawing software.

The results of the thermocycling experiments can be observed in Fig. 74 to Fig. 77. During the experiments when the temperature rises, the composites turn to deform as bending in the expected direction and when the temperature goes down the composite return to their original/permanent shape. A two-way response in the first and high-grade repeatability in subsequent cycles was found during the experiment. Nevertheless, a different response was found in SMCX samples; behavior further addressed as follow.

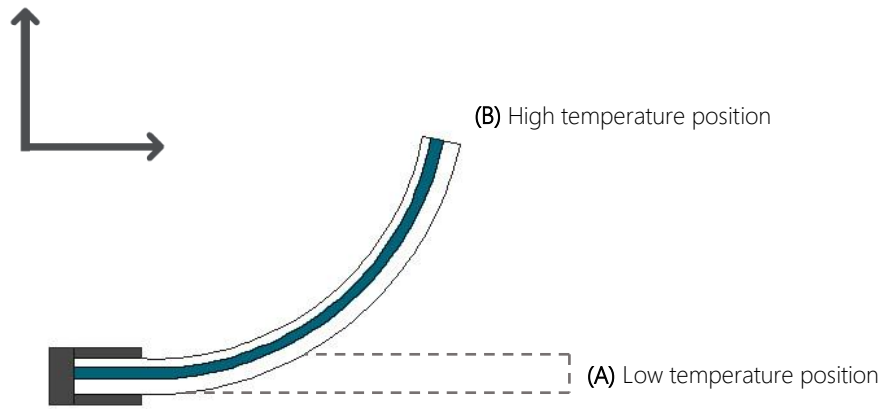


Fig. 74 Expected composite actuator response under thermal cycling

2D view

The actuation behavior in the first thermal cycle of SMC1 samples by pictures taken every 10 min. are summarized in Fig. 75. The experiment starts at room temperature and the temperature rises at $5^{\circ}\text{C min}^{-1}$ following the methods section. When the temperature rises to 45°C the sample starts to bend; although, the effect is more evident when 60°C is surpassed, and the full transverse displacement is observed at 70° . The most massive transverse displacement $64,56\text{ mm}$ where reached by SMC1 samples but the original shape does not be recover when the temperature is cooling down, in fact, by every new cycle the bending response is reduced, and the unrecoverable segment is increased as shown in Fig. 76 (A).

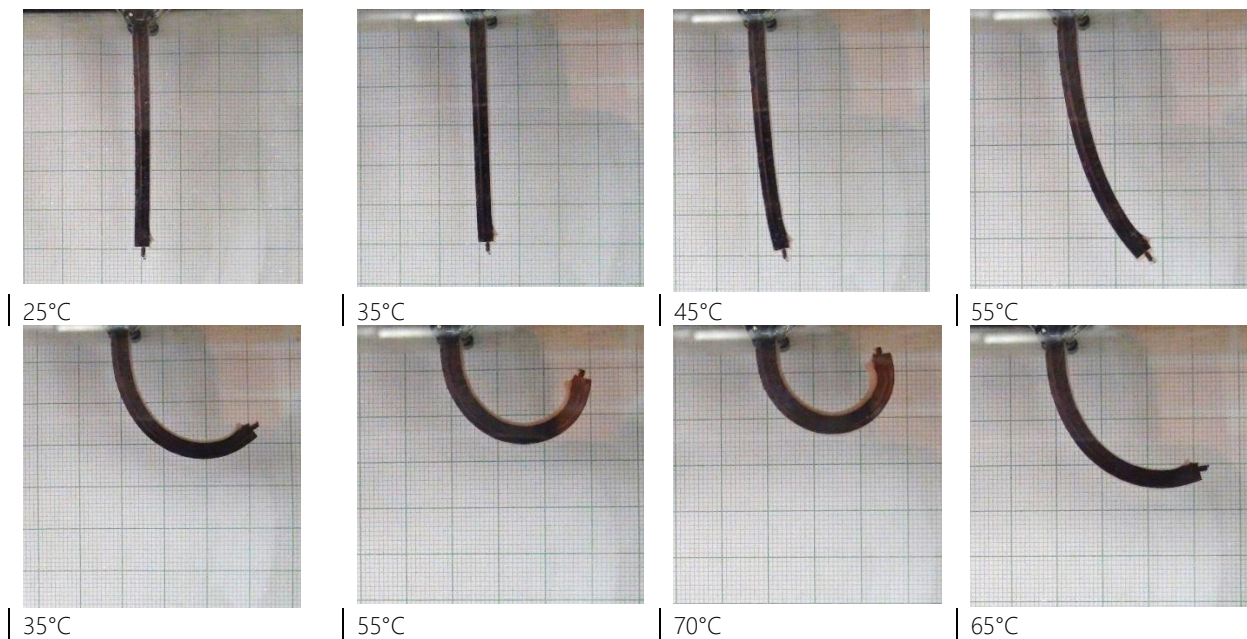
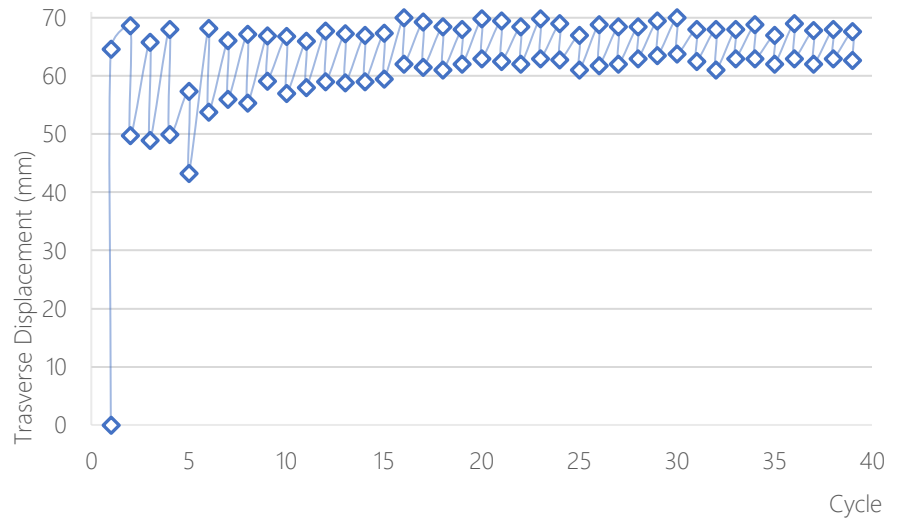


Fig. 75 Actuator response for the first thermal cycle SMC1 sample

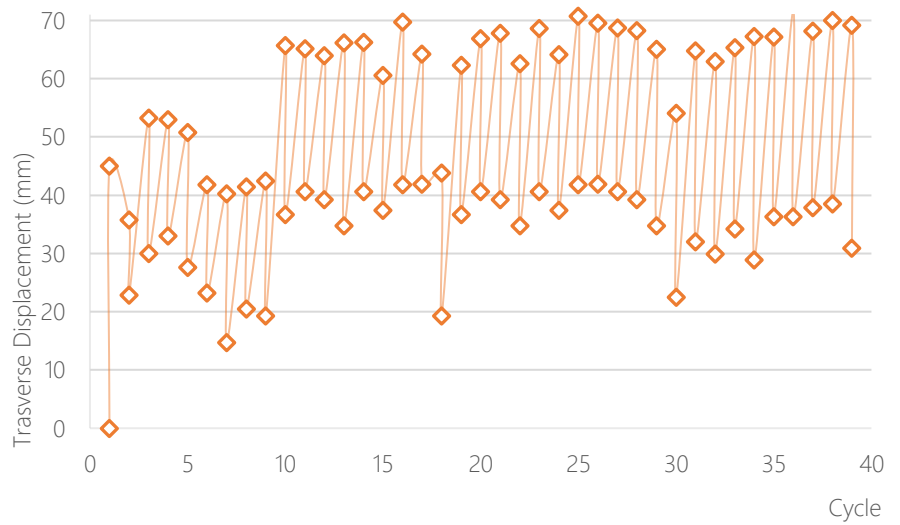
In the case of SMC2 samples, massive initial displacement is reached, but the unrecoverable segment is also found as shown in Fig. 77 and *video S4*, both initial transverse displacement and unrecoverable segment are less pronounced than SMC1 samples, and the response is more stable through the cycles. The highest bending actuation between cycles $38,35\text{ mm}$ is achieved by SMC2 samples as shown in Fig. 76 (B). The drop in the displacement values in 7, 18, 30, and 39 cycles is due to these were the first taken cycle of the day and starts at room temperature instead to starts at 35°C ; nonetheless, the transverse displacement behavior is similar through the experiment.

— SMC1
 — SMC2
 — SMC3

(A) SMC1



(B) SMC2



(C) SMC3

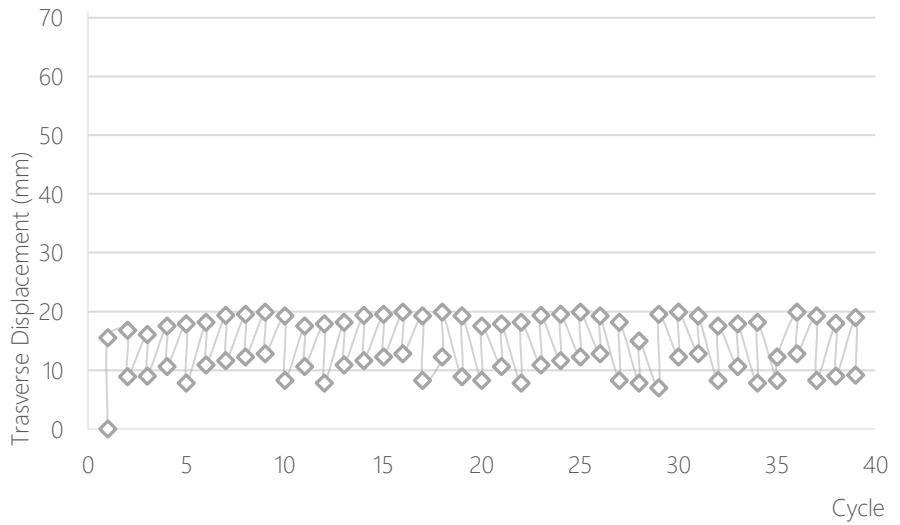


Fig. 76 Transverse displacement recorded during thermal cycling

Looking at Fig. 76 (C) it is apparent that substantial transverse displacement was not achieved by SMC3 samples as can be seen in *video S5*; nevertheless, the permanent shape was almost recovered in cooling cycles and the most stable bending effect ~ 10mm during the thermal cycling was found.

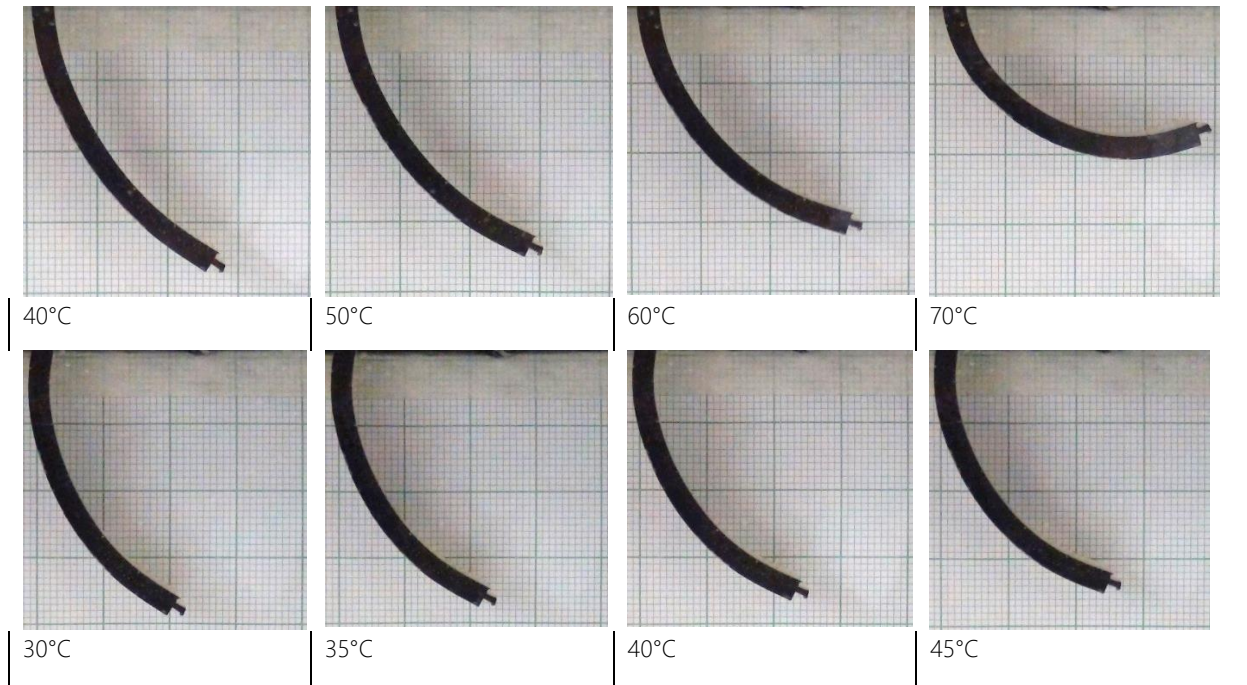


Fig. 77 second thermal cycle SMC2 samples

The behavior of the bending effect in the thermocycling experiments has two inflection points where the temporary shape is fixed, and the permanent shape is almost recovered. The temporary shape (highest transverse displacement) is reached up to 70°C temperature where the reinforced lamina crystals are partially melted. In the case of the permanent shape, at a temperature below 40°C the recovery of the shaping process (straight state), is most noticeable, may be due to at this temperature the crystalline segments of the reinforced lamina are crystallized in a preferred orientation allowing to reach that shape, but it needs to be further confirmed.

The differences in the SMCX samples during thermocycling experiments are directly related with the tensile strength, hardness and Young's modulus, lower values allow to obtain high transverse displacement, but the matrix cannot return to the original shape. Higher values lead to obtaining lower displacement values but more stable and reduced unrecoverable segments because of the matrix has the toughness to drive the reinforced lamina to their prestressed shape.

What was obtained

A further decay of the reverse effect was not seen when the number of cycles increase, just the differences found in the first cycles were evidenced.

4.4

CONCLUSIONS AND FURTHER WORKS

CONCLUSIONS

This section has presented the experimental study of a thermosensitive component through the synthesis of a composite based on a prestressed shape memory semicrystalline polymer. The purpose of this functional composite synthesis was to reach a displacement amplification, and a movement in a specific direction triggered through thermal differences that can be incorporated as an actuator without the need of electronic components into an architectural thermosensitive passive dynamic skin.

A directional bending movement driven by a crystallization induced elongation was achieved because of thermal variations as potential actuator based on a prestressed and functionalized shape memory polymer cured cEVA-DCP lamina encapsulated into poly (Ester-urethane) rubber with variation in hardness. After all, the following conclusions were obtained.

In accordance with the reinforcing shape memory lamina can be concluded:

To enhance the SME in cEVA-DCP cured samples the programming stress load must be up to 850kPa to obtain a reversible strain up to 30%.

AD and SD temperatures have an important role in achieving a two-way shape memory effect because of both drives partially the process of fixing and recovery of the shape.

In accordance with the shape memory composite SMC synthesis:

Surface wettability of cEVA-DCP cured samples can be enhanced by low-plasma exposure by the creation of polar groups in their surface.

The hardness, tensile strength, and Young's modulus have a significant effect on the thermosensitive behavior of reinforced shape memory composites as follows:

Matrix with hardness up to 30 Shore A conduct to obtain higher transverse values but just in the first cycle, can be used in applications where just one cycle must be performed.

Matrix with hardness up to 60 Shore A conduces to obtain the higher transverse displacement between thermal cycling, but an unrecoverable percent of the shape can be reached.

Matrix with hardness up to 80 Shore A lead to obtaining a more stable reversible bending actuation but higher transverse displacement cannot be achieved.

FURTHER WORKS

While this section presents an exploration into how programming processing parameters and encapsulating matrix hardness can be modified to obtain a directional movement, further development is needed to deep comprehend the phenomenon behind the effect and the uses of the material in real applications.

The study of the microstructure of the constituents and the interface region as well to know the mechanisms of the transfer of the load between the matrix and the reinforcement is needed because this is the crucial fact about the performance of the composite.

The toughness and Young modulus of the composite is still too low to be able to displace an architectural skin element. Nano-reinforcement to increase those properties must be developed.

Molecular customize must be done to adjust the thermal transition temperatures of the shape memory reinforcement to obtain bending displacement in response to the real temperatures (outside laboratory conditions), that can be found in an architectural skin.

Moreover, further development is needed to ensure actuator applications, as follow.

Further displacement amplifier methods such as flexible complaint mechanism, a type of mechanisms which the performance is based on the deformation of its members, which enlarge and allow the movement/actuation of more prominent elements is needed.

4.5

SUPPLEMENTARY INFORMATION

In this section audiovisual supplementary information access can be found

SUPPLEMENTARY VIDEOS

Please scan the following QR codes to access to the information.



S1



S2



S3



S4



S5



S6

4.6 REFERENCES

- [231] Y. M. Chen, P. Lin, Y. He, J. Q. He, J. Zhang, and X. L. Li, "Fast quantifying collision strength index of ethylene-vinyl acetate copolymer coverings on the fields based on near infrared hyperspectral imaging techniques," *Sci. Rep.*, vol. 6, no. 1, Aug. 2016.
- [232] Z. Zhang *et al.*, "Tunable shape memory behaviors of poly(ethylene vinyl acetate) achieved by adding poly(L-lactide)," *Smart Mater. Struct.*, vol. 24, no. 12, p. 125002, Dec. 2015.
- [233] H. Xie, L. Li, X.-Y. Deng, C.-Y. Cheng, K.-K. Yang, and Y.-Z. Wang, "Reinforcement of shape-memory poly(ethylene-co-vinyl acetate) by carbon fibre to access robust recovery capability under resistant condition," *Compos. Sci. Technol.*, vol. 157, pp. 202–208, Mar. 2018.
- [234] C. Qian, Y. Zhu, Y. Dong, and Y. Fu, "Vapor-grown carbon nanofiber/poly(ethylene-co-vinyl acetate) composites with electrical-active two-way shape memory behavior," *J. Intell. Mater. Syst. Struct.*, vol. 28, no. 19, pp. 2749–2756, Nov. 2017.
- [235] U. Nöchel, U. N. Kumar, K. Wang, K. Kratz, M. Behl, and A. Lendlein, "Triple-Shape Effect with Adjustable Switching Temperatures in Crosslinked Poly[ethylene-co-(vinyl acetate)]," *Macromol. Chem. Phys.*, vol. 215, no. 24, pp. 2446–2456, Dec. 2014.
- [236] M. Behl, K. Kratz, U. Noechel, T. Sauter, and A. Lendlein, "Temperature-memory polymer actuators," *Proc. Natl. Acad. Sci.*, vol. 110, no. 31, pp. 12555–12559, Jul. 2013.
- [237] L. Ionov, "Polymeric Actuators," *Langmuir*, vol. 31, no. 18, pp. 5015–5024, May 2015.
- [238] S. Iamsaard *et al.*, "Conversion of light into macroscopic helical motion," *Nat. Chem.*, vol. 6, no. 3, pp. 229–235, Mar. 2014.
- [239] Q. Ge, C. K. Dunn, H. J. Qi, and M. L. Dunn, "Active origami by 4D printing," *Smart Mater. Struct.*, vol. 23, no. 9, p. 094007, Sep. 2014.
- [240] O. Dolynchuk, I. Kolesov, and H.-J. Radusch, "Shape-memory actuators on the basis of binary and ternary blends of polyethylenes," 2015, p. 030002.
- [241] K. K. Westbrook *et al.*, "Two-way reversible shape memory effects in a free-standing polymer composite," *Smart Mater. Struct.*, vol. 20, no. 6, p. 065010, Jun. 2011.
- [242] J. Brandrup, *Polymer handbook*. Norwich, NY: Knovel, 2005.
- [243] A. Lendlein and M. Behl, Eds., *Shape-memory polymers*. Heidelberg ; New York: Springer, 2010.
- [244] D. Hull and T. W. Clyne, *An introduction to composite materials*. Cambridge: Cambridge University Press, 2003.
- [245] E. N. Bolbasov *et al.*, "Surface modification of poly(L-lactide) and polycaprolactone bioresorbable polymers using RF plasma discharge with sputter deposition of a hydroxyapatite target," *Mater. Lett.*, vol. 132, pp. 281–284, Oct. 2014.
- [246] L. S. Barbarash *et al.*, "Surface modification of poly-ε-caprolactone electrospun fibrous scaffolds using plasma discharge with sputter deposition of a titanium target," *Mater. Lett.*, vol. 171, pp. 87–90, May 2016.
- [247] S. I. Tverdokhlebov *et al.*, "Modification of polylactic acid surface using RF plasma discharge with sputter deposition of a hydroxyapatite target for increased biocompatibility," *Appl. Surf. Sci.*, vol. 329, pp. 32–39, Feb. 2015.
- [248] E. M. Liston, L. Martinu, and M. R. Wertheimer, "Plasma surface modification of polymers for improved adhesion: a critical review," *J. Adhes. Sci. Technol.*, vol. 7, no. 10, pp. 1091–1127, Jan. 1993.
- [249] S. Yoshida, K. Hagiwara, T. Hasebe, and A. Hotta, "Surface modification of polymers by plasma treatments for the enhancement of biocompatibility and controlled drug release," *Surf. Coat. Technol.*, vol. 233, pp. 99–107, Oct. 2013.
- [250] C. Cepedajimenez, "Surface modifications of EVA copolymers by using RF oxidizing and non-oxidizing plasmas," *Surf. Coat. Technol.*, vol. 174–175, pp. 94–99, Sep. 2003.
- [251] M. D. Landete-Ruiz and J. M. Martín-Martínez, "Surface modification of EVA copolymer by UV treatment," *Int. J. Adhes. Adhes.*, vol. 25, no. 2, pp. 139–145, Apr. 2005.
- [252] K. K. Chawla, *Composite materials: science and engineering*, 3rd ed. New York: Springer Science+Business Media, 2012.
- [253] S. Chen, J. Hu, and H. Zhuo, "Properties and mechanism of two-way shape memory polyurethane composites," *Compos. Sci. Technol.*, vol. 70, no. 10, pp. 1437–1443, Sep. 2010.
- [254] S. Chen, J. Hu, H. Zhuo, and Y. Zhu, "Two-way shape memory effect in polymer laminates," *Mater. Lett.*, vol. 62, no. 25, pp. 4088–4090, Sep. 2008.

- [255] H. Tamagawa, "Thermo-responsive two-way shape changeable polymeric laminate," *Mater. Lett.*, vol. 64, no. 6, pp. 749–751, Mar. 2010.
- [256] T.-H. Kang, J.-M. Lee, W.-R. Yu, J. H. Youk, and H. W. Ryu, "Two-way actuation behavior of shape memory polymer/elastomer core/shell composites," *Smart Mater. Struct.*, vol. 21, no. 3, p. 035028, Mar. 2012.
- [257] C. Hirschl *et al.*, "In-line determination of the degree of crosslinking of ethylene vinyl acetate in PV modules by Raman spectroscopy," *Sol. Energy Mater. Sol. Cells*, vol. 152, pp. 10–20, Aug. 2016.
- [258] X. Zhang, Q. Zhou, H. Liu, and H. Liu, "UV light induced plasticization and light activated shape memory of spiropyran doped ethylene-vinyl acetate copolymers," *Soft Matter*, vol. 10, no. 21, p. 3748, 2014.
- [259] A. . Vaughan, Y. Zhao, L. . Barré, S. . Sutton, and S. . Swingler, "On additives, morphological evolution and dielectric breakdown in low density polyethylene," *Eur. Polym. J.*, vol. 39, no. 2, pp. 355–365, Feb. 2003.
- [260] C. Jiao, Z. Wang, X. Liang, and Y. Hu, "Non-isothermal crystallization kinetics of silane crosslinked polyethylene," *Polym. Test.*, vol. 24, no. 1, pp. 71–80, Feb. 2005.
- [261] Y.-I. Yoo, Y.-J. Kim, D.-K. Shin, and J.-J. Lee, "Development of martensite transformation kinetics of NiTi shape memory alloys under compression," *Int. J. Solids Struct.*, vol. 64–65, pp. 51–61, Jul. 2015.
- [262] P. S. Lobo, J. Almeida, and L. Guerreiro, "Shape Memory Alloys Behaviour: A Review," *Procedia Eng.*, vol. 114, pp. 776–783, 2015.
- [263] R. J. Good, "Contact angle, wetting, and adhesion: a critical review," *J. Adhes. Sci. Technol.*, vol. 6, no. 12, pp. 1269–1302, Jan. 1992.
- [264] D. K. Owens and R. C. Wendt, "Estimation of the surface free energy of polymers," *J. Appl. Polym. Sci.*, vol. 13, no. 8, pp. 1741–1747, Aug. 1969.
- [265] K. A. Vijayalakshmi, M. Mekala, C. P. Yoganand, and K. Navaneetha Pandiyaraj, "Studies on Modification of Surface Properties in Polycarbonate (PC) Film Induced by DC Glow Discharge Plasma," *Int. J. Polym. Sci.*, vol. 2011, pp. 1–7, 2011.
- [266] D. G. Petlin, S. I. Tverdokhlebov, and Y. G. Anissimov, "Plasma treatment as an efficient tool for controlled drug release from polymeric materials: A review," *J. Controlled Release*, vol. 266, pp. 57–74, Nov. 2017.
- [267] M. Walo, G. Przybytniak, K. Łyczko, and M. Piątek-Hnat, "The effect of hard/soft segment composition on radiation stability of poly(ester-urethane)s," *Radiat. Phys. Chem.*, vol. 94, pp. 18–21, Jan. 2014

5.

OVERALL

CONCLUSIONS

AND

RECOMMENDATIONS FOR FUTURE WORKS

5.1 OVERALL CONCLUSIONS

5.2 RECOMMENDATIONS FOR FUTURE
WORKS

5.3 ARCHITECTURAL SKIN APPLICATION
PROPOSAL

5.4 REFERENCES

5.1

OVERALL CONCLUSIONS

In the second section of this work, active and passive responsive architectural envelope/skins were assessed, and mechanisms and protocols were reported, defining in this way state of the art and further lines of research were identified.

Nowadays most of the building envelopes have been restricted by their robust and rigid materiality to adapted to the micro-climate changes which takes place around it; a reason why the materiality has started to change and turned into small-scale pieces to reach a flexible interface.

At first place, active dynamic systems based on electromechanical components driven by sensors and actuators were introduced, and their adaptability has been shown; nevertheless, their rapid obsolescence triggered a different approach.

Not only are complex systems more prone to failure over an extended period—due to more points of failure in controllers, connections, energy supply, —but they also tend to be more unreliable when performing repetitive tasks.[268] pp. 68.

At second place, passive dynamic systems as jointless solutions without the need for electricity were proposed, based on the use of stimulus sensitive materials, this is state of the art. The reported new and exciting strategies to control microclimate variations have been shown promising results; however, soft actuators are an early-stage approach into architectural and building fields in contrast with minimally invasive surgery, robotics, and aerospace engineering areas where their development has been carried out for several years.

In this way, in the third section, the exploration into materials capable of conforming soft actuators conduced to stimulus-sensitive polymers, because of their advantage above others stimulus-sensitive materials. Semicrystalline shape memory polymers were selected as a target, because of being a low-complex synthesis system with thermal stimulus-sensitive features, make it capable of being scaled into building elements.

Once the experimental program was carried out in section fourth, the requirements of the further experimental development of large soft-actuators were evidenced. In fact, a movement in a preferred direction as actuator was achieved because of the response of the composite to a thermal-stimulus, but the toughness and mechanical potential of the system is still too low. The suggested system is not enough to trigger the displacement of any object but itself; at least envelopes made of fabric tiles or cushions of low-density materials could be an object of actuation nowadays.

RECOMMENDATIONS FOR FUTURE WORKS

Following the given facts, transdisciplinarity needs to be the key to the future expansion of soft actuators based on stimulus-sensitive materials, in order to achieve their development as the most promising direction of passive dynamic architectural skins. Moreover, in the coming developments, the soft and jointless approach must be maintained, and the uses of biomimicry in architecture [269]–[274] could be a pathway.

As an early advance for prospective studies, stimulus-sensitive materials and *compliant mechanisms* [275] must be merged as a system.

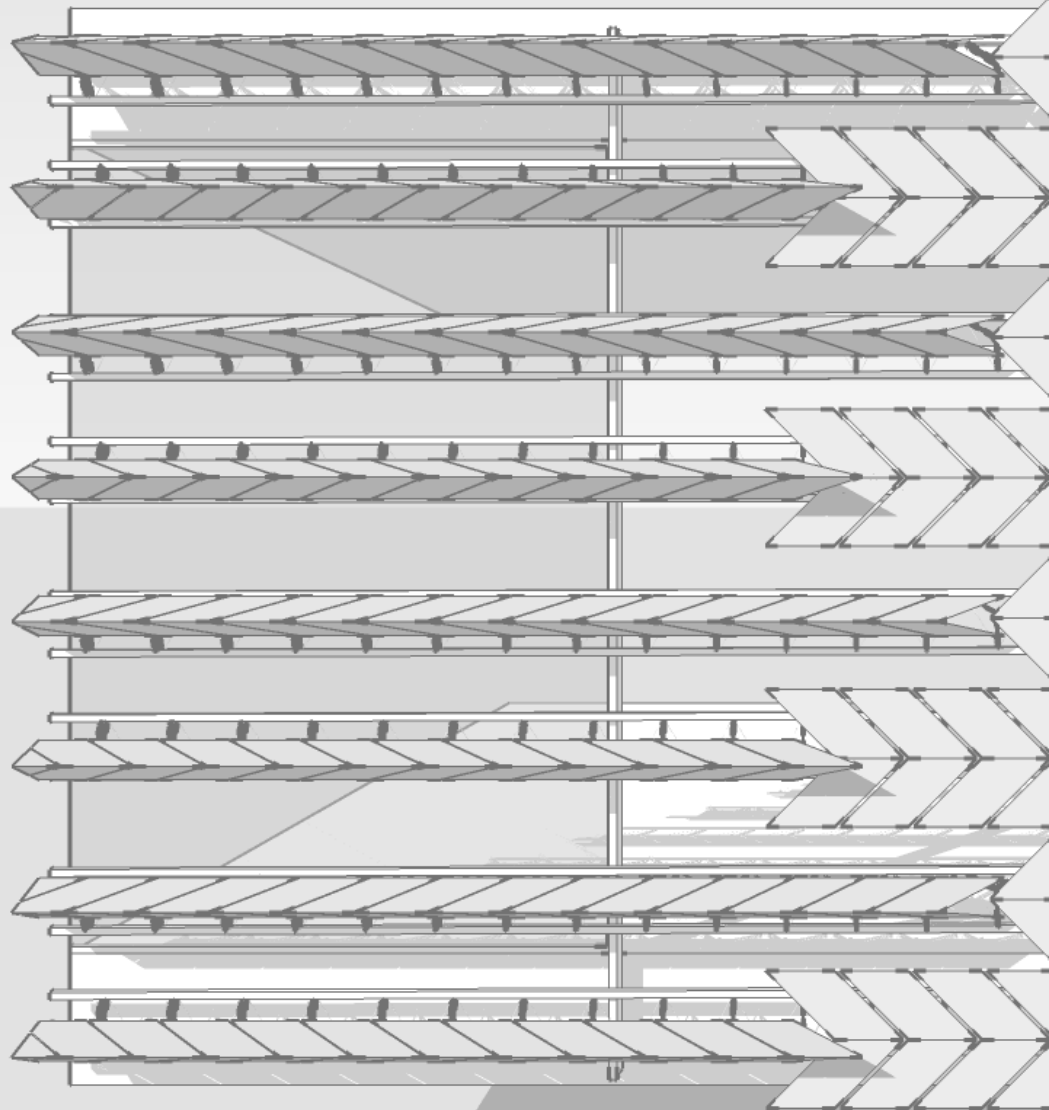
If something bends to do what it is meant to do, then it is compliant. If the flexibility that allows it to bend also helps it to accomplish something useful, then it is a compliant mechanism. The idea of using compliant mechanisms in products is catching on, but traditionally when designers need a machine that moves, they commonly use very stiff or rigid parts that are connected with hinges (like a door on its hinge or a wheel on an axle) or sliding joints. But when we look at nature we see an entirely different idea from rigid parts connected at joints – most moving things in nature are very flexible instead of stiff, and the motion comes from bending the flexible parts [276] pp. 2.

On the one hand, this kind of mechanisms can admit unconventional activation protocols, in contrast with rigid body mechanisms [277] which has a difficult response to these actuation schemes [278]. On the other hand, this integration in the way of translating properties from micro to macro-scale could be a second amplifying step.

5.3

ARCHITECTURAL SKIN APPLICATION PROPOSAL

Once the path for future studies according to the theoretical and experimental study was defined, an early proposal for an architectural skin application was developed with the aim of giving a closure returning in the architecture field and is presented as follow.



Following the biomimicry of process, which is based on the kinetics and dynamics of nature, *Mimosa pudica*, a plant with seismonastic movement features in leaves was taken as the biomimetic referent to define a dynamic architectural skin. Seismonastic movement in *Mimosa pudica* leaves are driven by an electrochemical and osmotic phenomenon [279] which triggers the bending of the pulvinus as shown in Fig. 78 and Fig. 79.

As the actuation response of the Mimosa, the obtained bending because of thermal differences of the composite material, as can be seen in Fig. 74, was used as the basis of a 3D displacement-amplifier compliant mechanism (DaCM) [276]. A compound bridge-type (CBT) [280] was used as the fundamental unit as shown in Fig. 80

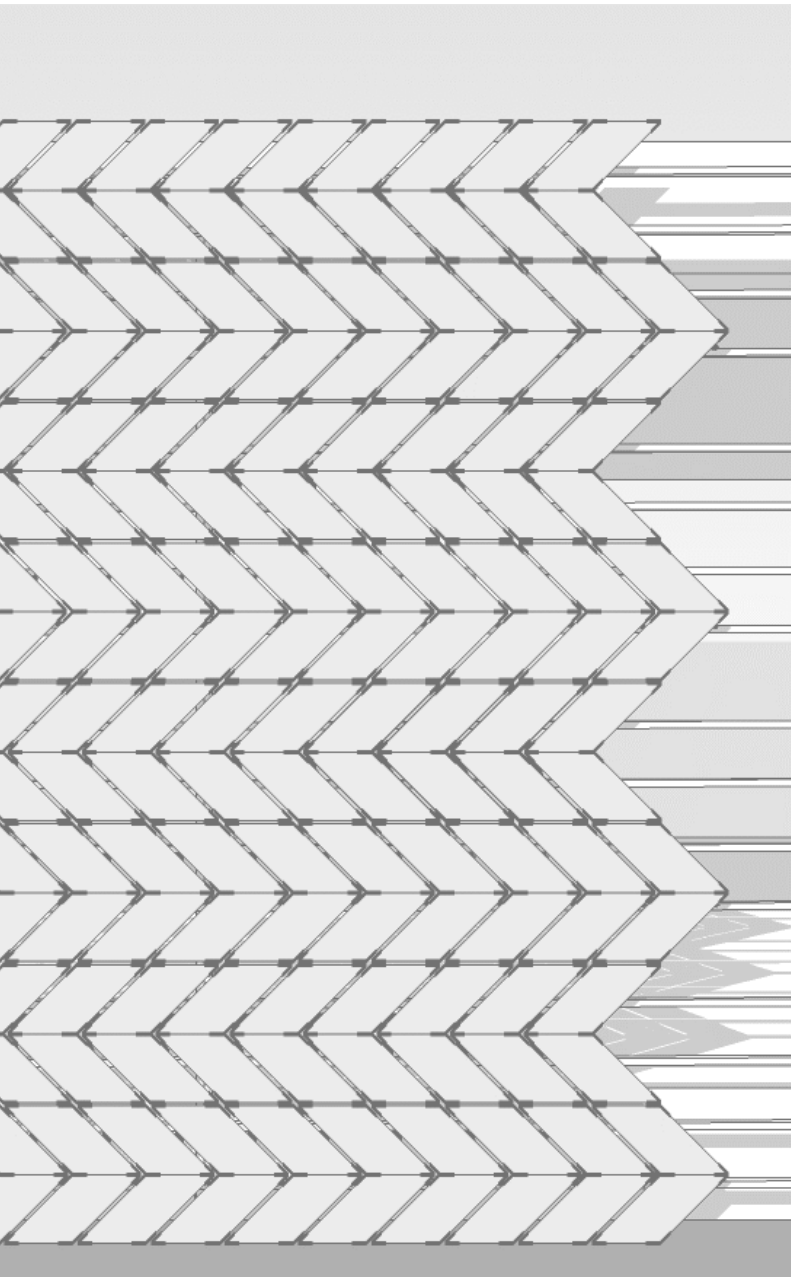


Fig. 78 *Mimosa pudica* pulvinus left. relaxed right. bended

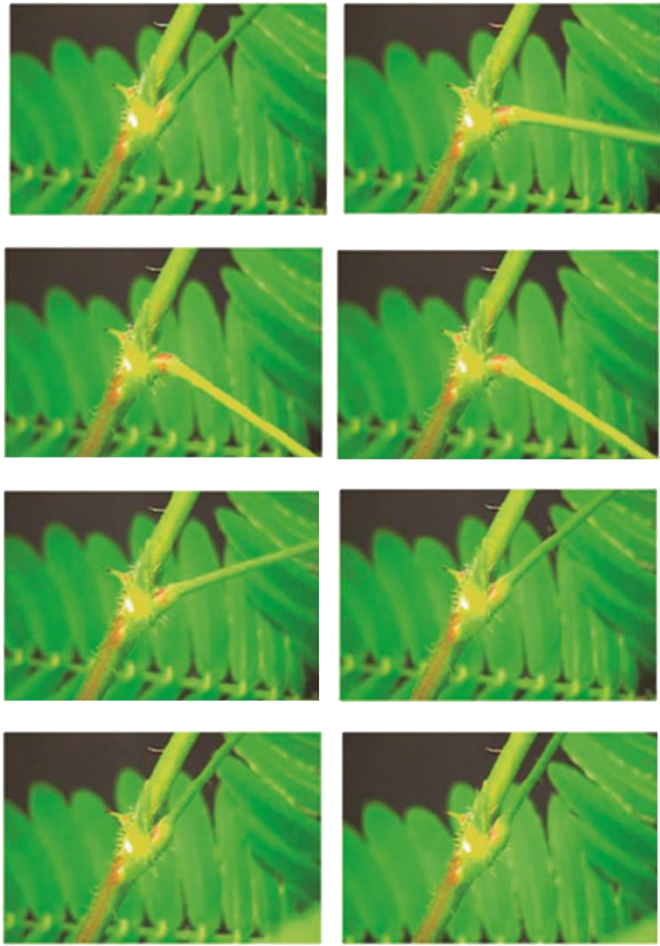
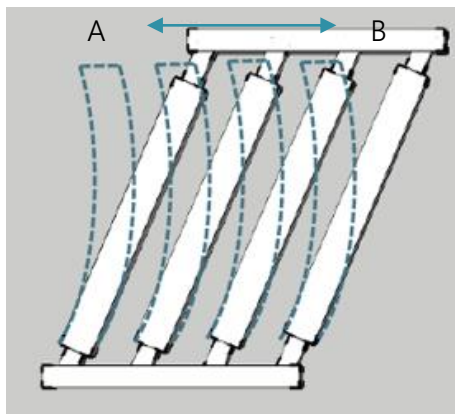
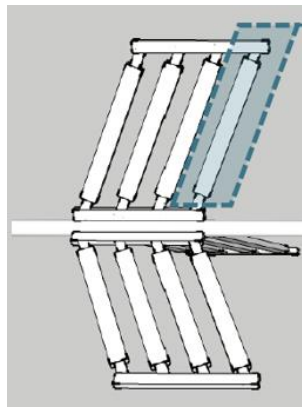


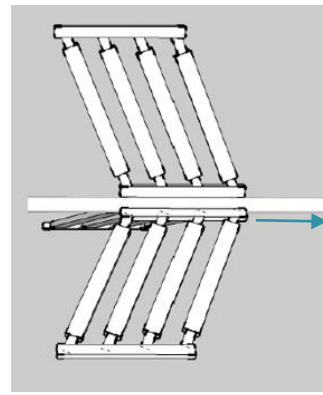
Fig. 79 Morphing structures of a pulvinus and a petiole movement of *Mimosa pudica* after thermal stimulation of pinnules and the top of a rachis by a flame, adapted from [281]



(A) A and B positions



(B) Actuation member



(C) Direction of the movement

Fig. 80 Fundamental unit of actuation DaCM

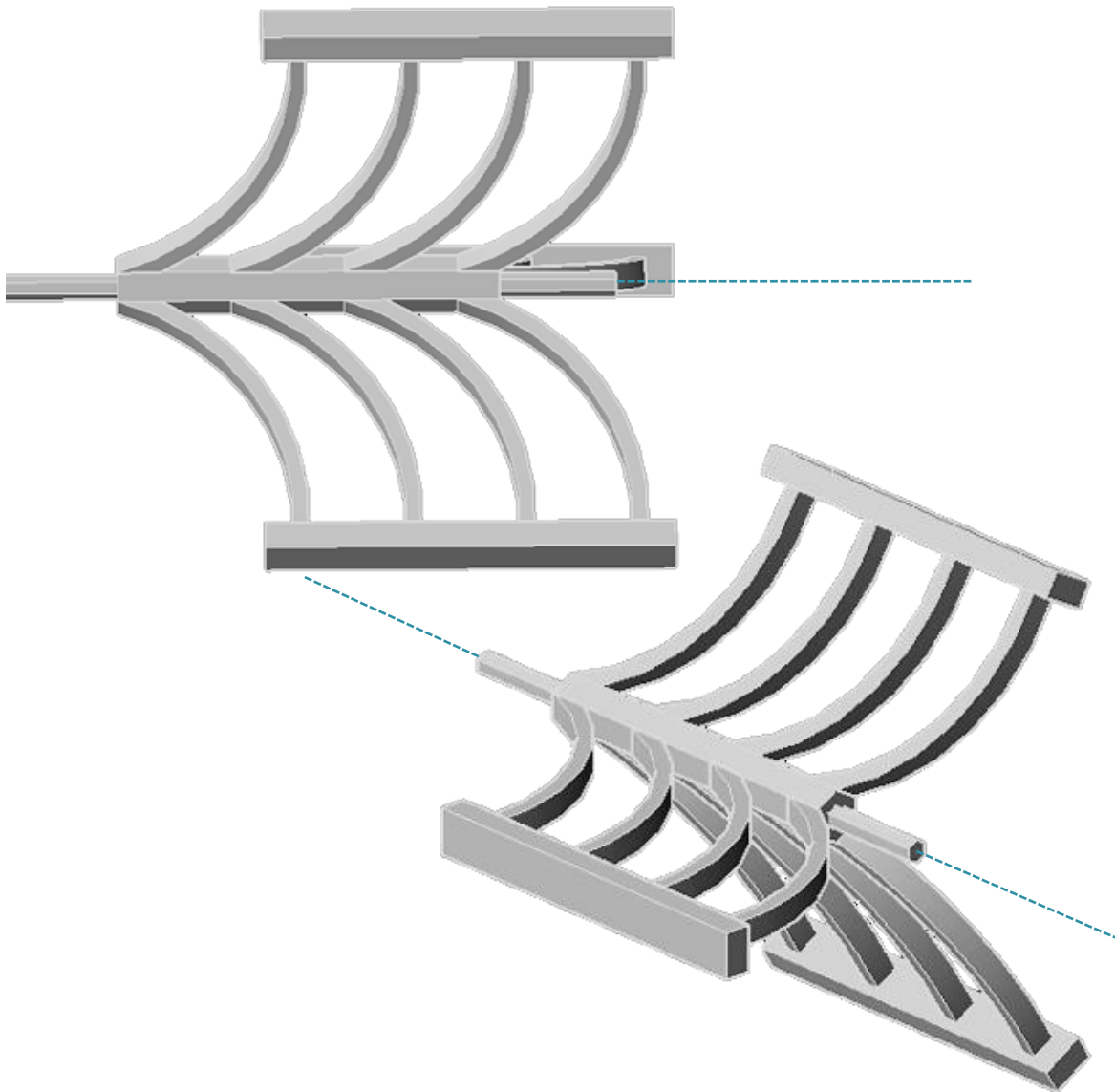
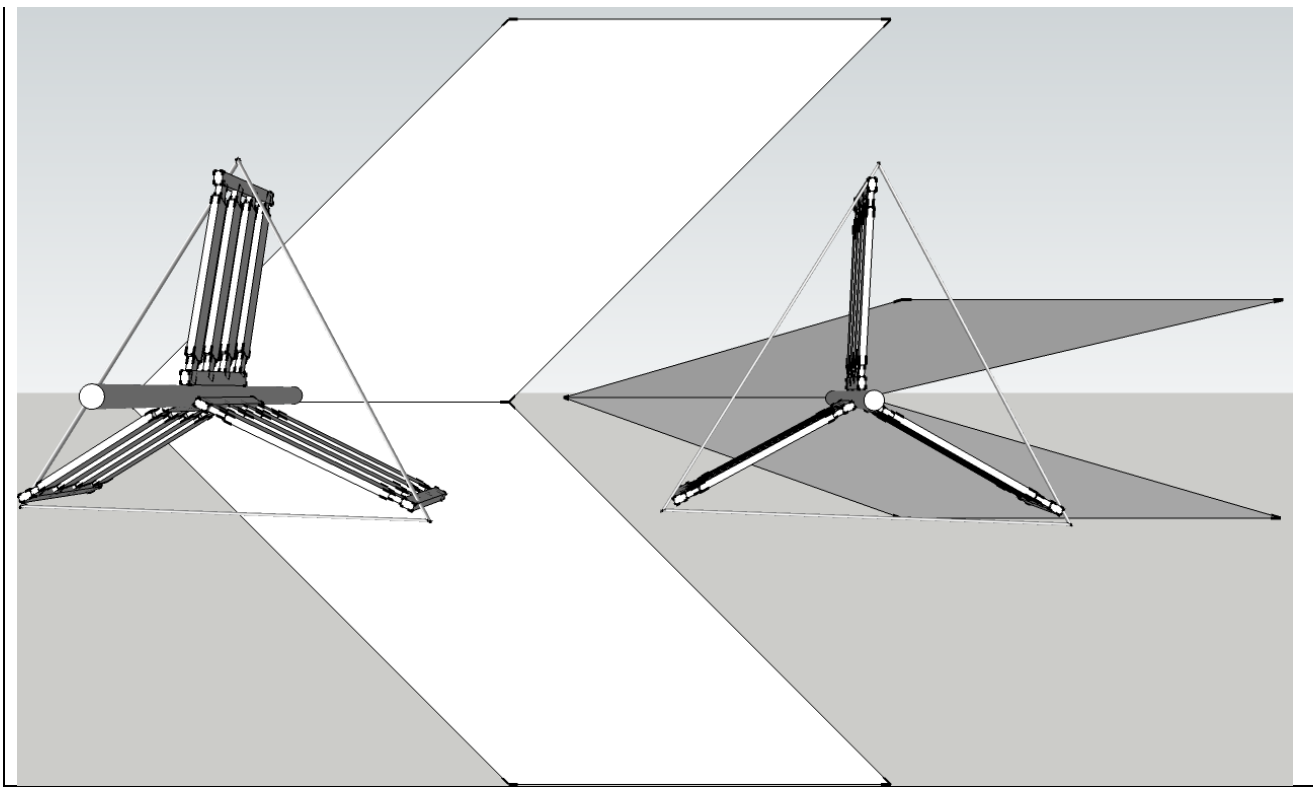
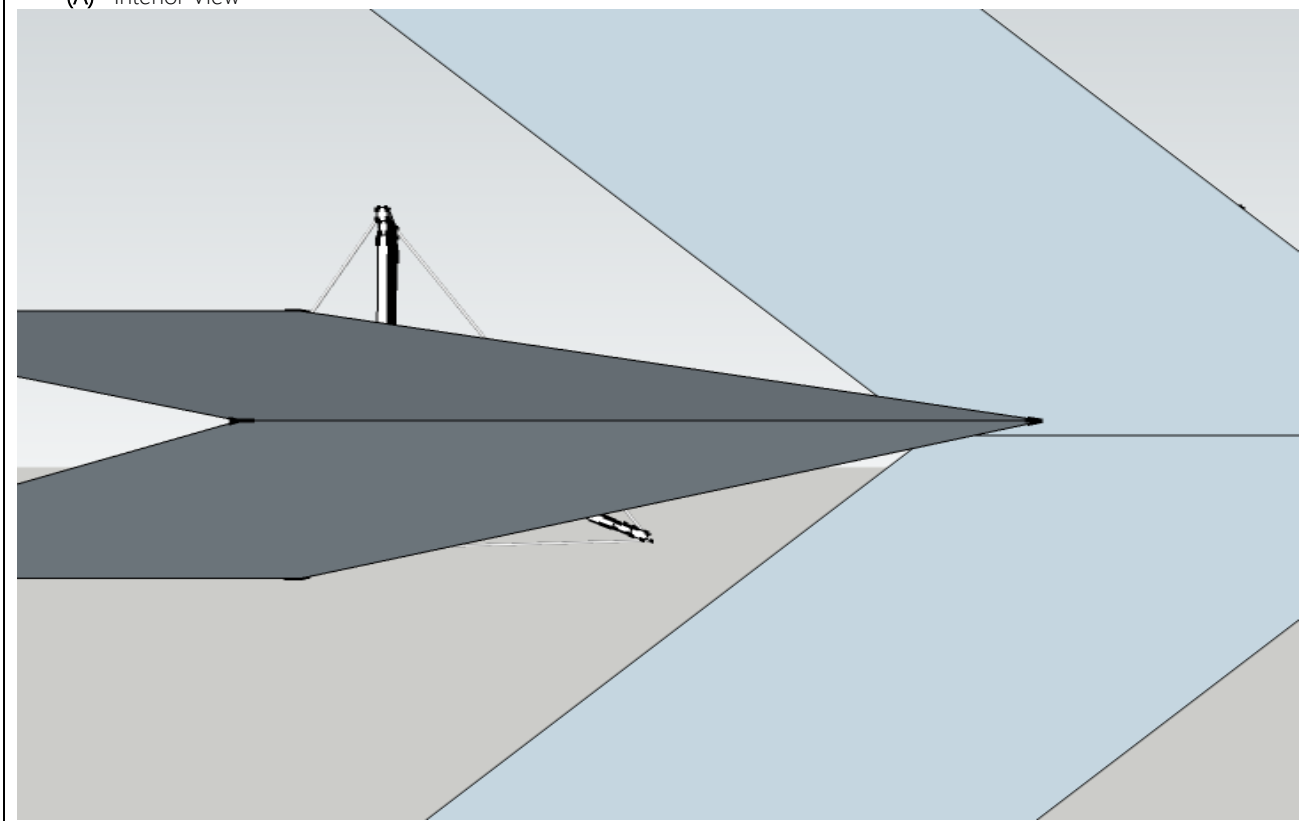


Fig. 81 DaCM 3D views



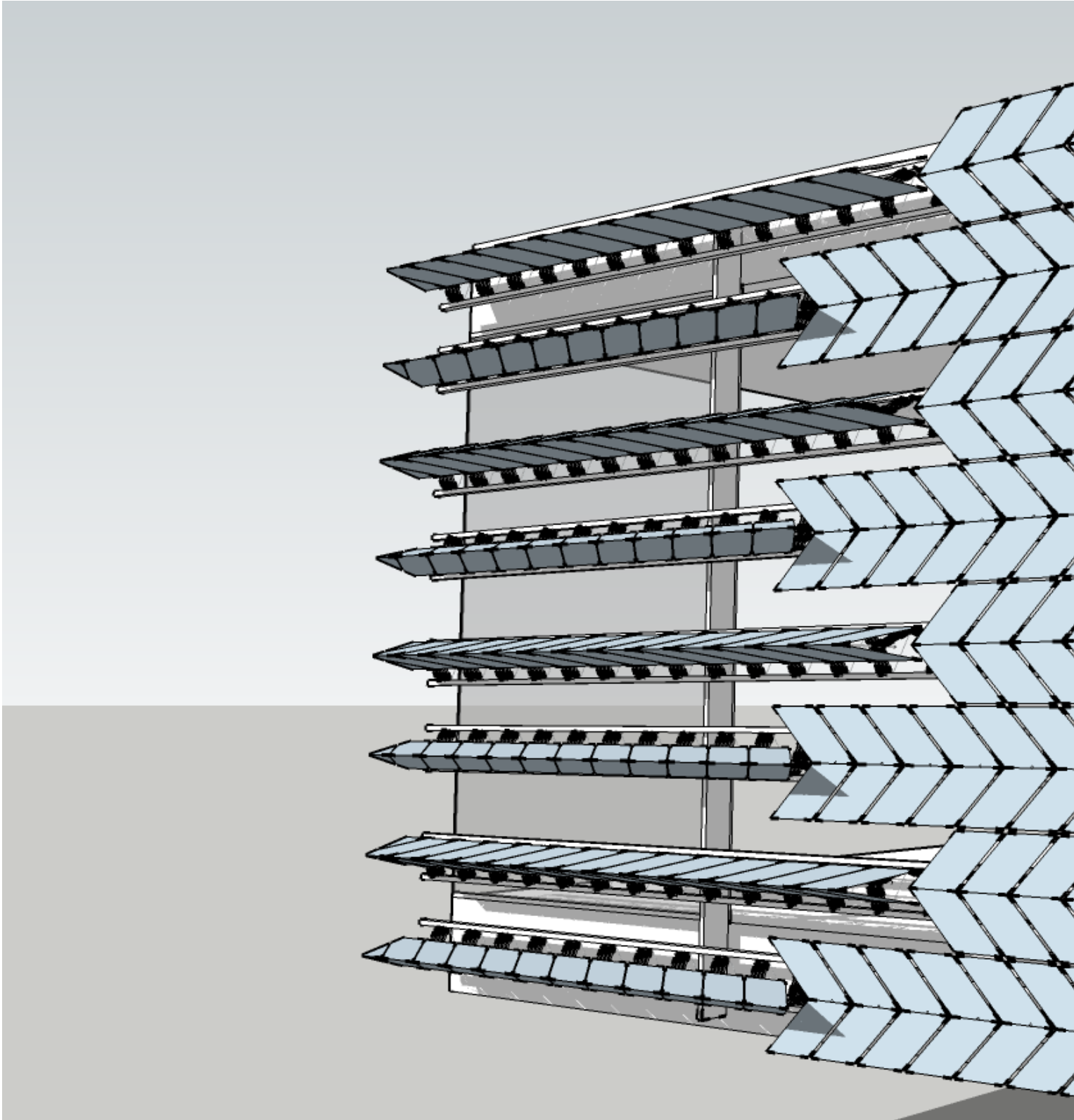
(A) Interior View

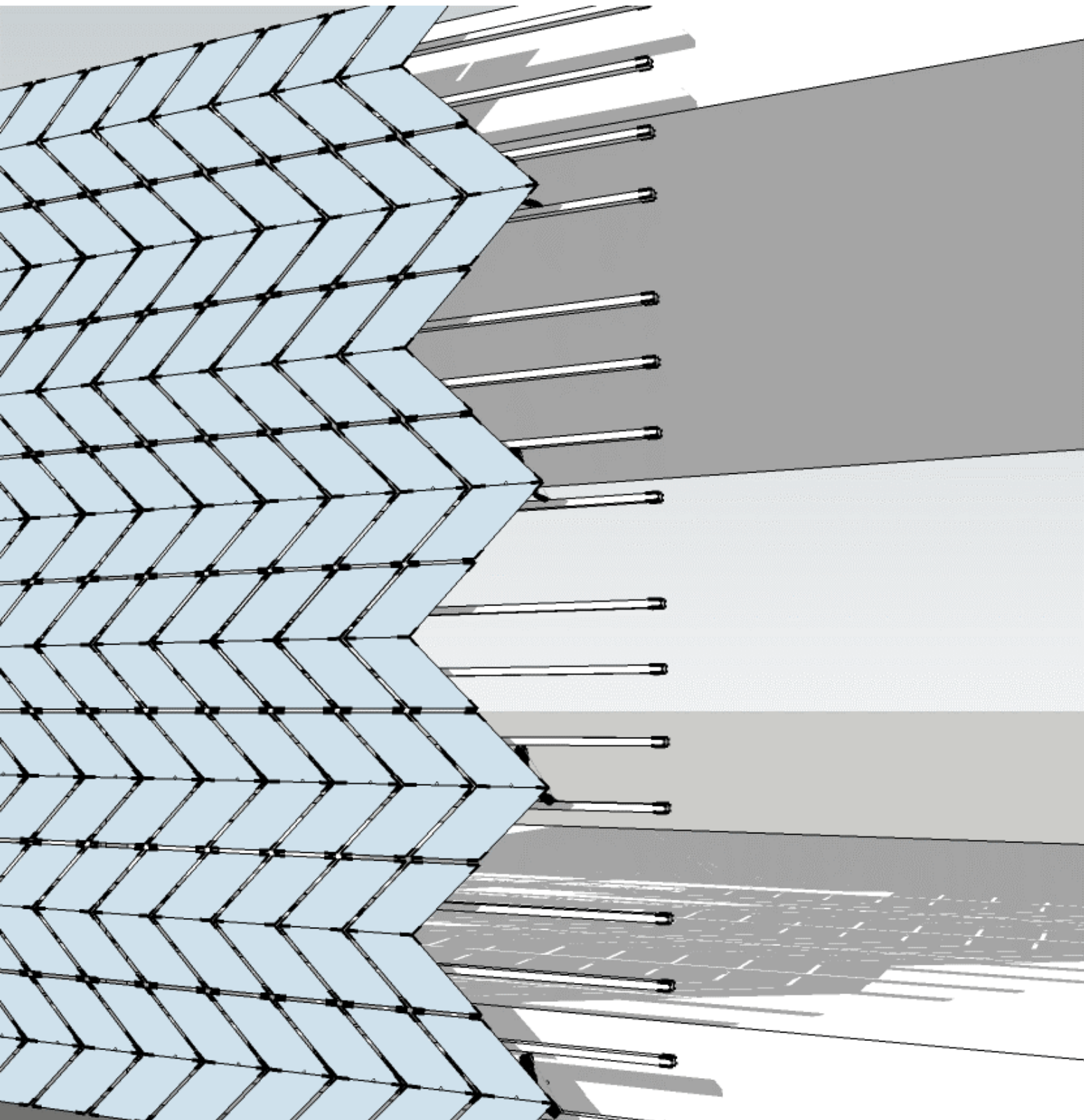


(B) Exterior View

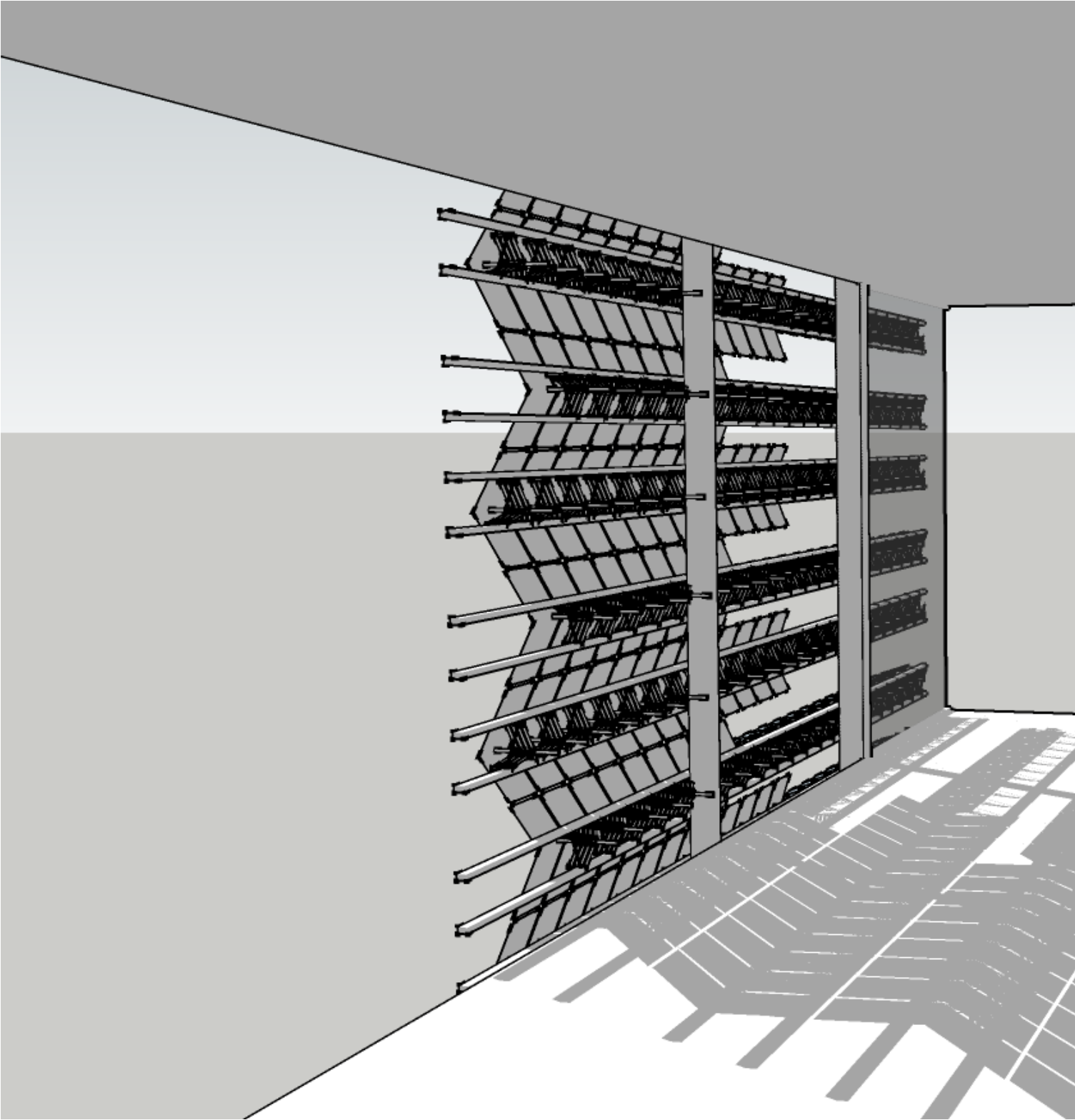
Fig. 82 Skin module open and close positions

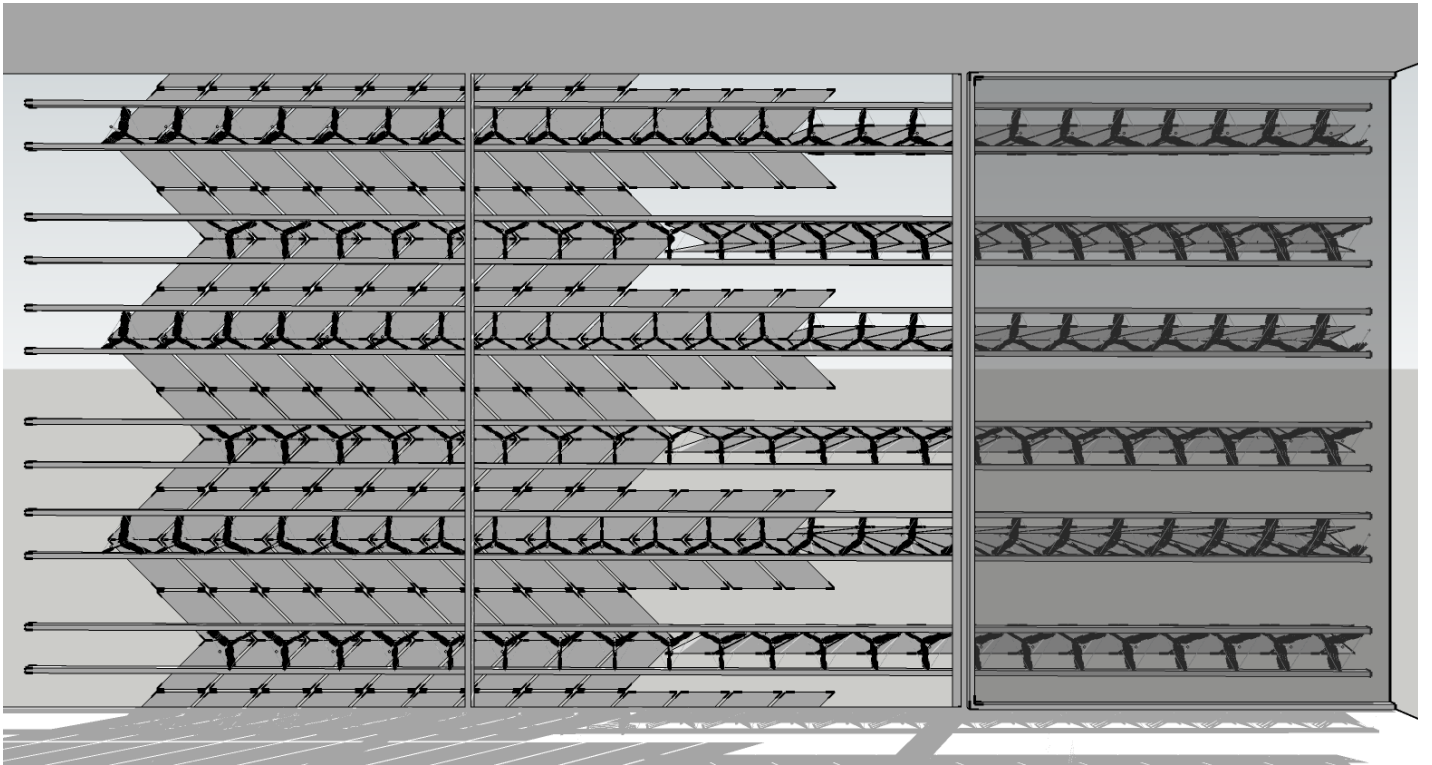
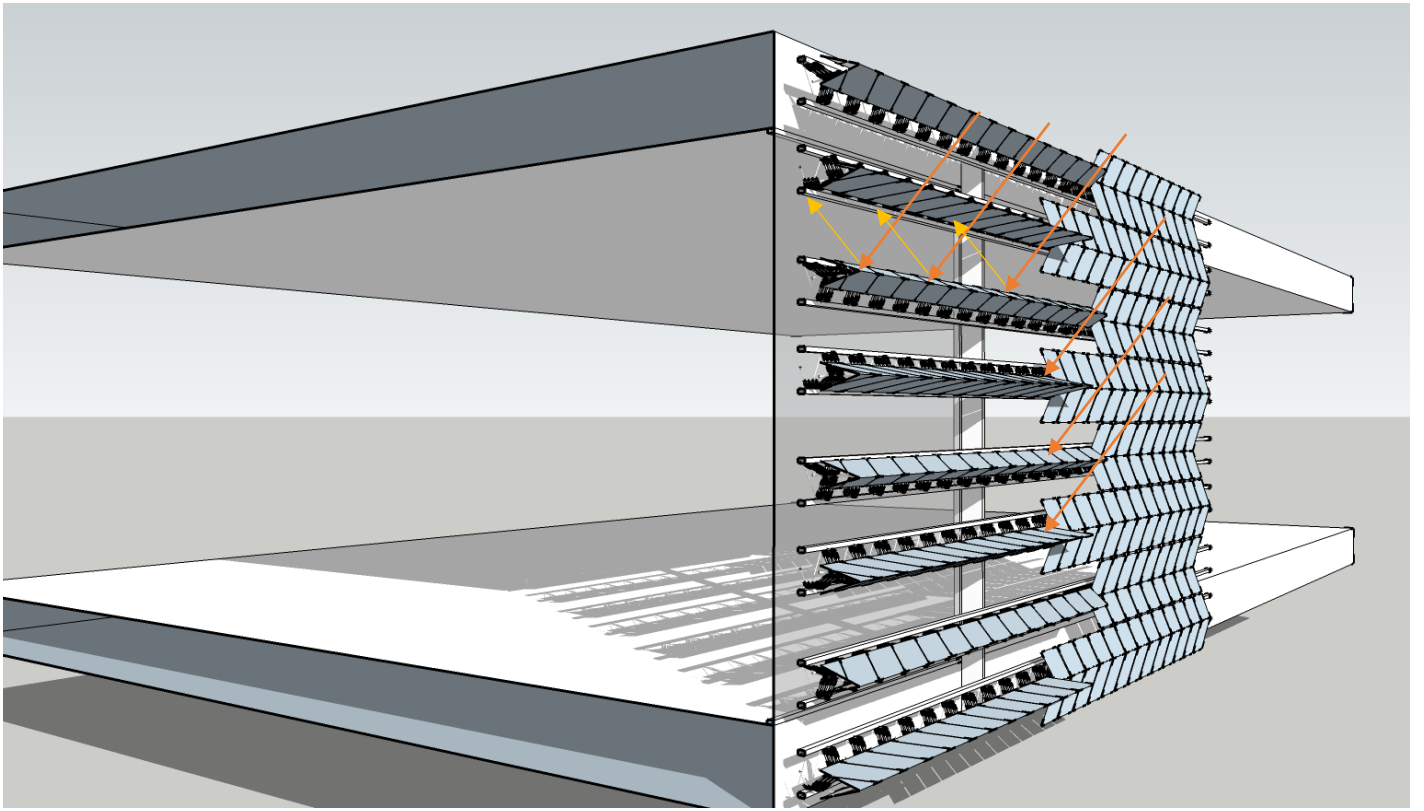
OUTSIDE VIEW





INSIDE VIEW & SUN CONTROL





5.4 REFERENCES

- [268] A. Menges and S. Reichert, "Performative Wood: Physically Programming the Responsive Architecture of the HygroScope and HygroSkin Projects," *Archit. Des.*, vol. 85, no. 5, pp. 66–73, Sep. 2015.
- [269] J. Lim, *Bio-structural: analogues in architecture*. Amsterdam: BIS-Publishers, 2009.
- [270] K. M. Al-Obaidi, M. Azzam Ismail, H. Hussein, and A. M. Abdul Rahman, "Biomimetic building skins: An adaptive approach," *Renew. Sustain. Energy Rev.*, vol. 79, pp. 1472–1491, Nov. 2017.
- [271] N. Oxman, *Design at the intersection of technology and biology*. 2016.
- [272] M. Garcia-Holguera, O. G. Clark, A. Sprecher, and S. Gaskin, "Ecosystem biomimetics for resource use optimization in buildings," *Build. Res. Inf.*, vol. 44, no. 3, pp. 263–278, Apr. 2016.
- [273] Y. Xing, P. Jones, M. Bosch, I. Donnison, M. Spear, and G. Ormondroyd, "Exploring design principles of biological and living building envelopes: what can we learn from plant cell walls?," *Intell. Build. Int.*, pp. 1–25, Nov. 2017.
- [274] S. Poppinga *et al.*, "Toward a New Generation of Smart Biomimetic Actuators for Architecture," *Adv. Mater.*, vol. 30, no. 19, p. 1703653, May 2018.
- [275] L. L. Howell, *Compliant mechanisms*. New York: Wiley, 2001.
- [276] L. L. Howell, S. P. Magleby, and B. M. Olsen, Eds., *Handbook of compliant mechanisms*. Chichester, West Sussex, United Kingdom ; Hoboken: John Wiley & Sons, Inc, 2013.
- [277] A. Müller, "Generic mobility of rigid body mechanisms," *Mech. Mach. Theory*, vol. 44, no. 6, pp. 1240–1255, Jun. 2009.
- [278] V. Kumar, J. Schmiedeler, S. V. Sreenivasan, and H.-J. Su, Eds., *Advances in Mechanisms, Robotics and Design Education and Research*, vol. 14. Heidelberg: Springer International Publishing, 2013.
- [279] A. G. Volkov, J. C. Foster, K. D. Baker, and V. S. Markin, "Mechanical and electrical anisotropy in *Mimosa pudica* pulvini," *Plant Signal. Behav.*, vol. 5, no. 10, pp. 1211–1221, Oct. 2010.
- [280] Q. Xu and Y. Li, "Analytical modeling, optimization and testing of a compound bridge-type compliant displacement amplifier," *Mech. Mach. Theory*, vol. 46, no. 2, pp. 183–200, Feb. 2011.
- [281] A. G. Volkov and V. S. Markin, "Active and Passive Electrical Signaling in Plants," in *Progress in Botany*, vol. 76, U. Lüttge and W. Beyschlag, Eds. Cham: Springer International Publishing, 2015, pp. 143–176.

FIGURES REFERENCES

Fig. 1 Werner, Bertholf (Photographer). (2007, May). *The Curia* [digital image]. Retrieved 12 February, 2018 from [/commons.wikimedia.org/wiki/Curia_Lulia](https://commons.wikimedia.org/wiki/Curia_Lulia)

Fig. 2 Nyetta, Ken (Photographer). (2013, December). *North Rose Window, Notre Dame* [digital image]. Retrieved 12 February 2018, from [/www.flickr.com/photos/kjfnjy/11553619656](https://www.flickr.com/photos/kjfnjy/11553619656)

Fig.3 Fernandez, Gabriel (Photographer). (2015, January). *Seagram building* [digital image]. Retrieved 12 February, 2018, from [/www.flickr.com/photos/gaf/16162990589](https://www.flickr.com/photos/gaf/16162990589)

Fig. 6 Melki, Serge (Photographer). (2009, March). *Arab World Institute, facade inside view* [digital image]. Retrieved 12 February 2018, from [/www.flickr.com/photos/sergemelki/3389136542](https://www.flickr.com/photos/sergemelki/3389136542)

Fig. 8 E. Giselbrecht, *Kiefer Technic Showroom*. 2007

Fig. 9 AHR (2012, June). *Al Bahar Towers* [digital image]. Retrieved 12 February, 2018, from [/www.ahr-global.com/Al-Bahr-Towers](https://www.ahr-global.com/Al-Bahr-Towers)

Fig. 10 Deutscher, Rob (Photographer). (2013, June). *RMIT Design Hub* [digital image]. Retrieved 12 February, 2018, from [/www.flickr.com/photos/bobarc/9100351902/](http://www.flickr.com/photos/bobarc/9100351902/)

Fig. 11 Arnoldious (Photographer). (2011, June). *Q1 ThyssenKrupp Quarter* [digital image]. Retrieved 12 February, 2018, from [/commons.wikimedia.org/wiki/File:ThyssenKrupp_Quartier_Essen_07.jpg](http://commons.wikimedia.org/wiki/File:ThyssenKrupp_Quartier_Essen_07.jpg)

Fig. 12 Modlar John from: [/modlar.com/photos/1749/one-ocean-thematic-pavilion-expo-2012-concept-design/](http://modlar.com/photos/1749/one-ocean-thematic-pavilion-expo-2012-concept-design/)

Fig. 14 Meagher, M. (2014). Responsive Architecture and the Problem of Obsolescence. *International Journal of Architectural Research: ArchNet-IJAR*, 8(3), 95. <https://doi.org/10.26687/archnet-ijar.v8i3.498>

Fig. 17 Correa Zuluaga, D., & Menges, A. (2015). 3D Printed Hygroscopic Programmable Material Systems. *MRS Proceedings*, 1800. <https://doi.org/10.1557/opl.2015.644>

Fig. 18 B. Torres, "Programmable Matter Hygroscopic actuation of multidirectional lattice structures," Master Thesis, University of Stuttgart, Stuttgart, Germany, 2014.

Fig. 24 Cohan, Joe (Photographer). (2013, August). *Adaptive Architectural skins* [digital image]. Retrieved 12 February, 2018, from [/www.evolo.us/architecture/adaptive-architectural-skins-and-dynamic-environmental-conditions/](http://www.evolo.us/architecture/adaptive-architectural-skins-and-dynamic-environmental-conditions/)

Fig. 28 phase change materials based on Pazrev 29 October 2014 retrieved 18 March, 2018 https://commons.wikimedia.org/wiki/File:Phase_Change_Materials.png

Fig. 30 M. Decker, "Nanotechnology and Emergent Materials in Architecture," presented at the Tectonics of Teaching, Tectonics of Teaching, 2013, vol. 2013, pp. 1–7

Fig. 31 M. Decker, "Nanotechnology and Emergent Materials in Architecture," presented at the Tectonics of Teaching, Tectonics of Teaching, 2013, vol. 2013, pp. 1–7 Fig. 33 Gesimat (2009) , retrieved 12 February, 2018 [/www.gesimat.de/](http://www.gesimat.de/)

Fig. 35 R. shambayati, ece Tankal, and B. Efilena, "Translated Geometries," Master Thesis, Institute for advanced architecture of Catalonia, Barcelona, 2014.

CONSTRUCTION

MASTER

THESIS



Construction master degree
Construction school
Architecture faculty
Universidad Nacional de Colombia